David José Rodrigues dos Santos Costa

Licenciado em Ciências da Engenharia Civil

Dynamic stiffness of the piled foundation of a onshore wind turbine

Dissertação para obtenção do Grau de Mestre em Engenharia Civil

Orientador: Paul Hölscher, Senior Advisor, Deltares
Co-orientador: José Nuno Varandas, Professor Auxiliar, FCT/UNL

Júri:

Presidente: Prof. Doutor Carlos Chastre Rodrigues
Arguente: Prof. Doutor João Bilé Serra
Vogal: Prof. Doutor José Nuno Varandas

FACULDADE DE CIÊNCIAS E TECNOLOGIA
UNIVERSIDADE NOVA DE LISBOA

Setembro 2014

Dynamic stiffness of the piled foundation of a onshore wind turbine

Acknowledgments

First of all, I would like to thank all the professors that were involved in my education as civil engineer. Thank you for all your expertise, advices, critics and great talks that ultimately inspired me to be the best I can. I feel grateful to have been your student in this long journey that is university. All of you were somehow important and for that a big thank you.

I am very thankful to professor Paul Hölscher. Thank you for this opportunity and for being always helpful and available in the necessary arrangements prior to my stay in Delft. Thank you for the way you receiving me at TU Delft, showing the greatest care and concern that I could ever expect. I am very grateful for all the knowledge you shared with me and for all the critical comments that helped improving my master thesis. I thank professor José Varandas for all the help and guidance. This thesis was never possible if there was not for the effort, patience and dedication shown during the process. Thank you very much for being always available for discussion and ready to give insightful advices. To both, from the bottom of my heart, I thank you for the friendship. I will always keep with me what you thought me and I am very grateful for your presence in my last step as an engineering student. I feel privileged to have had the opportunity to work with both of you.

Finally, I thank my family, friends and loved ones. All of you gave me extraordinary support in this chapter of my life and I believe if university was crucial for my development as civil engineer, you gave me the best self development i could ever wish. It wouldn't be possible to finish this chapter of my life if there wasn't for all the love, care, laughs and support i had. To all, I will always keep you in my heart.

Abstract

One of today's biggest concerns is the increase of energetic needs, especially in the developed countries. Among various clean energies, wind energy is one of the technologies that assume greater importance on the sustainable development of humanity. Despite wind turbines had been developed and studied over the years, there are phenomena that haven't been yet fully understood. This work studies the soil-structure interaction that occurs on a wind turbine's foundation composed by a group of piles that is under dynamic loads caused by wind. This problem assumes special importance when the foundation is implemented on locations where safety criteria are very demanding, like the case of a foundation mounted on a dike.

To the phenomenon of interaction between two piles and the soil between them it's given the name of pile-soil-pile interaction. It is known that such behavior is frequency dependent, and therefore, on this work evaluation of relevant frequencies for the intended analysis is held. During the development of this thesis, two methods were selected in order to assess pile-soil-pile interaction, being one of analytical nature and the other of numerical origin. The analytical solution was recently developed and its called *Generalized pile-soil-pile theory*, while for the numerical method the commercial finite element software PLAXIS 3D was used. A study of applicability of the numerical method is also done comparing the given solution by the finite element methods with a rigorous solution widely accepted by the majority of the authors.

Keywords: Dynamic Stiffness; Pile-soil-pile interaction; Wind turbines; FAST; PLAXIS 3D

Resumo

Uma das maiores preocupações hoje em dia é o aumento das necessidades energéticas, principalmente nos países desenvolvidos. Deste modo, entre as várias energias limpas, a energia eólica é uma das tecnologias que assume maior relevo no desenvolvimento sustentável da humanidade. Apesar das turbinas eólicas terem sido largamente desenvolvidas e estudadas ao longo dos anos, há fenómenos ainda não totalmente compreendidos. Este trabalho estuda a interação solo-estrutura que ocorre numa fundação composta por um grupo de estacas de uma turbina eólica que está sujeita às cargas dinâmicas induzidas pelo vento. Esta problemática assume especial relevância quando a fundação está assente em locais onde os critérios de segurana da fundação sejam muito exigentes, como é o caso de uma fundação que esteja assente num dique.

Ao fenómeno de interacção entre duas estacas e o solo entre estas, dá-se o nome de interacção estaca-solo-estaca. É sabido que tal comportamento é dependente da frequência de excitação e, sendo assim, neste trabalho procede-se também à avaliação das frequências relevantes para a análise em questão. Durante o desenvolvimento desta tese, dois métodos são seleccionados para estudar a interacção estaca-solo-estaca, sendo um de natureza analítica e outro de origem numérica. A solução analítica foi recentemente desenvolvida e é denominada de *Generalized pile-soil-pile theory*, enquanto que para a análise numérica recorre-se ao *software* comercial de elementos finitos PLAXIS 3D. É ainda efectuada um estudo de aplicabilidade do método numérico para este tipo de problemas procedendo à comparação da solução obtida pelo método dos elementos finitos com uma solução rigorosa vastamente aceite pela maioria dos autores.

Palavras chave: Rigidez dinâmica; Interação estaca-solo-estaca; Turbinas eólicas; FAST; PLAXIS 3D

Contents

List of Figures

List of Tables

List of Symbols

Latin Symbols

A_b	Pile tip area
A_s	Pile shaft area
$A_{v_{ij}}$, $A_{h_{ij}}$	Dynamic interaction matrix for vertical and horizontal motions
a_0	Dimensionless frequency
$\boldsymbol{C}$	Damping matrix
c	Damping coefficient
c'	Soil cohesion
C_1, C_2	Relaxation coefficients
C_d	Damping coefficient
c_p	Soil compression wave velocity
c_{LA}	Lysmer's analog velocity
c_s	Soil shear wave velocity
c_{vg}, c_{hg}, $c_{\theta g}$	Vertical, horizontal and bending damping coefficients of the pile group
C_z^G	Vertical Damping coefficient of a group of piles
d	Plate element thickness
D_f	Foundation cap diameter
D_p	Pile diameter
E	Soil deformation modulus
E_p	Pile deformation modulus
F	Generic force
$\hat{F}$	Force amplitude

f	Linear frequency
F_G	Vertical forces applied on the foundation cap
F_j	Force acting on pile j
F_M	Additional total vertical force on the cap due to the bending moment
$F_{M;max}$	Additional maximum vertical force on a single pile due to the bending moment
F_{max}	Embedded pile foot resistance
F_r	Normalized friction ratio
f_s	Sleeve friction
F_{vert}	Vertical force on all piles
F_{vp}	Maximum total vertical load on a pile
G	Soil shear modulus
I_c	Soil behavior type index
$\boldsymbol{K}$	Stiffness matrix
K	Lateral earth pressure coefficient
k	Stiffness coefficient
K_0	Lateral earth pressure coefficient "at-rest‘
$\mathscr{K}_d$	Dynamic stiffness of a single pile
K_d	Dynamic stiffness coefficient
k_n, k_t	Elastic normal stiffness of the embedded pile element
k_s	Elastic shear stiffness of the embedded pile
K_{vg}	Vertical dynamic stiffness of a group of piles
k_{vg}, k_{hg}, $k_{\theta g}$	Vertical, horizontal and bending stiffness coefficients of the pile group
$\overline{K}_z^G$	Vertical dynamic stiffness coefficient of a group of piles
K_z^s	Static stiffness of a single pile
l_e	Average finite element size
l_p	Pile length
$\boldsymbol{M}$	Mass matrix
M	General bending moment

$\hat{M}$	Amplitude multiplier
m	Cap mass
M_x, M_y, M_z	Bending moment around x, y and z axis
N	Normal force
n_p	Total number of piles
q_c	Cone resistance
Q_t	Normalized cone penetration resistance
R	Foundation cap radius
r_0	Pile radius
R_b	Pile tip resistance
r_e	Relative finite element size factor
R	Foundation radius
R_f	Friction ratio
R_s	Pile shaft resistance
s/d	Dimensionless pile spacing
s_u	Undrained shear strength
t	Time
t_c	Foundation cap thickness
t_{total}	Total calculation time
T_{max}	Embedded pile skin resistance per meter
$\hat{u}$	Displacement amplitude
u_z	Vertical cap displacement
V_x, V_y	Shear force in x and y directions
W_{cap}	Foundation cap weight
w_i	Displacement of pile i
w_{vert}	Vertical displacement of all piles

Greek Symbols

α	Dimensionless adhesion coefficient
α_r	Rayleigh coefficient for mass influence in the damping of the system
α_s	Static interaction factor
β	Soil damping ratio
β_r	Rayleigh coefficient for stiffness influence in the damping of the system
γ, γ_t	Total unit weight
γ_w	Water unit weight
δ	Soil-structure friction angle
Δ_{ij}	Spacing between pile i and pile j
Δt	Time step
δ_t	Time difference between excitation and response
θ_{ij}	Angle between pile i and j
θ_j	Angle between pile j and the foundation center
λ	Wavelength
ν	Poisson ratio
ξ	Damping ratio
ρ	Material density
σ_n	Normal stress
σ'_v	Mean vertical effective stress along pile shaft
σ'_{v0}, σ'_0	Vertical stress
τ	Shear stress
ϕ	Foundation cap rotation
ϕ'	Soil friction angle
ϕ_0	Initial phase angle
φ	Phase angle
ω	Angular frequency

Abbreviations

BEM	Blade element momentum
CPT	Cone penetration test
DLC	Design load case
DOF	Degree of freedom
FEM	Finite element method
GDW	Generalized dynamic wake
NTM	Normal turbulence model
NREL	National renewable energy laboratory
SBT	Soil behavior type
SBT_N	Normalized soil behavior type

Chapter 1

Introduction

1.1 General context

Over the years and with the increase of industrialized nations, energy demand has been a subject of great importance to the humanity. Over the past century and specially after the oil crisis in the mid 1970's, renewable energies have been a matter of study and development, with wind energy leading the way to achieve reliable, effective and clean energy. Wind turbines are nowadays an usual element on the landscape of many European countries (Castro, 2009). Among Germany, Denmark or the USA, The Netherlands has been one of the countries that deposits high expectations on this technology with extensive experience on both off-shore and on-shore wind turbines.

Although onshore wind turbines are reasonably well studied, some effects are not yet fully understood, namely the interaction between a foundation composed by a group of piles and the surrounding soil. In order to assess the wind turbine foundation response when dynamically loaded, the dynamic stiffness must be properly evaluated. Many designers approach this problem from a static point-of-view which does not allow to estimate the damping of the foundation and thus no proper estimation of the dynamic stiffness is possible, leading to a choice of a very safe value for the stiffness (Hölscher, 2014a). This matter assumes major importance if the wind turbine is implemented on a dike. Dike safety its been a subject of great concern over the country's safety, specially after the big flood of 1953 where 100 000 people were evacuated and a total of 1836 casualties occurred (Gerritsen, 2005). Therefore, full understanding of wind turbine foundation behavior is required in order to increase sustainable energy spacial implementation. Proper estimation of foundation's dynamic stiffness is then crucial to fully describe the response of a foundation, dynamically loaded by a wind turbine.

1.2 Aim of research

The aim of the present thesis is to properly evaluate the dynamic loads caused by a wind turbine on its foundation which is composed by a piled group and the computation of the dynamic stiffness, estimating both the stiffness and damping coefficients. This problem is approached using two different methods. An analytical method called general pile-soil-pile interaction developed by Hölscher (2014a) and a numerical approach using a finite element analysis using the software PLAXIS 3D. Also, it is investigated the applicability of the finite element approach to this type of problems and if the method is capable of describing the pile-soil-pile interaction in terms of value and trend. The analysis is based on real scenario data, more precisely, the investigation is made for a potential implementation of a wind turbine mounted on a dike located in Lauwersoog, The Netherlands.

1.3 Outline of the Thesis

Chapter 2 starts by introducing the phenomenon of pile-soil-pile interaction. A brief description of the work made so far on pile group interaction is made showing the differences between the static and dynamic behavior of a piled foundation. The main conclusions on previous studies on dynamic soil-structure interaction is presented where is clear the frequency dependent behavior of this type of foundation.

In chapter 3, wind turbine behavior is studied. The wind action is described using real wind data from a weather station. The computation of the dynamic wind loads is made using the software FAST where the plotted results are three dimensional time series of loads on every direction. Also, the evaluation of the natural frequency of the wind turbine is made as well as the response frequencies of the system.

After the calculation of wind loads on the base of the tower, Chapter 4 defines the missing variables in order to perform a pile-soil-pile interaction analysis. Here a geotechnical model is built by first characterizing the soil medium, using cone penetration tests. After, a foundation preliminary design was held using the computed loads on the previous chapter. This foundation preliminary design was made using to Eurocode 7 specification and respecting its safety requirements.

Finally in Chapter 5 the dynamic pile-soil-pile interaction analysis is performed using results from the previous chapters. As already mentioned, this analysis was made using analytical and numerical solutions. Both solutions are fully described and compared. Also the applicability of the finite element method is studied and compared with the rigorous

solution of Kanya and Kausel (1982).

Chapter 6 sums up the main conclusions of the present work and presents recommendations and possible future developments.

Chapter 2

Problem Description

The dynamic response of dynamically loaded foundation depends on many factors such as the excitation, foundation type and geometry and soil characteristics. The final goal of an engineer is to properly design a foundation that verifies both safety and economical requirements. In this thesis the dynamic action is the wind excitation of an onshore wind turbine. The load is transmitted from the tower to the foundation which is composed by a group of piles connected by a concrete cap.

Many engineering models simplify the problem by considering that the soil-structure model is represented by a spring-dashpot system as schematized in Figure 2.1 (Santos, 2002). The piles and the soil in the between provide additional stiffness and dissipative contributions to the system, so it is necessary to incorporate these contributions into equivalent springs and damping coefficients.

It is then, important to properly define the foundation stiffness and damping since it plays

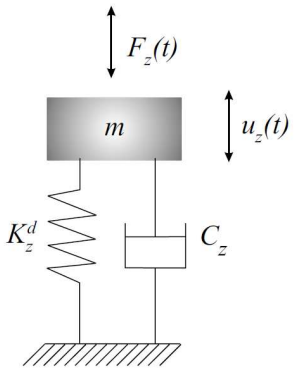

Figure 2.1: Spring-dashpot model

an important role on the foundation behavior. As said, foundation stiffness is dependent on the strength and stiffness of the soil as well as on the foundation elements. Since a group of piles is the object of study, special care must be taken since the response of a group of piles is influenced by the parameters mentioned above and also by the excitation frequencies.

Over the years, behavior of pile foundations have been the subject of deep research. Most studies focused and still focus mainly on pile behavior when subjected to static loading. If one pile of a piled foundation is under static loading, all piles within the deformation field of this pile tend to move in the same direction. Figure 2.2 illustrates an example of two piles where one is subjected to a static vertical force. Due to this load, the pile on the left moves downwards and the pile on the right moves in the same direction. Consequently, in many cases a group of piles will suffer greater displacements than if these were isolated carrying the average load. This means that for groups with high pile density the group efficiency, i.e, the ratio between the total group displacement and the sum of isolated piles displacements if these were loaded separately is smaller than 1. Among many studies of reference, it is important to refer the work of Poulos (1968) and Poulos (1971) where the concept of *interaction factors* presented in Expression 2.1 was introduced and showed that the total group effect can be represented by overlapping the effects of only two piles. However, static pile behavior studies did not provide sufficient information when evaluating dynamic response of pile groups.

$$\alpha_s = \frac{additional\ displacement\ caused\ by\ the\ nearby\ pile}{displacement\ of\ the\ pile\ when\ subjected\ to\ it's\ own\ load} \tag{2.1}$$

If the load is dynamic the previous assumption is not always true. When subjected to an harmonic load, both piles will exhibit an harmonic motion. However, the phase of this motion depends on the loading frequency, distance between piles and wave velocity in the soil (Hölscher, 2014b). Depending on such parameters, the group efficiency may change considerably exhibiting values much higher or smaller than the unity by simply changing the frequency of excitation. This harmonic interaction between two piles is shown in Figure 2.3.

With the increasing demand on machine foundations such as nuclear power plants, offshore structures or wind turbines, significant research was made on this subject. First, dynamic analysis of isolated piles with relevance for the work of Liu and Novak (1994), then for pile groups with the proposed solutions of Kanya and Kausel (1982) and Dobry and Gazetas (1988). The main focus is to accurately describe soil-structure interaction under dynamic solicitation and the transmission of loads from the piles to the soil which is commonly associated with a problem of ground wave propagation. The rigorous solution by Kanya

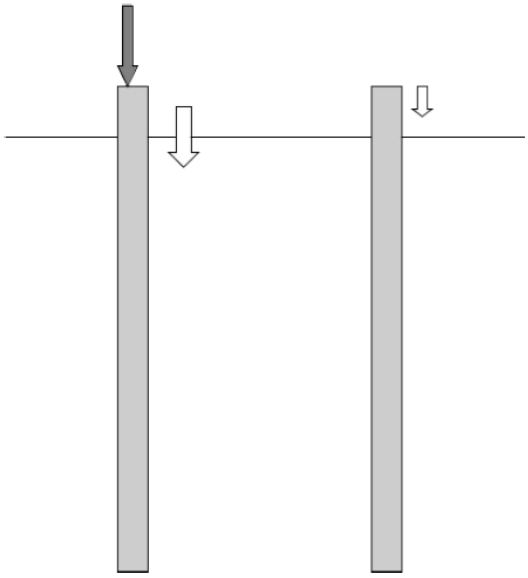

Figure 2.2: Static interaction between two nearby piles, Hölscher (2014b)

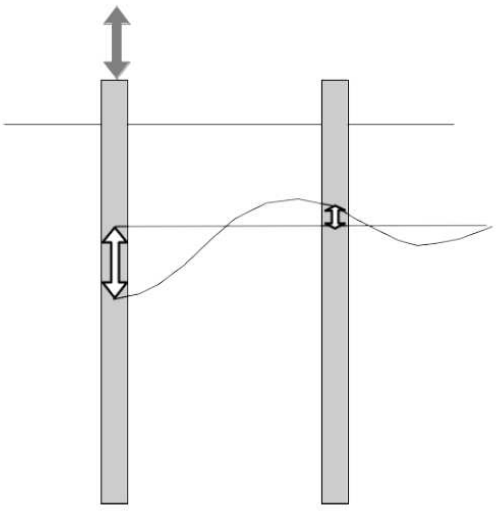

Figure 2.3: Dynamic interaction between two nearby piles, Hölscher (2014b)

and Kausel (1982) uses a numerical solution for the evaluation of the soil flexibility matrix and analytical solutions for the pile stiffness and flexibility matrices. The main disadvantage of this and other methods at the time was that these were all of numerical nature and involved discretizing each pile and supporting soil, hence, the application would imply substantial computational effort. Given this, Dobry and Gazetas (1988) developed a simple analytical solution to the problem. According to the authors this simple method could be summarized as:

(i) Simple enough to be taught in a course on soil dynamics, and can be well understood and applied by the engineer, even without the help of a computer.

(ii) For a wide range of material parameters, pile separation distances, and frequencies of oscillation, the results of the method are in excellent accordance with rigorous solutions.

(iii) Capable of being applied to all modes of oscillation while retaining its simplicity.

(iv) The procedure can be extended to handle pile installation effects in a simplified but physically sound way.

Figure 2.4 compares the simple method developed by Dobry and Gazetas (1988) with the rigorous solution of Kanya and Kausel (1982) for a vertically loaded group of 4 fixed head piles in a homogenous halfspace. These are plotted for different dimensionless s/d spacings as function of dimensionless frequency(see Equation 2.2) and the dynamic stiffness(a) and damping(b) factors. These factors are defined as the ratio between the dynamic stiffness($\overline{K}_z^G$) or dashpot(C_z^G) coefficient and the sum of the static stiffness of the individual single piles(K_z^s).

$$a_0 = \frac{\omega\, d}{c_s} \tag{2.2}$$

where,
ω - Angular frequency $[rad]$
d - Pile diameter $[m]$
c_s - Shear wave velocity of the soil $[m/s]$

As seen, for each frequency and spacing the foundation presents different behavior. Notice that if there was no pile-soil-pile interaction, the group factor curves would coincide with the dashed line which corresponds to the response of the single pile. Depending on spacing

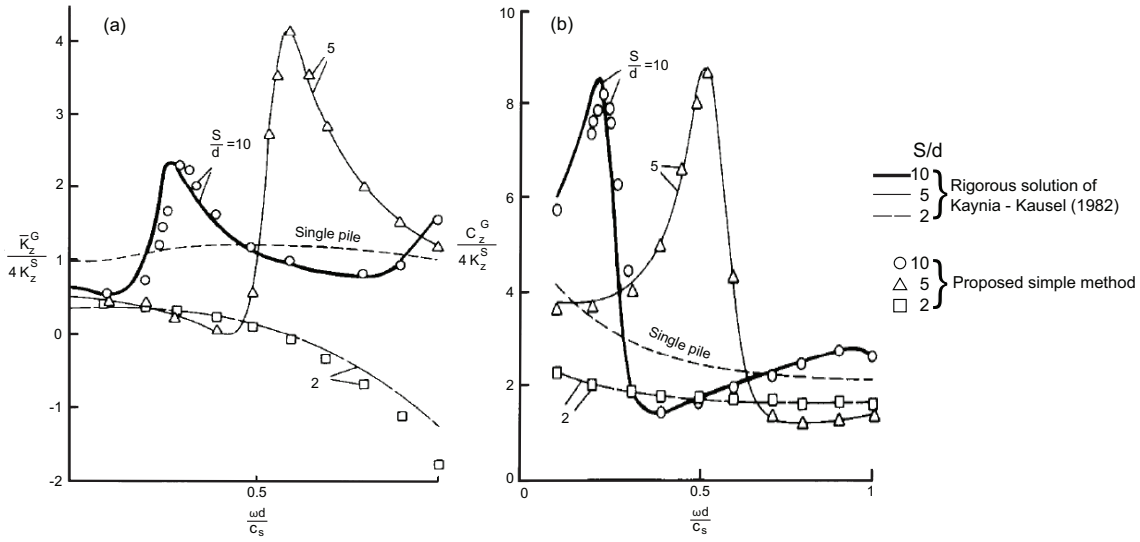

Figure 2.4: Vertical dynamic stiffness and damping group factors for a group of 2x2 fixed head piles, Dobry and Gazetas (1988)

and frequency the plots exhibit a behavior with the curves for stiffness and damping coefficients having pronounced peaks and valleys. It is easily seen that for a small frequency change the dynamic stiffness of the group may considerably change having group factors that lead to safe situations where the dynamic stiffness exceeds by far the unity or potential dangerous cases where this considerably decreases to values bellow the well known static group efficiency. For these reasons, dynamically loaded piled foundations require a thoughtful approach, specially for the case of wind turbines working on a dike, since dike safety is of extreme importance in The Netherlands. The main conclusions from Kanya and Kausel (1982) and Dobry and Gazetas (1988) pile-soil-pile interaction studies are:

- Behavior of dynamically loaded pile groups is strongly frequency dependent.
- Spacing and number of piles have a considerable effect on dynamic stiffness.
- Lateral interaction effects are minor when compared with vertical and rocking solicitations.

Results seen in Figure 2.4 show very good agreement between the different methods. The proposed solution of Kanya and Kausel (1982) is usually referred as the rigorous solution but is taken as a not so practical approach from the day by day engineering point of view. As for the simple method developed by Dobry and Gazetas (1988), it is indeed a simple method but also has its limitations. First it is referred by the authors that the method tends to overestimate the peak values of both stiffness and damping coefficients

for pile groups embedded in very stiff soils, typically when the elastic modulus of the soil, E_s, is greater than $E_p/300$, where E_p is the Young's modulus of the pile. Also, according to the authors, pile groups with high number of piles (typically > 16) the method may slightly overpredict the peaks. With increasing number of piles, the method may become time consuming since the distance between all piles must calculated as well as all *interaction factors*. In order to face with previous challenges, Hölscher (2014a) came up with a generalized pile-soil-pile theory, where its solution is derived from the simple method proposed by Dobry and Gazetas (1988). Generalized pile-soil-pile theory uses the same simplifications as the simple method but approaches the problem using a matrix formulation for spacing and *dynamic interaction factors*, where it allows the calculation of dynamic stiffness for foundations with higher number of piles and many different configurations while keeping its simplicity and low computational effort. Detailed description of the solution is given in section 5.2.

Given the continuous progress on computer technology and the fast increase and availability of computational resources, numerical methods have been attractive tools for the soil-structure interaction problems. Specially the finite element method(FEM) due to its efficiency in dealing with complex geometries and soil heterogeneity. Schoenmaker (2014) approached the problem of a single pile dynamically loaded using to the commercial FEM software PLAXIS and comparing with other numerical and analytical solutions. Overall, results show good agreement with other solutions. However, for high frequencies computer efforts may increase to unfordable calculation times on daily engineering practice.

As mentioned, dike safety in The Netherlands is a matter of great concern. Any failure is unacceptable since the consequences would be catastrophic both in terms of human lives and economically. Therefore, before implementing any technology on this geotechnical constructions, understanding of the behavior and its consequences ought to be fully studied and described in order to fulfill all safety requirements. The right evaluation of the dynamic stiffness of an on-shore wind turbine is then very important, since this knowledge allows to properly describe the foundation response when dynamically loaded. Furthermore, the pile-soil-pile interaction phenomenon plays a role key when it comes to computing the dynamic stiffness of a wind turbine foundation composed by a group of piles. Achieving same solution from different approaches to the same problem allows to increase the degree of confidence in the methodology and verifying results. For this reason, the analytical solution named Generalized pile-soil-pile theory developed by Hölscher (2014a) and a numerical approach using the commercial finite element method software PLAXIS 3D will be developed in the present thesis. Both solutions have their inherent complexity but at the same time are relatively simple to implement , and, for this reason, the proposed methods may be used in a common engineering practice without neglecting important

aspects of this problem.

Chapter 3

Wind-Turbine Interaction Analysis

3.1 Introduction

This chapter presents a methodology on how to compute the dynamic loads that a wind turbine is subjected to. The loads transmitted to the foundation due to wind action are calculated using FAST code. A brief explanation of how the software works and the theories involved in the process is made. The wind turbine is briefly described and the natural frequency of the system is calculated. The end of this chapter studies the dynamic wind loads as well as the relevant frequencies of the wind turbine system.

3.2 FAST - Fatigue, Aerodynamics, Structures and Turbulence

FAST its a aero-hydro-servo-elastic code created by National Renewable Energy Laboratory (NREL) capable of computing the dynamic response of both two and three bladed, conventional horizontal-axis wind turbines. The code was evaluated by Germanischer Lloyd who provided its suitability for the calculation of wind loads for design and certification of wind turbines (Germanischer Lloyd, 2005).

The FAST code employs a combined modal and multibody dynamics formulation, where the wind turbine is modelled as a combination of rigid and flexible bodies. The multibody dynamic analysis is cast within the framework of nonlinear finite element methods, and the element library includes rigid and deformable bodies as well as joint elements (Bauchau, 2009). This tool was first developed for modeling mechanisms with only rigid bodies,

but rapidly evolved to the point where is capable of handling flexible systems. FAST considers, for example, the nacelle and hub as rigid bodies and the tower and blades as flexible. Figure 3.1 represents a general multibody system. As shown, the elements of the model are bodies, force elements, joints and a global reference frame. On the surface of the bodies there are parts, called nodes, at which the joints and force elements are attached. The force elements are used to model applied forces and torques. These elements may represent external forces, e.g due to gravity or interaction forces between the bodies, resulting from dampers, springs, actuators or contact. The joints represent any devices that constrain the relative motion of the nodes on the bodies. Joint deformations as a result of the interaction between the system bodies are not considered. Finally, the global reference frame is used to model a known global system motion in the inertial space.

The FAST code connects all these bodies with up to 24 degrees of freedom (DOF), which one can turn on or off individually depending on the intended analysis. Some of the considered degrees of freedom by the code are:

- Platform translation (surge, sway and heave) and rotation (roll, pitch and yaw).
- Tower motion.
- Nacelle yaw.
- Generator motion.
- Blade flexibility, and, tip and flap motion.

Although FAST considers many DOFs, not all of them may be relevant for the required analysis. It is up to the user to understand and define which degrees of freedom to take into account. Figure 3.2 illustrates more specifically some of the available degrees of freedom in the FAST code.

FAST defines a coordinate system depending where and what the input and output parameters are. In order to avoid extensive characterization of this subject, it was chosen to only present the coordinate system relevant for the outputs analyzed in the present thesis. Since the relevant outputs are the actions transmitted from the tower to the foundation, the tower-base coordinate system is chosen as the relevant one. This coordinate system is fixed in the support platform so that it translates and rotates with the platform. Figure 3.3 gives a visualization of the tower-base coordinate system. The origin is at the intersection of the tower axis with the support platform. The x_t-axis is the axis pointing at downwind direction (0°) while y_t points to the left when looking in the downwind direction. Finally z_t is the vertical axis, pointing upward.

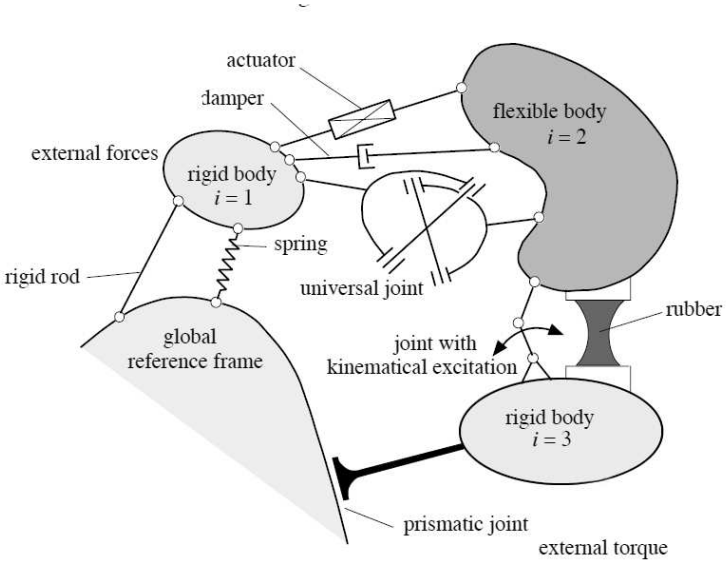

Figure 3.1: General multibody system and its elements, Schwertassek and Shabana (1999)

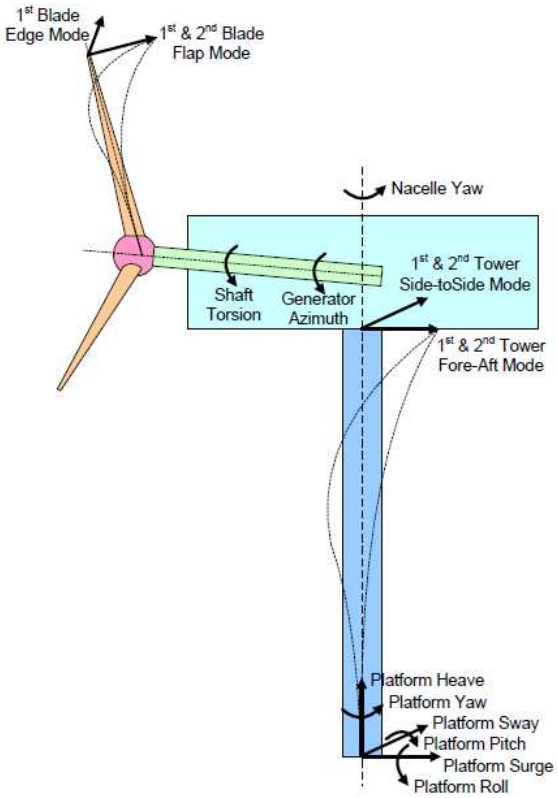

Figure 3.2: Degrees of Freedom considered in FAST

Figure 3.3: Tower base coordinate system considered by FAST (Jonkman and Jr, 2005)

FAST allows the user to model the support platform with a mass-spring-dashpot system, being able to represent an onshore foundation, a fixed bottom offshore foundation or a floating offshore configuration. Not considering any platform type will cause FAST to rigidly attach the tower to the ground through a fixed connection (Jonkman and Jr, 2005). If the user takes platform behavior into account, the software will run a file with mass and inertia parameters of the foundation as well as any considered platform loading. Considering platform loading a user-defined routine is used to compute these effects and returning loads on the platform. This routine contains contributions from any external load acting on the platform other than load transmitted from the wind turbine. For example, these loads should contain contributions from foundation stiffness and damping. Also, the routine assumes that the platform loads are transmitted through a medium like soil (Jonkman and Jr, 2005). Apart from the platform input parameters mentioned before it is necessary to specify damping and stiffness properties in all three translation and rotation components.

FAST works by interacting with different modules in order to fully achieve time-domain aero-hydro-servo-elastic simulations of wind turbines (see Figure 3.4). Wind flow is created by external programs such as TurbSim and IECWind. FAST with AeroDyn account for the applied aerodynamic and gravitational loads, the behavior of the control systems and the structural dynamics of the wind tower. HydroDyn is a module that computes the applied hydrodynamic loads (Jonkman, 2007). Modeling onshore wind turbines is possible by disabling the hydrodynamic module.

As shown, neither Fast nor AeroDyn are stand-alone programs, but designed to interface

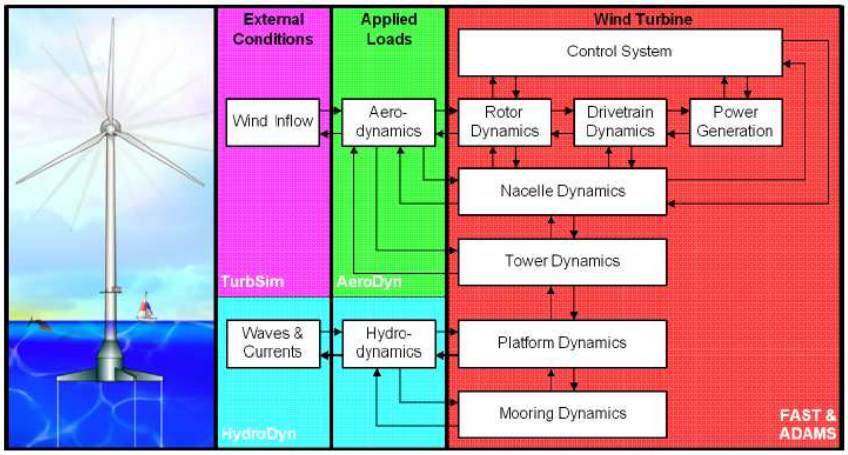

Figure 3.4: FAST code working scheme, Jonkman (2007)

with other software, both need several input data to generate outputs that are a valid input of the following simulator and so on until the requested output by the user is returned by the codes.

3.2.1 Generation of wind field

Wind field is input data for FAST. In order to simulate this wind profiles in x, y and z directions over time, NREL provides two preprocessors called TurbSim and IECwind that were developed to provide a numerical simulation of wind conditions.

TurbSim is a stochastic, full field, turbulent-wind simulator. It uses a statistical model to numerically simulate time series of wind speed vectors at points in a two-dimensional vertical rectangular grid (Jonkman and Kilcher, 2012). Figure 3.5 gives an example of a typical TurbSim grid as well the coordinate system used by the code. The capital letters point along the inertial reference frame while the others refer to the system aligned with the mean wind. As said before, TurbSim output can be used as input into AeroDyn which later makes the connection with FAST. The code simulates wind flows that contain bursts of turbulence. It generates aleatory components of varying wind speed, wind shear and direction around mean parameters provided by the user. TurbSim allows the creation of many broad spectrum wind scenarios. Also, the software has the possibility of changing the wind model suggested by the IEC 61400-1 [1] norm.

IECwind generates discrete hub-height wind-speed history cases, it allows the user to simulate constant mean flow, direction change (over a certain period of time) and other events recommended by IEC 61400-1. Just like TurbSim, IECwind creates a wind file that

[1] IEC 61400-1 is the international standard for minimum design requirements of onshore wind turbines.

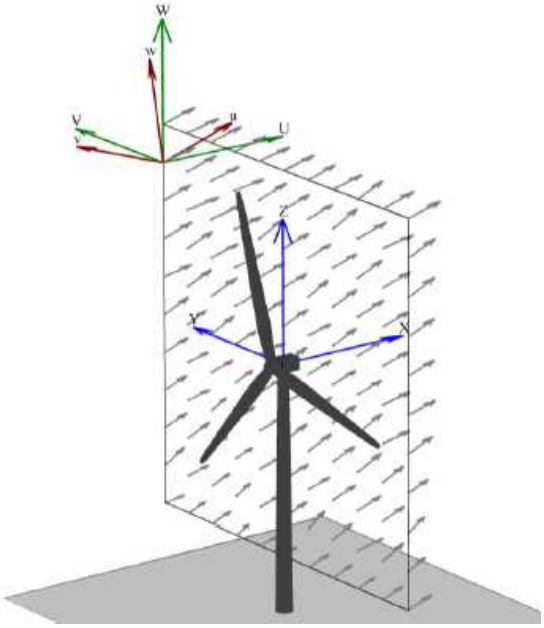

Figure 3.5: Example of a grid and the coordinate system used in TurbSim, Jonkman and Kilcher (2012)

is a valid input in AeroDyn.

3.2.2 AeroDyn

AeroDyn is responsible for transforming wind speeds into loads on the blades caused by wind. It does this by first breaking each blade into a number of segments and continuously gathering information about the turbine geometry, operating condition, blade-element velocity and location, and wind inflow from wind input files. Then, it uses this information to calculate the various forces on each segment, which are used to calculate the distributed forces along the turbine blades. The code obtains wind input data from simple hub-height(IECwind) wind files or full-field(TurbSim) wind files that contain turbulent velocity components at points on a grid that covers an area larger than the rotor disc and tower.

Several different aerodynamic models are used in AeroDyn. The user has the option of selecting which of these are most applicable to their simulation needs. The most relevant of these aerodynamic models are the wake models which are the blade element momentum theory (BEM) and the generalized dynamic wake theory(GDW).

The blade element momentum theory is one of the oldest and most commonly used methods for the calculation of forces on wind turbine blades. This theory actually is the coupling of two theories, blade element theory and momentum theory. Blade element the-

ory assumes that blades can be divided into small elements. Then, the elemental forces are summed along the span of the blade to calculate the total forces and moments acting on the turbine. The other part, the momentum theory, assumes that the loss of pressure or momentum in the rotor plane is caused by the work done by the airflow passing through the rotor plane on the blade elements. This affects the inflow in the rotor plane and therefore also affects the forces calculated by blade element theory. This coupling of both theories ties together blade element theory and sets up an iterative process to determine the aerodynamic forces and also the induced velocities near the rotor.

Although BEM it one of the most used theories so far, it has several limitations. One assumption is that the calculations are assumed as static, and therefore, it is assumed that the airflow is always in equilibrium. It's is known that this is not completely true and it takes some time for the airfoil to adjust to a changing wake resulting from new inflow or turbine operating conditions. In order to properly model this time lag effect it is recommend that the user primarily chooses the generalized dynamic wake (GDW) model (Moriarty and Hansen, 2005). Although this recommendation is made, AeroDyn switches to the BEM method when the mean wind speed is below 8 m/s, due to instability of GDW model at low wind speeds.

The generalized dynamic wake model was originally developed for the helicopter industry and later on adopted to wind turbine aerodynamic calculations. The method assumes that the induced velocities are small compared to the mean wind speed and regard the rotor as an infinite number of slender blades (Moriarty and Hansen, 2005). The consequence of this approach is that the model allows for a more general distribution of pressure across a rotor plane than the BEM theory.

The main advantages of general dynamic wake theory over BEM is that includes inherent modeling of the dynamic wake effect and other phenomena that blade element momentum theory either doesn't account for or it needs extra corrections in the model. As said before, the dynamic wake effect is the time lag in the induced velocities created by vorticity . Figure 3.6 illustrates an example of this time lag effect on the power production of a wind turbine. More precisely the example shows the measured power output of a wind turbine operating at a 10.6 m/s mean wind speed and where the blades are pitched from 0.2° to 3.9° and then back again to 0.2°. As seen, after the pitch change, the power production changes quickly and then gradually returns to a new equilibrium state. When comparing both methods with the measurement it's clear that BEM theory shows no time lag while GDW does. It should also be noted that despite general dynamic wake theory reproduces the time lag phenomena the time taken to reach the new equilibrium is faster than the real measured time lag.

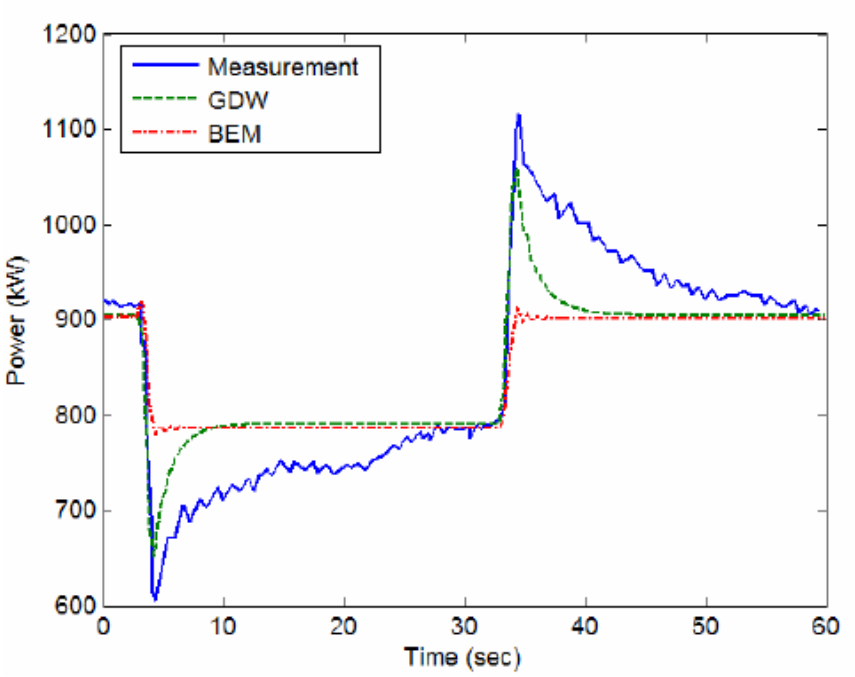

Figure 3.6: Generator power output during pitch change, Moriarty and Hansen (2005)

Like the blade element theory, the GDW method has some limitations. The generalized dynamic wake method was developed for lightly loaded rotors and assumes that the induced velocities are small relative to the mean flow. This assumption leads to instability of the method at low wind speeds and that is why AeroDyn switches to the blade element momentum theory for speeds smaller than 8 m/s.

3.3 Model Parametrization

We are now in conditions to fully define the model for the studied case. Wind action will be defined as well as the wind turbine main parameters. The relevant input parameters are also mentioned in this section.

3.3.1 Wind Turbine Model

Due to the complexity of the code, FAST creators advise to use the code mostly to analyze existing turbines. This does not mean that FAST is not adequate for the design of new wind turbines, but for this purpose it becomes too complex and it takes long time to fully master the software. Nevertheless, it should be noted that the code fits both analysis and design approaches. For the matter of the present thesis, the usage of a pre-built wind

turbine model is considered to be enough in order to meet the intended objectives.

As mentioned before, FAST has several horizontal axis wind turbine models inbuilt. This models were created and made available so all users can have a wind turbine with the same features that are characteristic of a certain wind turbine class and still compare results between them. For this study the turbine chosen is called NREL 5-MW Baseline Wind Turbine. It is a 5 megawatt wind turbine with variable speed and pitch controlled. The following table resumes the main characteristics of the chosen wind Turbine:

Table 3.1: Gross properties of NREL 5-MW Baseline wind turbine, Jonkman et al. (2009)

Rating	5 MW
Control	Variable speed Blade-Pitch-to-Feather
Blades	3
Rotor orientation	Upwind
Hub height [m]	90
Rotor diameter [m]	126
Blade length [m]	61,5
Cut-in speed [m/s]	3
Rated speed [m/s]	11,4
Cut-out speed [m/s]	25
Rotational speed range [rpm]	6.9 to 12.1
Tower mass [kg]	347500
Blade mass (each) [kg]	17740
Hub mass (minus the blades) [kg]	56780
Nacelle mass (minus hub and blades) [kg]	240000
Base diameter [m]	6
Base thickness [m]	0,027
Top diameter [m]	3,87
Top thickness [m]	0,019

NREL 5-MW Baseline wind turbine was "built" gathering available information from manufacturers and from the conceptual models used in the WindPACT [2], RECOFF [3] and DOWEC [4]. It is a conventional upwind horizontal axis wind turbine with three blades and two main control systems, generator-torque controller and rotor collective blade pitch controller. The two control systems are designed to work independently. For the first control the goal is to maximize power capture bellow rated wind speed. When the turbine is working above rated wind speed blade-pitch-to-feather controller is called to regulate the generator speed and also to protect the blades structurally when the wind speed is greater than cut-out wind speed.

[2]The land-based Wind Partnerships for Advanced Component Technology.
[3]Recommendations for Design of Offshore Wind Turbines.
[4]Dutch Offshore Wind Energy Converter.

The tower has a circular hollow steel section with variable diameter and thickness from the base to the top. The base diameter is 6 m and 3.8 m at the top. The thickness is 0.027 m at the base decreasing to 0.019 m at the top. It is also worth mentioning some mechanical properties of the tower material. The elastic modulus was taken to be 210 GPA and the shear modulus 80.8 GPA. Steel density was increased from the typical value in order to account for paint, bolts and welds that were not accounted for in the tower thickness. Hence, the density was chosen to be 8500 kg/m^3.

(van der Tempel and Molenaar, 2002) suggest that the structural dynamics of a flexible wind turbine system can be modeled as a beam with a top mass as shown in Figure 3.7. This model was used in order to effectuate a Rayleigh-Ritz modal analysis to calculate the natural frequency of the system. This analysis was made using the engineering tool PTC Mathcad Prime 3.0 and it is presented in appendix A. In order to avoid resonance, the structure should be designed such that its first natural frequency does not coincide with either 1P or 3P intervals. These intervals are rotational frequencies of the rotor, where 1P is given by the rotational speed range shown in table 3.1 and 3P interval is the turbine's number of blades times 1P frequencies. Results from Rayleigh-Ritz analysis confirm that the natural frequency lies outside these intervals. As seen in Figure 3.8, the tower has a natural frequency of 0.302 Hz.

3.3.2 Wind Model

As mentioned in section 3.2.1, a wind profile must first be defined. There are two options, either TurbSim for full-field turbulent wind flows or IECWind for discrete wind profiles. IEC 61400-1 norm requires running a series of design load cases (DLCs) to determine the ultimate and fatigue loads expected over the lifetime of the machine. These design load cases include several wind scenarios and design situations such as normal power production, occurrence of fault while producing power, emergency shut down, among others. Although this is an important matter to take into account when pursuing certification, this is not the intended case and running all the DLCs would take much more than the available time for this thesis. Also, the goal is to simulate loads on the wind turbine foundation and not other effects on the wind turbine itself. For this reason only one wind scenario and operating condition will be dealt in this thesis.

As known, wind action is not constant over time. There are gusts, the wind speed and direction are changing constantly and there is turbulence. Hence, it is wise to choose a model and program capable of simulating all these effects. TurbSim seems appropriate to model these conditions and also it has inbuilt several wind models suggested by IEC 61400-1. Regarding the turbulence type, the normal turbulence model(NTM) was chosen .NTM

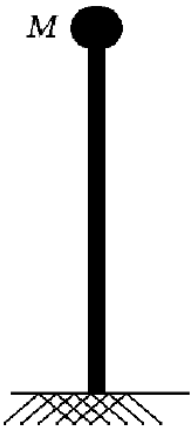

Figure 3.7: Structural model of a flexible wind turbine system, van der Tempel and Molenaar (2002)

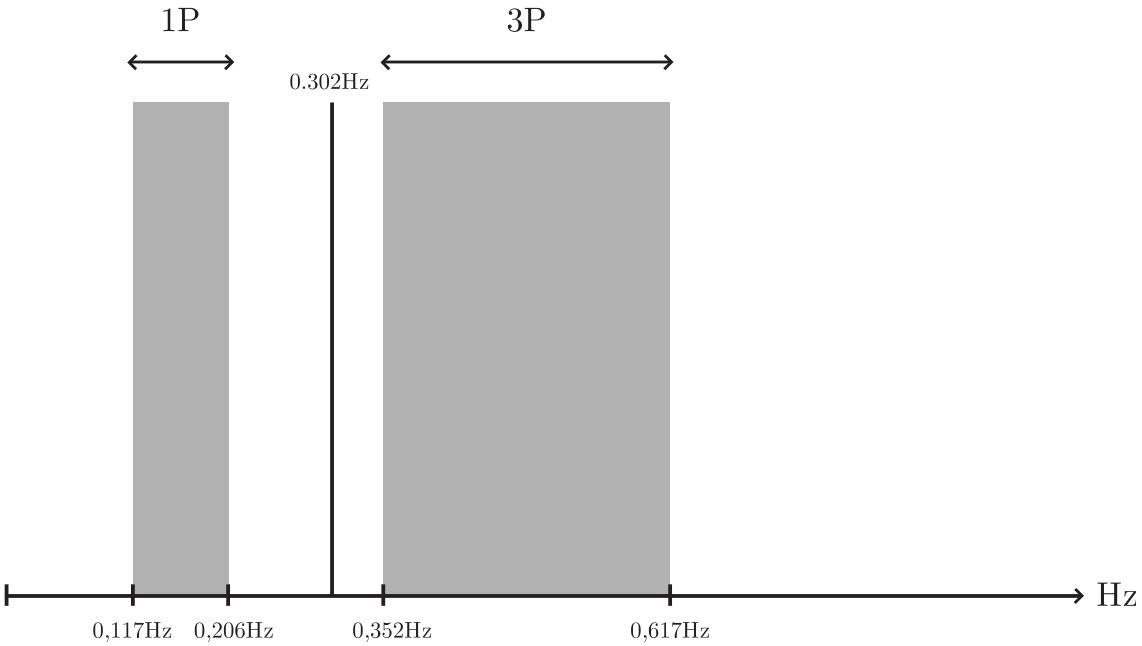

Figure 3.8: 1P and 3P intervals and natural frequency plot for NREL 5-MW Baseline wind turbine

is defined by a mean value and standard deviation. The norm suggests this turbulence model for several DLCs and (Jonkman, 2007) recommends this model for casual wind turbine evaluation.

In this thesis, wind data was provided from measurements performed in a weather station close to Lauwersoog, The Netherlands. The provided data can be seen in Figure 3.9 and it represents the hourly wind speed measured over 15552 days. Although this was the only available data , it is important to refer that in terms of wind input data, TurbSim does not need other wind inputs in order to create a reasonable wind spectra.

As Figure 3.9 shows, the most common wind speed observed was around 10 m/s while the maximum verified speed over the period of measurement was 33.4 m/s. TurbSim requests a wind speed to serve as mean, and after creates a wind profile that oscillates around this given velocity. This parameter is `URef` . Although the mean speed given by the data is about 10 m/s, dike security is an important matter, and hence, with greater wind speeds, higher loads are expected on the dike. For this reason, `URef` is set to have the maximum wind speed observed in the whole time of data gathering, i.e, `URef` is 33.4 m/s.

Apart from the mean wind speed considered, TurbSim has several other input parameters. Jonkman (2007) refers that "'*To generate IEC-type turbulence, many of the parameters in the TurbSim input file can be ignored*"'. Given this, Jonkman (2007) gives some guidelines for the parameters that typically do not need to change and those that change every simulation or are dependent on the wind turbine being analyzed. The following parameters should be changed based on the particular wind turbine for which the wind field is being generated:

- `NumGrid_Z`: This parameter controls the number of vertical grid points. It should be large enough to ensure that there is sufficient vertical grid resolution.

- `NumGrid_Y`: This parameter controls the number of lateral grid points. Once again, it should be large enough to ensure that there is sufficient lateral grid resolution.

- `HubHt`: This is the hub height (in meters) of the wind turbine.

- `GridHeight`: Here the grid height is defined. Typically the grid height should be at least 10% larger than the rotor diameter (in meters).

- `GridWidth`: The same as the grid height but for width.

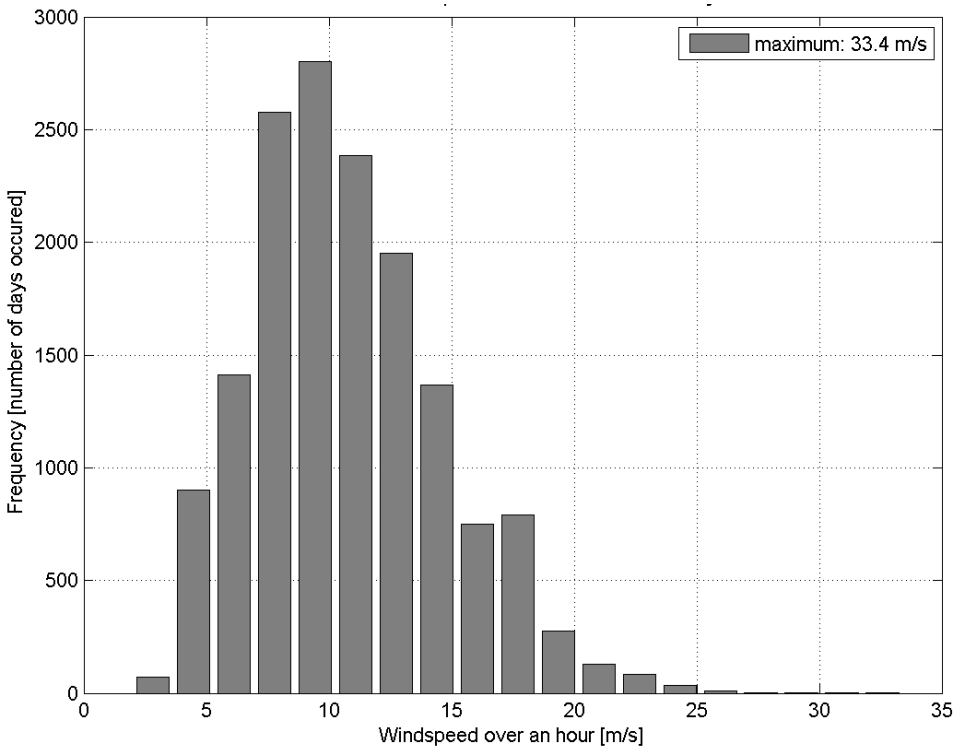

Figure 3.9: Maximum windspeed measured in Lauwersoog weather station over 15552 days

- `IECtrubc`: Defines the turbulence category according to 61400-1 norm.

- `RefHt`: This parameter defines the reference height which is the height (in meters) where the input wind speed is defined. Typically it is the same as `HubHt`.

Next, the parameters that should be changed for each simulation case:

- `RandSeed1`: This the random seed parameter. Here a number is given which initializes the pseudo-random number generator. The random seed should be changed every simulation in order to create different random wind distributions. When running the same random seed number, the same random phases will be reproduced.

- `IEC_WindType`: Here the wind condition for the turbulent IEC 61400-1 load cases is selected. As mentioned before the chosen wind condition was NTM.

- `Uref`: This is the reference wind speed (in meters per second) the `RefHt`. Again, as mentioned before in this section this parameter will have a value of 33.4 m/s.

Since FAST has already the wind turbine model inbuilt some of the parameters are already written on the files provided in the package. Anyhow, the input file was properly filled with the correct values and following Jonkman (2007) guidance it was decided to assume default values for the parameters that would not interfere considerably in the wind simulation. Appendix B.2 contains TurbSim input file (file extension `.inp`) with the values used for this specific simulation.

3.3.3 AeroDyn Model

In order to run AeroDyn, at least two other input files are necessary apart from AeroDyn input file it self. One is a wind file (`.wnd`), which is the output resulting from TurbSim and the other(s) is an airfoil data file (`.dat`) that is used to properly represent the aerodynamic properties of the problem. The airfoil data is different for every wind turbine and it should be constructed by the user. In this case, the airfoil data is already available and therefore the calculation of drag, lift and pitching moment coefficients (for each angle of attack) was not required.

AeroDyn input file (`.ipt`) has also some input parameters that do not need to be changed. For this specific case, only the following parameters were altered, leaving the others with their default value:

- `InfModel`: This input controls the dynamic inflow option. The user has two options, either `DYNIN` or `EQUIL`, which represent generalized dynamic wake model and BEM theory respectively. Given the high wind speeds and the reasons pointed in section 3.2.2, `DYNIN` is the chosen option for this calculation.

- `WindFile`: Here, the name of the file containing wind data is requested. The input should be something like `windfilename.wnd`.

- `HH`: Just like `RefHt` this parameter requests the wind turbine hub height.

The full AeroDyn input file can be consulted in appendix B.3.

3.3.4 FAST Model

For the present study, all calculations using FAST were made using version 7.02.00 which was the latest available version at the time of modeling. FAST program and input file

(`.fst`) are what makes everything work together. This input file is responsible for the full definition of the model, operating conditions and requested outputs. Since FAST input file has over 180 input lines not all parameters will be listed in this text. Only the relevant ones and those that need proper explanation. Nevertheless, appendix B.1 shows FAST input file.

IEC 61400-1 design standard requires for turbulent wind simulations an analysis time of 10 minutes. Also, it is good practice to include another 30 seconds in the simulation in order to mitigate model start-up interference. Hence, `TMax` was set to be 630 seconds. This is the total run time of the simulation. Note that when generating wind scenario, the user has to create a time-series at least as big as `TMax` on TurbSim or other wind generator software. If not, FAST will keep running using the last wind input line. It is also worth mentioning that the time step is separately defined in all three files but it is recommended to be the same in all different codes. So, the integration time step (`DT`) was defined to be 0.0125 seconds.

Operating condition may change depending on the simulation or design load case in question. For this, FAST input file includes a turbine control section in order to properly simulate special events. Hereafter, the main control inputs are explained:

- `PCmode` and `VSContrl`: Both of this parameters are used to turn on or off pitch-control-mode(`PCmode`) and generator torque for variable speed machines(`VSContrl`).

- `BlPitch` and `B1PitchF`: `BlPitch` controls the initial pitch angle in degrees while `B1PitchF` specifies the final pitch angle for pitch maneuvers. These angles must be defined for each blade separately.

- `TPitManS` and `TPitManE`: These parameters stand for the start (`TPitManS`) and final (`TPitManE`) time in seconds for which the pitch override maneuver occurs. Again, these parameters have to be defined for each blade.

- `TYawManS` and `TYawManE`: This entry parameters refer to the same times as the previous point but for the yaw over ride maneuver.

- `NacYawF`: Here the final yaw angle is defined.

As mentioned in section 3.3.2 wind speed oscillates around 33.4 m/s. This wind speed is clearly above cut-out speed, thus the turbine is not rotating for security purposes. To

make sure that the generator is not working i.e not producing power, the generator degree of freedom must be disabled causing the rotor inability to rotate. This means changing `GenDOF` to false and `RotSpeed` assumes a value of 0 rpm. Then, all blades must be set to a feathering setting. For this, `BlPitch` and `B1PitchF` assume a angle of attack of 90 degrees for all the blades. Also, `TPitManS` and `TPitManE` must be greater than the simulation time. This allows the blades to be in a feathering position the entire simulation and therefore minimizing structural effects due to wind loading. Another thing worth mentioning is that no yaw misalignment is assumed. Hence, nacelle yaw angle (`NacYaw`) is set to 0 degrees and the yaw DOF(`YawDOF`) is set to false.

In terms of outputs, forces and bending moments at the base of the tower over time were requested in x, y and z directions. Also, to confirm that no power was produced and therefore the control parameters were set correctly, the rotor speed over time was plotted. Table 3.2 shows the necessary commands to write on `OutList` to return the desired outputs. Note that the results are printed every 0.05 seconds.

Table 3.2: Requested outputs from FAST

Output Name	Description	Units
`WindVxi`	Wind speed directed along x_t axis	m/s
`WindVzi`	Wind speed directed along y_t axis	m/s
`WindVzi`	Wind speed directed along z_t axis	m/s
`TwrBsFxt`	Tower base shear force directed along x_t axis	kN
`TwrBsFyt`	Tower base shear force directed along y_t axis	kN
`TwrBsFzt`	Tower base axial force (directed along z_t axis)	kN
`TwrBsMxt`	Tower base roll moment (about x_t axis)	kNm
`TwrBsMyt`	Tower base pitching moment (about y_t axis)	kNm
`TwrBsMzt`	Tower base yaw or torsional moment (about z_t axis)	kNm
`LSSTipVxa`	Rotor angular speed	rpm

3.4 Numerical Simulation

For time-marching analysis the output file contains columns of time-series data with one column for each parameter requested in the input file. These files have a `.out` extension but are possible to open using a regular `.txt` reader. For post processing the software Matlab was used. A matrix with all the values was created with each column referring to a certain output parameter. This made plotting and result treatment easier and considerably faster.

3.4.1 Wind Speeds

Figure 3.10 presents the wind speeds generated at hub-height by TurbSim in all three axis directions plotted over the simulated time. As seen, wind speed in x_t direction is greater than wind speed components in y_t and z_t directions. This is easily understandable if we think that despite wind direction changes, the wind primarily blows in one direction. Also, FAST and TurbSim assume x_t axis as default downwind direction.

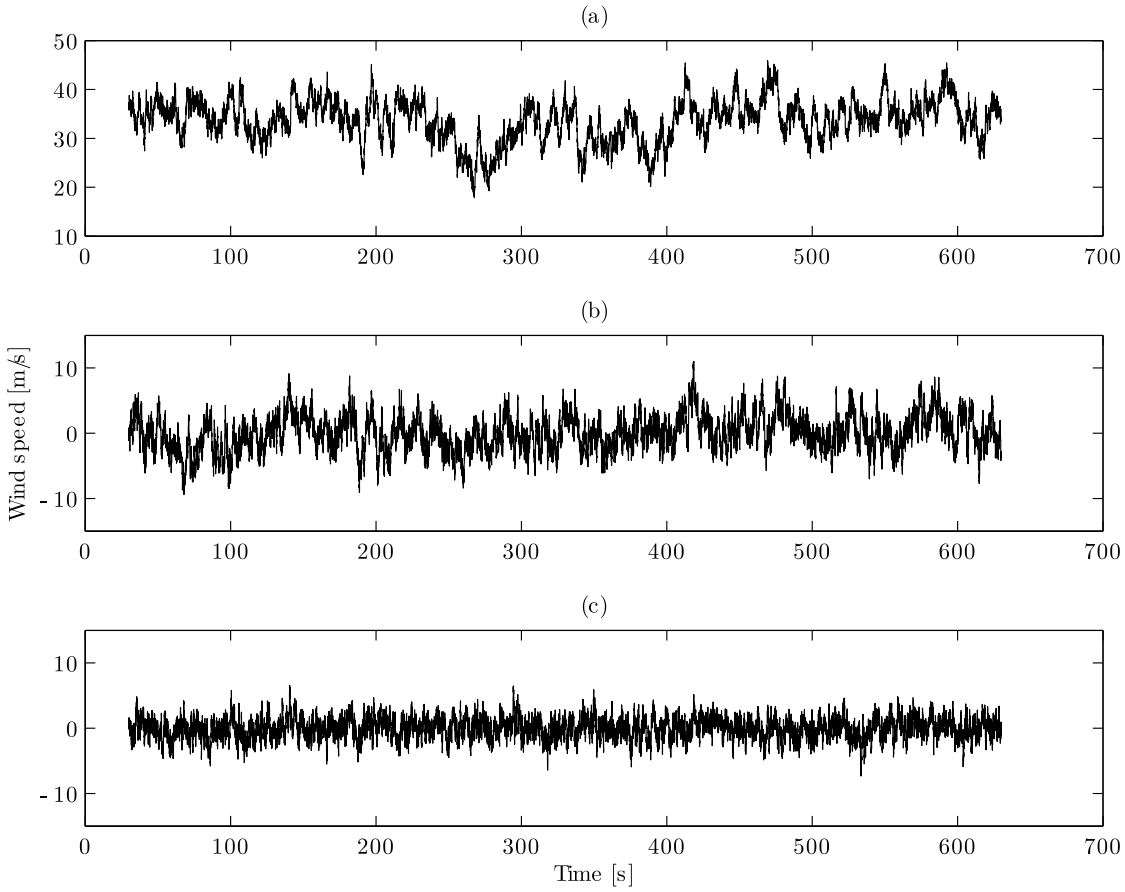

Figure 3.10: Wind speed in x_t(a), y_t(b) and z_t(c) directions

3.4.2 Loads on wind turbine base

The plots for shear and normal forces are shown in Figure 3.11. As expected, shear force along x_t(a) direction is the relevant one when it comes to ultimate loads. The y_t(b) shear force starts relatively high and in the end of the simulation oscillates close to zero 0 kN. The normal force plotted in Figure 3.11-c is not constant, exhibiting small variations. This might have to do with some wind disturbances in the vertical direction and the dynamic

nature of the problem.

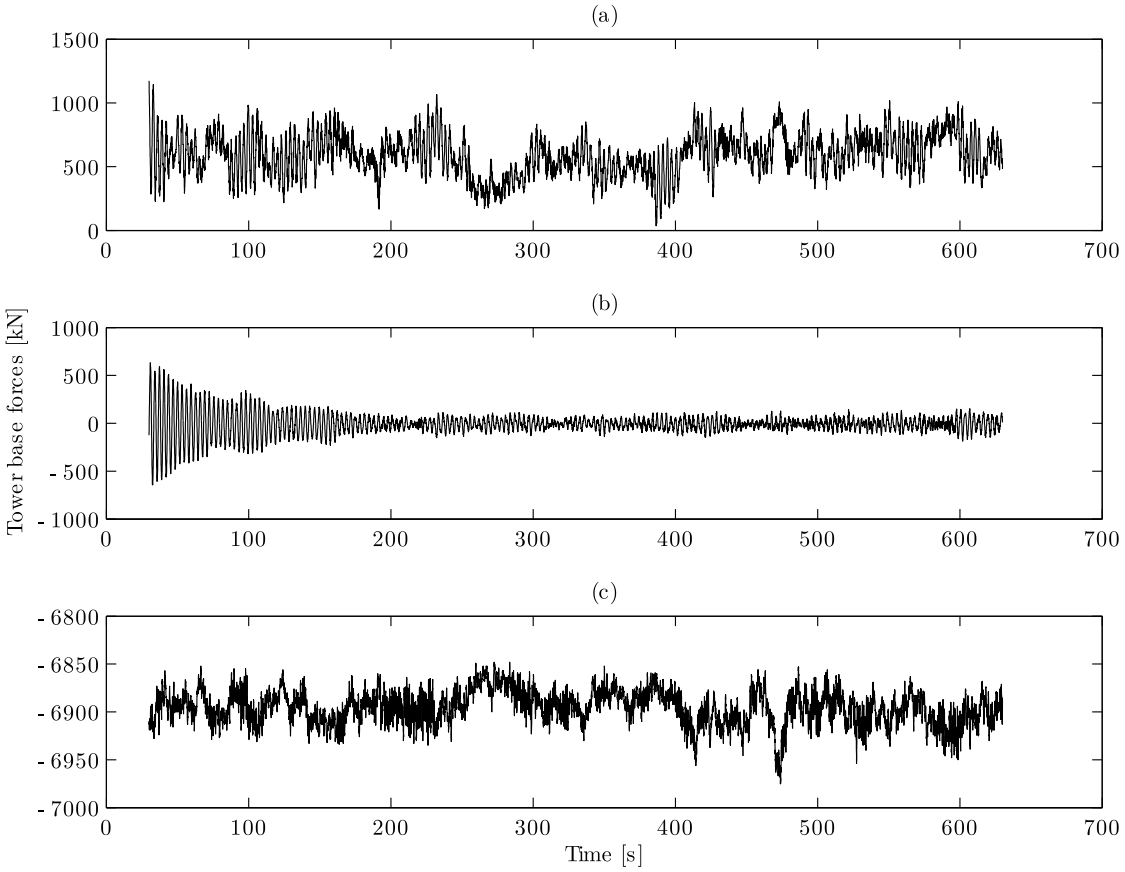

Figure 3.11: Tower base shear forces directed along x_t(a), y_t(b) and z_t(c) direction

The results for the bending moments can be seen in Figure 3.12. Since the bending moments are function of shear force, the behavior is similar to the one seen in Figures 3.11-a and 3.11-b but now the mean bending moment around x axis is clearly greater than zero. Still, the mean bending moment around y axis is much higher than the one registered around x axis. Figure 3.12-c presents the plot for the torsional moment. Giving the low speeds in the transverse direction and the fact that the nacelle is aligned with the wind direction, the torsional moment is small as expected.

Figure 3.13 confirms that no power is being produced during the entire simulation. The figure shows some "'noise"' in the plot but when looking to the magnitude of the rotations, one can see that the rotations are very small and oscillate around the mean value of 0 rpm.

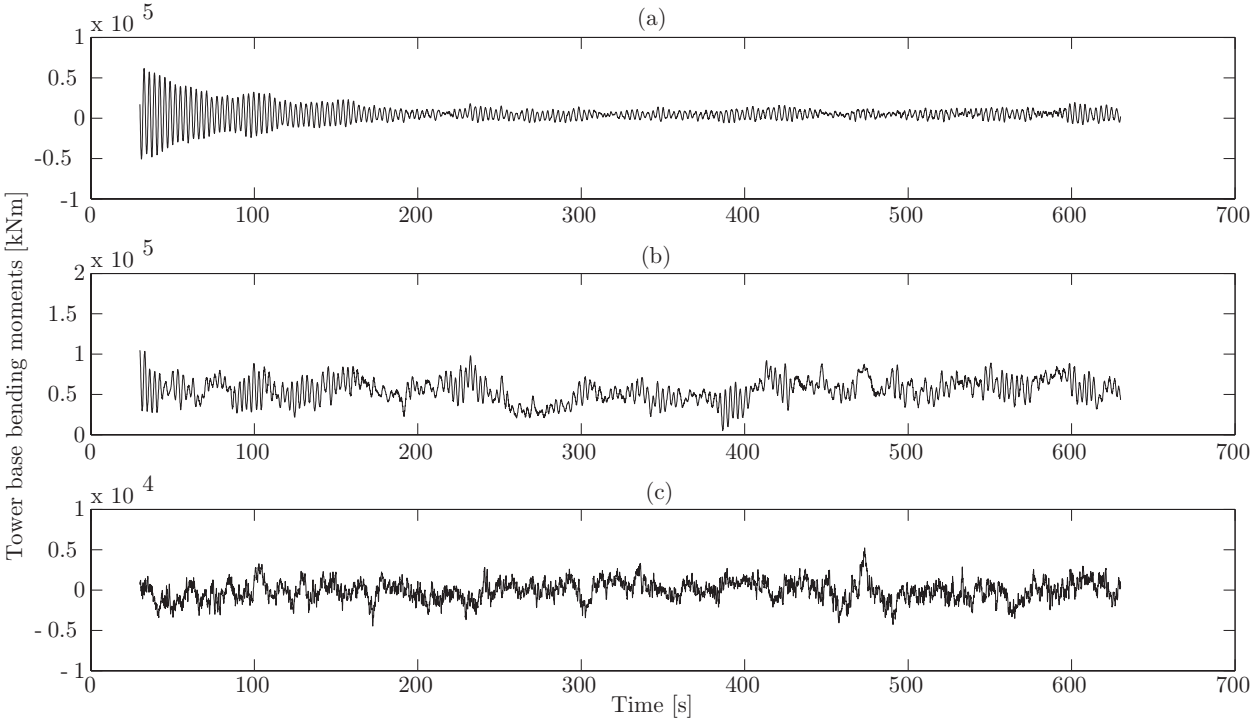

Figure 3.12: Tower base moment around x_t(a), y_t(b) and z_t(c) axis

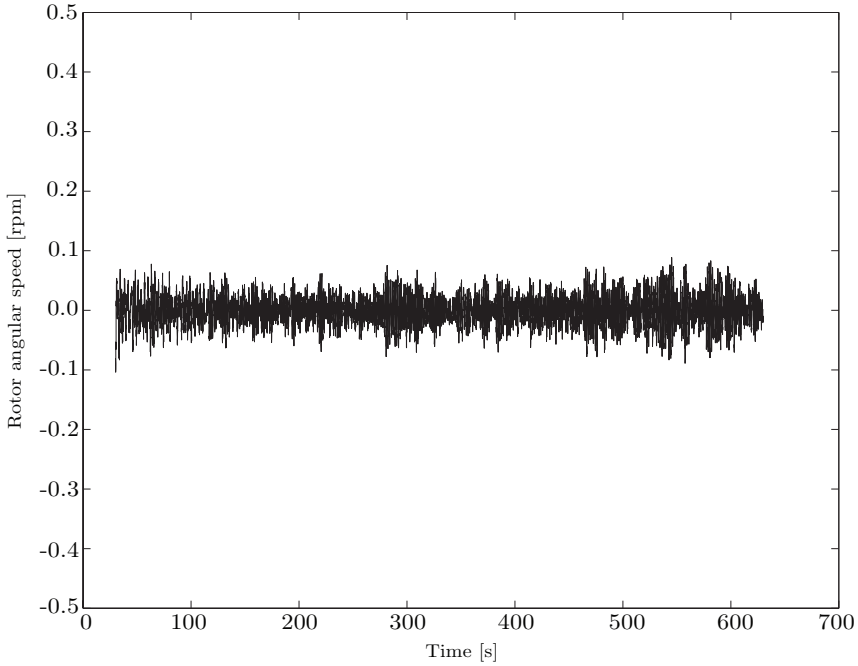

Figure 3.13: Rotor angular speed over the simulated time

3.5 Discussion

When comparing wind speeds in Figure 3.10, wind speed in x_t(a) direction shows greater wind speeds than the ones exhibited in y_t(b) and z_t(c) directions. While cross-wind and vertical components of wind speed have mean values (at hub-height) close to zero, the wind speed for the nominally downwind component has a mean value of 33.65 m/s. Note that this value is extremely close to the input value `Uref`. It is also important to refer that despite y_t and z_t directions have almost null mean values (over the simulated period) these present variations during the simulation. Cross-wind speed component varies from -9.41 m/s to 10.99 m/s while vertical wind speed exhibits a variation from -7.35 m/s to 6.57 m/s. Given these relatively important variations , actions in these directions can not be neglected *a priori* because it may influence turbine behavior over the time of simulation. As mentioned in section 3.3.2, TurbSim generates for the nominally downwind component a profile that oscillates around a mean given wind speed. In this case, the wind speed profile for x_t direction presents a variation of 28 m/s with a minimum value of 17.87 m/s and a maximum of 45.87 m/s.

Figure 3.11-a confirms that wind in x direction leads to the higher shear forces that the wind turbine is subjected to. Since a wind turbine problem can be seen as a cantilever beam with a concentrated mass at the hub height and the wind action as a horizontal force, the bending moments are expected to be the conditional loads. That is why the plots for the bending moments show such greatness in their values, specially the tower base pitching moment around y_t axis seen in Figure 3.12-b, i.e, the bending moment caused by the x_t axis shear forces. This rocking motion assumes high importance not just for the wind turbine tower but as well as for the foundation which transmit these forces vertically to the soil underneath.

The plots for y_t shear forces seen in Figure 3.11-b and bending moment around x_t axis in Figure 3.12-a show different behavior. Here the loads progressively decrease until a stationary state is reached. This is related to start up effects where the wind turbine suffers an initial impact (caused by the first wind input) followed by weak solicitation by the wind in y_t direction. Due to low damping the structure takes a while to dissipate the effects of this initial impact.

In section 3.4.2 it was mentioned that the normal force was not constant during the entire simulation. When analyzing Figure 3.11-c and although there are variations, these are actually quite small. The difference between the maximum and minimum registered values is smaller than 2% and therefore the results suggest that the additional normal loading caused by the vertical wind component may be neglected. Also, Figure 3.12-c which is related to the torsional moment does not exhibit a significant magnitude when

compared to the pitching moment plotted in Figure 3.11-b. This result is because no yaw misalignment was considered for this simulation. Nevertheless, it is important to refer that some design load cases in 61400-1 standard request yaw misalignment to be considered and this might increase considerably the moment around z_t axis.

As mentioned, results from FAST are plotted in the time domain. However, analyzing results in the frequency domain might give some further conclusions. Fourier transforms allows to take discrete time domain solutions and change them into the frequency domain through the combination of a series of periodic functions sine and cosine which allow one to analyze the importance of each frequency component in the original signal. Figure 3.14 presents the plots for the response amplitude over frequency on all directions after applying fast Fourier transform to the given results by FAST. The results for Figure 3.14-a and 3.14-b refer to plots in x_t and y_t directions, where it can be seen that the returned frequency for the highest response is about 0.3017 Hz. These plots exhibit similar behavior, which was expected since no major changes between directions x_t and y_t can be seen. Also, the natural frequency given by the response spectrum has values very close to the natural frequency of the wind turbine calculated from the Rayleigh-Ritz method in section 3.3.1. On the other hand, the plot for z_t direction seen in Figure 3.14-c shows different sensibility in the frequency domain. Here the frequency that returns the strongest response is situated about 1.088 Hz.

Figure 3.15 shows the Fourier spectrum for the wind action in all three directions. As it can be seen, the wind action presents a disperse spectrum with higher amplitude for frequencies below 0.5 Hz being, as expected, x_t direction the one that produces results with higher magnitude. Also, Figure 3.15 helps explaining the response for the first frequencies seen in Figure 3.14-a and 3.14-c, being these due to the wind excitation.

3.6 Conclusions

In this chapter the wind-turbine problem was successfully handled. Introductory concepts about FAST and all the codes related to the software were given as well as the theories behind. This is a multidisciplinary subject and requires a vast knowledge of different areas to fully understand and define all phenomena that take place on a turbine loaded by wind. After plotting the loads caused by the high wind problem in all three x, y and z directions, the following conclusions were drawn:

- The normal force at the tower base is not greatly influenced by the vertical wind component. This is because the wind vertical action is of small value. Therefore the

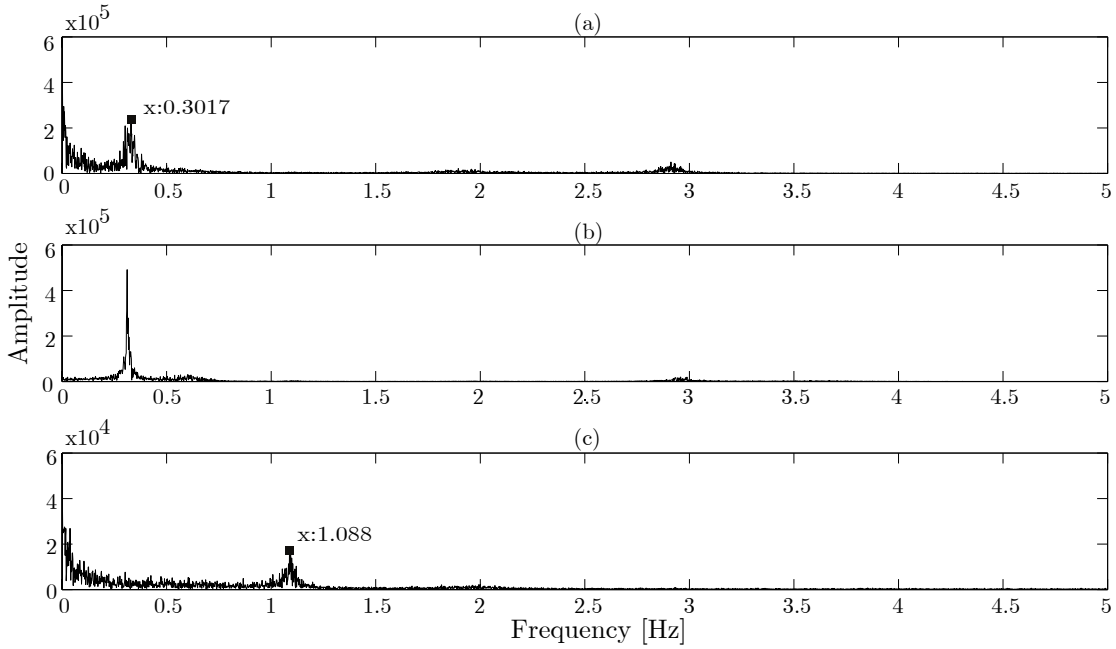

Figure 3.14: Amplitude spectrum of the wind turbine's response calculated using fast Fourier transforms in x_t(a), y_t(b) and z_t(c) directions

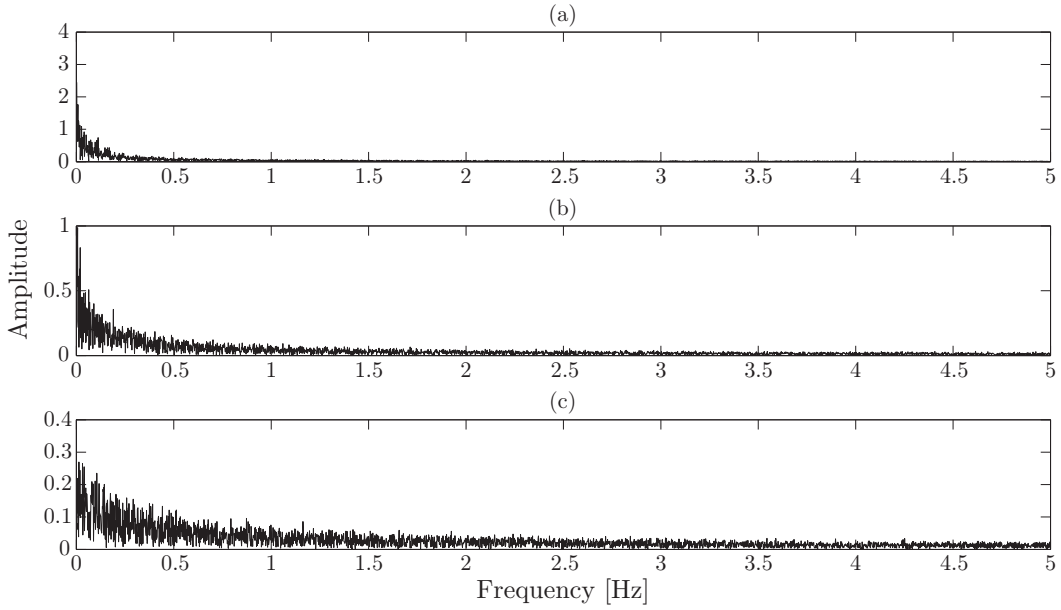

Figure 3.15: Amplitude spectrum of the wind action calculated using fast Fourier transforms in x_t(a), y_t(b) and z_t(c) directions

normal force can be assumed constant and equal to the turbine weight.

- The shear force in y_t direction and the bending moment around x_t axis exhibit decaying behavior over the entire simulation. The initial transient behavior is a consequence of the simulation initialization where the first wind input causes an impact on the wind turbine. For this reason, this effect must be neglected and therefore, it is clear that the loads in this directions are very small when compared with the loads caused by the primary wind direction.

- When no yaw misalignment is considered, the torsional moment does not play a relevant role. This is expected when the wind turbine is properly working (even if the rotor is not producing power). Nevertheless, it is important to refer that fault conditions might create conditions for yaw misalignment and therefore increasing torsional solicitation of the wind turbine.

- Plots for the horizontal x_t force and pitching moment confirm that the highest solicitation is due to wind action directed along x_t axis.

- Finally, response frequency analysis show that the frequencies that return higher response are close to 1 Hz and below.

The loads caused by wind action will be used in Chapter 4 in order to proceed with the intended analysis.

Chapter 4

Geotechnical and Foundation Model

4.1 Introduction

After building a wind interaction model that allowed the computation of the dynamic wind loads acting at the foundation of the wind turbine, it is necessary to define and evaluate all the parameters of the geotechnical model. Figure 4.1 represents schematically the model in question. As said, the wind turbine foundation is implemented on the top of a dike which it's materials and also the foundation are yet not defined. All these variables are defined using a case-study site which is developed in this Chapter.

First the evaluation of the soil is made using CPT data from three soil tests carried out on the dike. Afterwards, load definition is made using results from Chapter 3 and finally a foundation preliminary design is performed. After this chapter all conditions will be met towards a pile-soil-pile interaction analysis.

4.2 Soil Characterization

4.2.1 Field Data

As said in Chapter 3, the field location is in Lauwersoog, The Netherlands. Both wind and geotechnical data were provided in order to properly define real world problem variables. For this case, the provided data was from three cone penetration tests(CPT) that were made on a dike just outside the local port. The red circles in Figure 4.2 show the exact

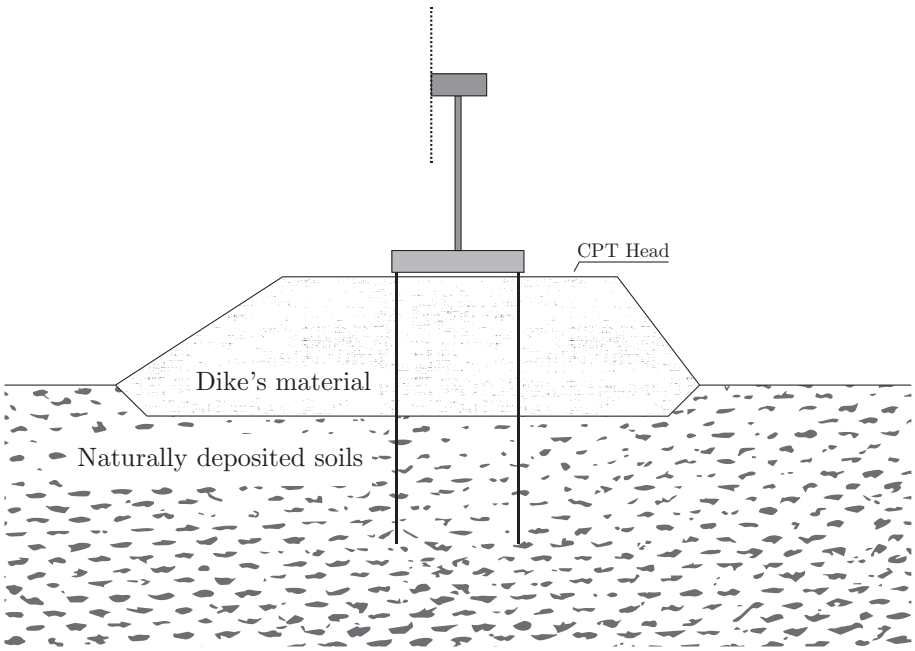

Figure 4.1: Schematic profile of the geotechnical model being defined

location where the *in-situ* tests were made and their corresponding names. The coordinates for each CPT can be seen in table 4.1. As for the data, this is of public domain and made available by DINOloket . DINOloket is a public access website that gathers information of geotechnical testing performed in The Netherlands territory. For the present thesis, all the chosen soil parameters are derived from the CPT data available on DINOloket, more specifically by 3 tests: S02G00190, S02G00208 and S02G00206.

Table 4.1: Cone penetration tests coordinates

CPT name	Coordinates
S02G00190	5324'28.52"N 6 9'18.08"E
S02G00208	5324'32.37"N 6 9'31.13"E
S02G00206	5324'35.59"N 6 9'42.05"E

From CPT data the gross given parameters are:

- The beginning elevation or the head (m)
- Depth (m)
- Cone resistance, q_c (MPa)
- Sleeve friction, f_s (MPa)

Figure 4.2: Local of CPT testing, taken from Google Earth version 7.1.2.2041

- Friction Ratio, R_f (%)

From these measurements and through several correlations, a CPT test offers soil profiling, material identification and evaluation of geotechnical parameters. CPT is a soil test with extensive applications in a wide range of soils. Although the CPT is limited primarily to softer soils, with modern large pushing equipment and more robust cones, the CPT can be performed in a stiff to very stiff soils (Robertson and Cabal, 2012). It should be noted that an ideal soil characterization should have different types of *in-situ* soil testing and also samples to perform laboratory tests.

Figure 4.3 presents the measured gross parameters over depth returned by CPT S02G00190. In section 4.2.2 CPT interpretation is made in order to define the required soil parameters for the intended analysis. For the present thesis, these are shear strength, state and elastic parameters. However, different types of analysis and constitutive models may change the required parameters that are necessary to estimate.

4.2.2 Data interpretation

Numerous semi-empirical correlations have been developed to estimate geotechnical parameters from CPT for a wide range of soils. (Robertson, 2012) classifies CPT testing to be perceived with moderate to high applicability for use in different ground conditions. Also if pore pressure and seismic readings are added to the CPT, reliability to estimate certain parameters grows favorably.

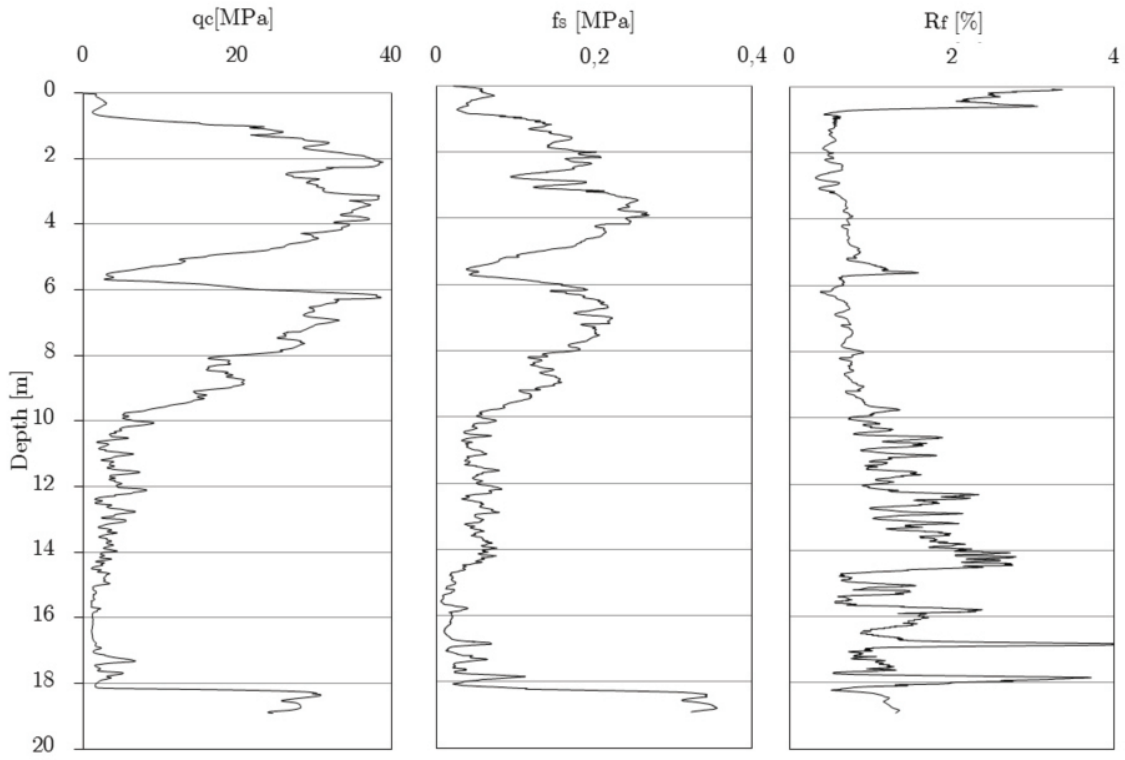

Figure 4.3: Measured field data from CPT S02G00190

One of the major applications (and advantages) of the CPT test is for soil profiling and defining soil type. Typically, at first sight one can identify different soil mechanical behavior by analyzing the cone resistance and the friction ratio. When q_c has a high value and R_f returns a low one, it means that a sandy-type behavior is expected. The contrary is verified when dealing with soft soils. Figure 4.3 illustrates exactly this. In the beginning higher cone resistance values and small friction ratio are observed, which give a sandy soil expectation. With increasing depth and specially after -2 m elevation a change in these parameters can be seen. R_f increases while q_c starts decreasing. This is clearly a layer transition and a cohesive soil is expected. The same line of thought can be made for the other CPTs.

The best way to calculate the total unit weight of a soil is by obtaining an undisturbed sample and weighting a known soil volume. When such procedure is not possible, relationship 4.1 (Robertson, 2010) can be used to estimate the total unit weight from CPT results:

$$\frac{\gamma}{\gamma_w} = 0.27\,[\log R_f] + \left[\log \frac{q_t}{p_a}\right] + 1.236 \tag{4.1}$$

Here,q_t is the corrected cone resistance. This correction is usually suggested when pore pressure measurement is made. This is because the cone resistance is influenced by interstitial pressure acting on uneven areas of the cone (Guedes de Melo, 2012). Since no pore pressure was measured, no cone resistance correction is made and hence, it is considered $q_t \approx q_c$. The value used for the atmospheric pressure(p_a) was 0.101 MPa. Estimating the total unit weight is important in order to calculate the stresses and help in the soil identification process.

In order to facilitate soil identification processes, Robertson et al. (1986) suggested a soil behavior type(SBT) chart. This chart uses the basic CPT parameters of cone resistance and friction ratio. Knowing that the increase in the penetration resistance and the sleeve friction with depth due to the increase in effective overburden stress, a new normalized SBT chart was suggested by Robertson (1990). This new chart requires normalization of these parameters. The normalized soil behavior type(SBT_N) chart shown in Figure 4.4 apart from identifying results for most young, un-cemented, insensitive normally consolidated soils also identifies ground response, such as increasing soil density, over consolidation ratio, age and soil sensitivity. The soil type corresponding to the numbers seen in Figure 4.4 can be consulted in table 4.2. Nevertheless, it should be reminded that these charts are meant to provide guidelines to the soil behavior type.

To simplify the application of the normalized soil behavior type chart shown in Figure 4.4, the normalized parameters can be combined into one soil behavior type index(I_c), where I_c is the radius of the essentially concentric circles that represent the boundaries between each SBT zone (Robertson and Cabal, 2012). I_c is defined as:

$$I_c = \sqrt{(3.47 - \log Q_t)^2 + (\log F_r + 1.22)^2} \tag{4.2}$$

where, the normalized cone penetration resistance (Q_t) is expressed in a non-dimensional form and taking into account the *in-situ* vertical stresses:

$$Q_t = \frac{q_t - \sigma_{vo}}{\sigma'_{vo}} \tag{4.3}$$

The normalized friction ratio(F_r) can be expressed as:

$$F_r = \frac{f_s}{q_t - \sigma_{vo}} \times 100 \tag{4.4}$$

Boundaries of soil behavior types are then given in terms of the index I_c as can be seen

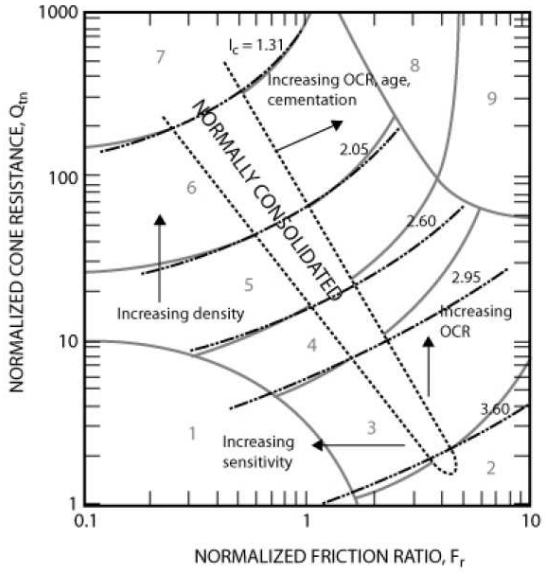

Figure 4.4: Normalized CPT soil behavior type chart, Robertson (2010)

in table 4.2. Note that this index does not apply to zones 1,8 and 9 shown in Figure 4.4. Profiles of I_c provide extra help to identify the continuous variation of soil behavior based on CPT results. Figure 4.5 illustrates for CPT S02G00190 a profile using a color code developed to aid the visual representation of SBT on a CPT profile. This method was also used on the layer definition process.

Table 4.2: Soil behavior type index boundaries, Robertson and Cabal (2012)

Zone	Soil Behavior Type	I_c
1	Sensitive, fine grained	N/A
2	Organic soils clay	> 3.60
3	Clays silty clay to clay	$2.95 - 3.60$
4	Silt mixtures clayey silt to silty clay	$2.60 - 2.95$
5	Sand mixtures silty sand to sandy silt	$2.05 - 2.60$
6	Sands clean sand to silty sand	$1.31 - 2.05$
7	Gravelly sand to dense sand	< 1.31
8	Very stiff sand to clayey sand	N/A
9	Very stiff, fine grained	N/A

As seen in Figure 4.5, the soil profile suggests that granular and cohesive soil may be found with depth. It is then important to estimate both friction angle and undrained shear strength parameters depending on the type of soil. Also, these parameters might indicate what kind of soil we are dealing with. Soils that exhibit a drained behavior have particularly high friction angles(ϕ') while undrained like soils have low ϕ' and high undrained shear strength(S_u).

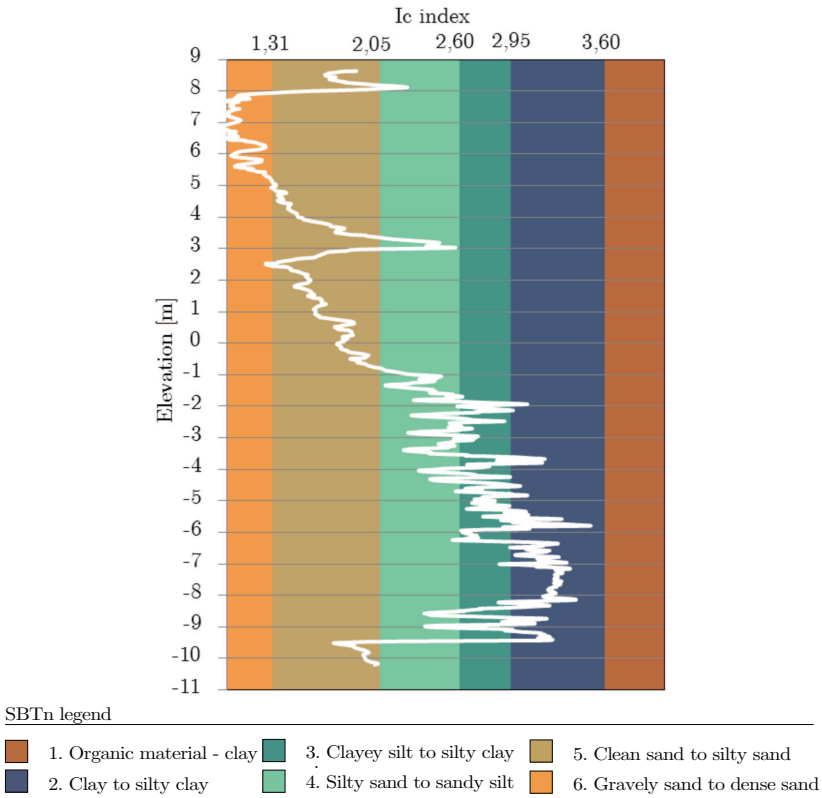

Figure 4.5: Soil behaviour type index ploted over elevation for CPT S02G00190

For the friction angle, two correlations are used. This allows to have a greater number of results and to evaluate if different correlations give alike results. The first relation presents the Robertson and Campanella (1983) correlation and latter Kulhawy and Mayne (1990) relationship:

$$\tan \phi' = \frac{1}{2.68} \left[\log \left(\frac{q_c}{\sigma'_{vo}} \right) + 0.29 \right] \tag{4.5}$$

$$\phi' = 17.6 + 11 \times \log (Q_t) \tag{4.6}$$

For undrained shear strength the correlation most commonly suggested in bibliography is from Lunne and Eide (1976):

$$s_u = \frac{q_t - \sigma_{vo}}{N_{kt}} \tag{4.7}$$

N_{kt} is the cone factor and constant for each soil. This constant typically varies from 10

to 18 and tends to increase with increasing plasticity and decrease with increasing soil sensitivity. Undisturbed soil samples must be obtained in order to properly define N_{kt} but when such resources are not available Bowles (1998) suggests a value of 14 to be satisfactory to use in Equation 4.7.

The last estimated soil parameter is Young's modulus(E). This modulus has been defined as that mobilized at about 0.1% strain. This is referred by (Robertson and Cabal, 2012) to be highly to moderately applicable to foundation design. The young modulus is then defined as:

$$E = \alpha_E \left[q_t - \sigma_{vo}\right] \tag{4.8}$$

where,

$$\alpha_E = 0.015 \left[10^{(0.55 I_c + 1.68)}\right] \tag{4.9}$$

Correlations for estimation of angle of friction, undrained shear strength and elastic modulus were presented in this section. However, as referred by (Bowles, 1998), a user should use them cautiously and these correlations should be plotted into charts. As the trend for each parameter develops, equation results may be revised.

4.2.3 Layer definition and obtained results

CPT results refer purely and only to the volume of soil tested and not for all the area of implementation. For this reason it is important to treat results all together and separate what might be reasonable results from singularities and isolated characteristics of a single CPT profile. The true soil characteristics should lay somewhere in between all results and the more tests, greater the degree of confidence in the estimations made. For this matter and to avoid extensive result presentation, the results shown in this section are charts containing all the data together.

As mentioned in the previous section, when looking at readings of cone resistance and friction ratio together it is possible to start defining the type of soil that the CPT is penetrating. When this trends tend to change with depth a layer change can be anticipated. This is what can be seen in Figure 4.6. The figure shows q_c(a) and R_f(b) plotted over elevation for all the CPT executed. At first, all the CPTs return high cone resistance values and relatively low friction ratios which make anticipate a granular type of soil. Then, and especially after a -2 meter elevation a change in the trend can be seen. The friction ratio

values increase while the cone resistance decreases. This variation suggests a change in the material leading to the impression that a layer with finer particles is being penetrated. As it was shown in Figure 4.1, the CPT readings start at the top of the dike, therefore, the first encountered material is naturally associated as the dike's soil material. After, we may describe the next materials as being the naturally deposited layers on site.

Some small variations from the general tendency can be seen sometimes for different CPTs. This is usually attributed to singularities or tinny deposits, but what is important is to focus on if this deviations are important enough to be taken into consideration or if soil homogenization is enough. As a starting point no special attention is made to this variations, nevertheless, this type of conclusions may change over time if results start suggesting the other way.

In the interest of making a better evaluation of the dike materials, a chart with the continuous soil behavior type index was elaborated. This plot shown in Figure 4.7 returns SBT_N index using a standard color code which is very helpful on the soil definition. According to (Robertson and Cabal, 2012) independent studies have shown that SBT_N charts typically have greater than 80% reliability when compared with soil samples. For this reason and that no samples were available, special attention should be made to the results returned by this method when defining the layer materials.

As evidenced by Figure 4.7 and already seen in Figure 4.6 the results indicate a first layer of mostly sand material with occasional silt particles, then from 1 m to -2 m a transition zone with the fine particles growing and after -2 m a change to a cohesive soil layer is clear. As mentioned before, the material after the dike's soil is the naturally deposited, and hence, this second layer is where the dike is built on. Both S02G00206 and S02G00208 stop at approximately -7.5 m. One of the reasons for this may be that the equipment was not able to continue penetrating or a sufficient strong layer was encountered. Analyzing carefully, with depth evolution I_c and cone resistance for this CPTs start increasing while the friction ratio decreases. This indicates a material change and most certainly a new granular soil. This tendency occurs later on S02G00190 but confirms the line of though. Hence, a third layer can be defined as being a cohesionless soil type. Due to the natural essence of the soil it is easy to understand that layers are not purely horizontal and therefore soil tests made in different (but close) locations might indicate different layer transition depths. This is exactly what happens when trying to determine a transition height from second to third layer. All CPTs display the same tendency but at different depths. S02G00208 starts this transition at about -4 m while S02G00206 at -6 m and S02G00190 at about -8 m. The transition height was chosen to be at -6 m because at this elevation two of the three profiles already are in the third layer and if special attention is taken in Figure 4.6(b) the friction ratio plot for S02G00190 and S02G00206 suffer a

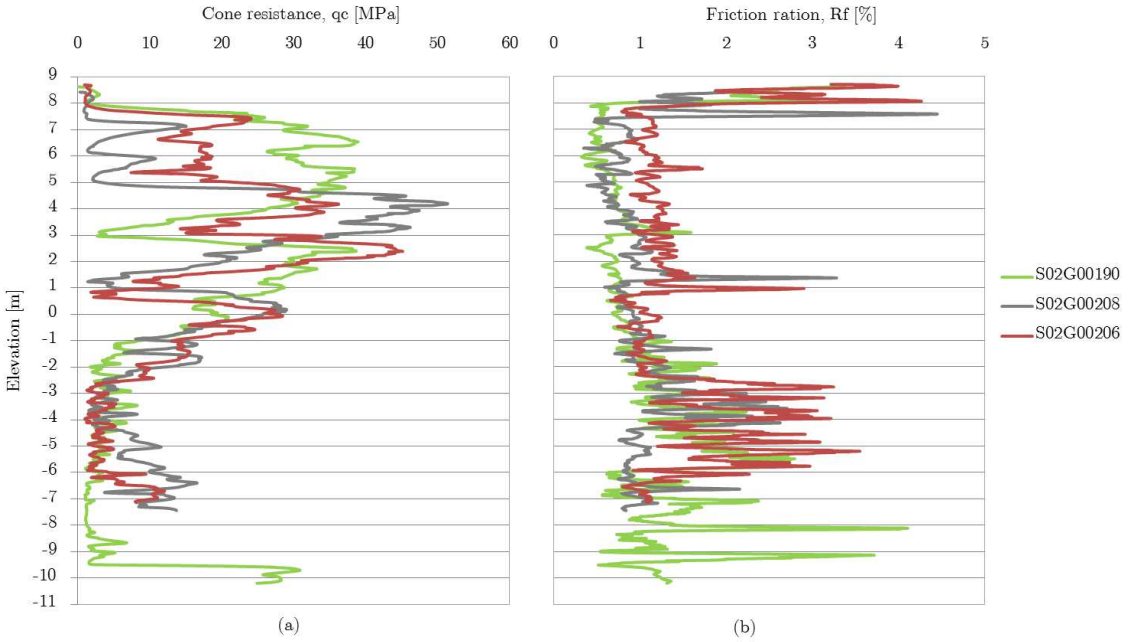

Figure 4.6: Cone resistance (a) and Friction ratio (b) CPT results

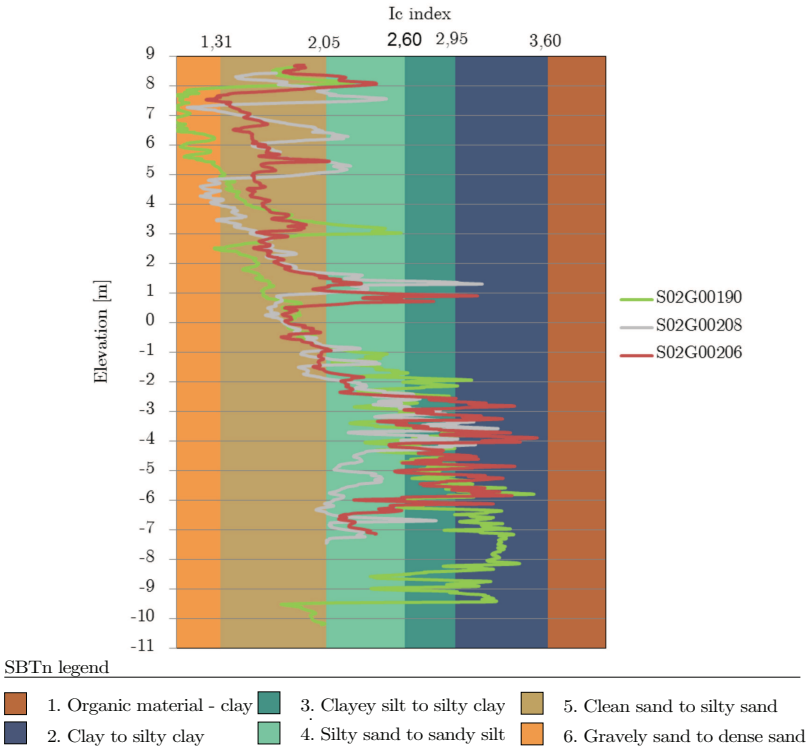

Figure 4.7: Continuous plot of soil behavior type index for all CPTs executed

considerable drop announcing a potential behavior change. Nonetheless, when estimating soil parameters the assumed layer transition depth is the one given on each CPT test.

Apart from soil layer definition also mechanical parameters are important in order to fully define a model for the soil. Applying correlations mentioned in section 4.2.2 it is possible to built a cloud of points with each point indicating the return value of a certain relationship for each CPT reading. First results for the total unit weight on each layer are presented in Figure 4.8. Results for the first layer show some peak deviations on the normal trend exhibited by all CPT results. Although this is normal to find in a natural material, there is the need to standardize the material on each layer. Hence, the peak deviations shown in the first layer may be ignored when it comes to select a total unit weight. Also for the third layer, difference is found when comparing results for S02G00206 and S02G00208 with S02G00190. Here the plot for the first pair suggests a higher value for γ than for S02G00190 CPT. Once again, when deliberating this parameter one should have attention to this outcome and chose a value that is capable of representing all results.

Chart 4.9 shows correlation results for the friction angle. These display similar tendency to the ones observed in Figure 4.8 for γ estimation. For the case of ϕ' on the third layer, returned values have a difference between S02G00190 and the other two of about 10°. Anyway, it is clear that when CPT S02G00190 reaches a certain depth this parameter rapidly increases, which leaves the impression that this layer has good conditions to found the piles tips if necessary.

As for the undrained shear strength, the results shown in Figure 4.10 appear to be relatively close together if we ignore the registered peaks in the beginning and end of the layer. Most points locate between 150 and 300 kPa leaving a reasonable confidence when attributing an s_u value to the layer.

Finally elastic modulus charts are presented in Figure 4.11. Also here the results show the same peaked tendency as the first layer plots for γ and ϕ' and significant difference on third layer. When dealing with this results variation, caution is advised and some conservatism may be taken when choosing this parameters. On the contrary plots for the second layer present points close together with minimal deviations which enhance the confidence for the young modulus on the second layer.

4.2.4 Adopted Soil Parameters

After gathering and examining all returned results it is time to fully define all model parameters. For the present work the parameters of interest for each layer are:

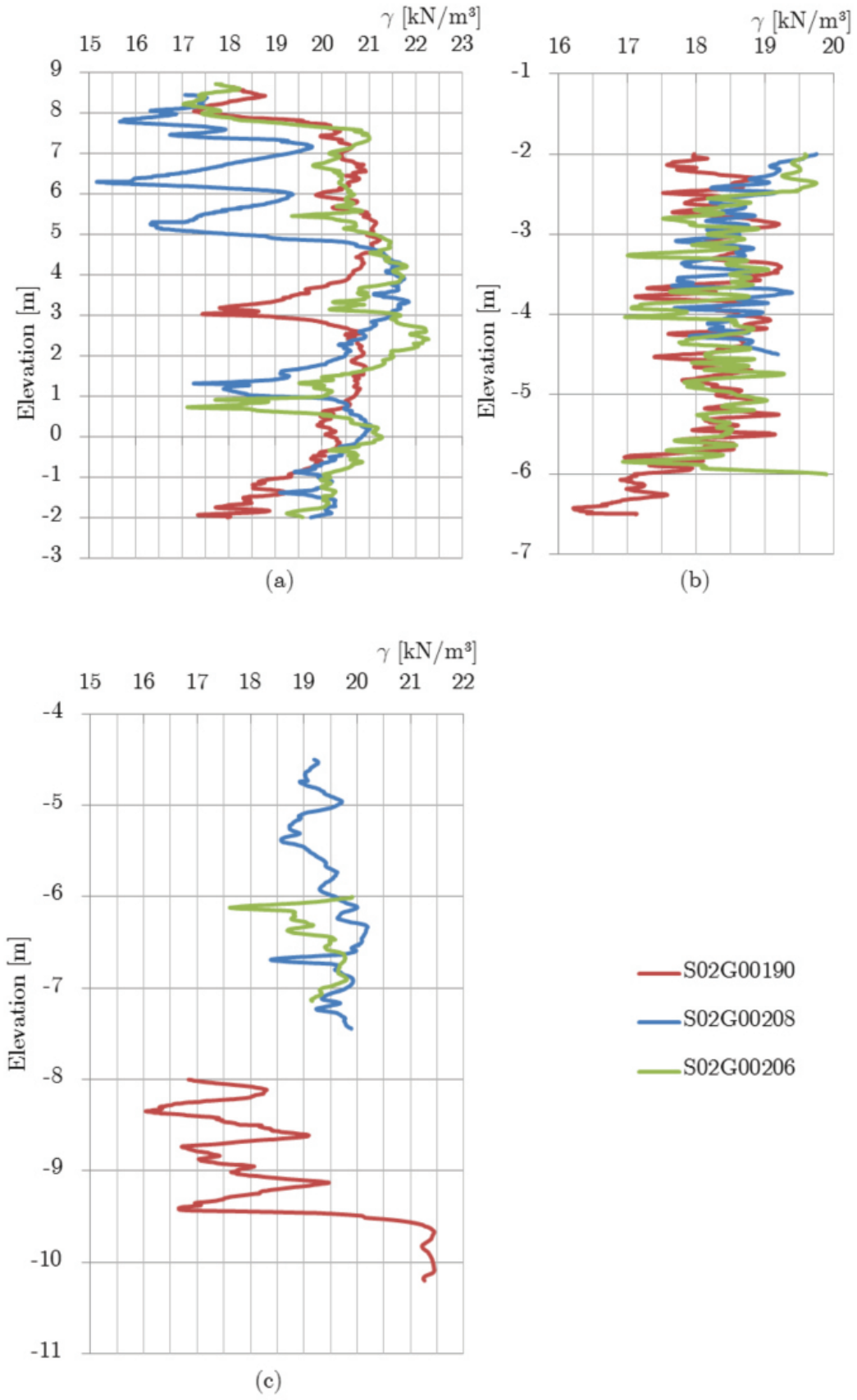

Figure 4.8: Plotted results for the total unit weight on each layer

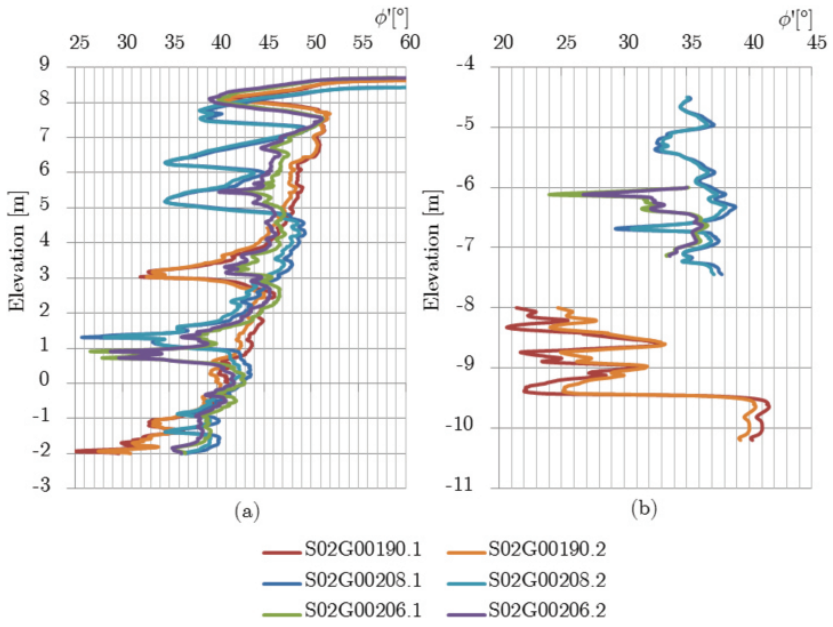

Figure 4.9: Plotted results for the angle of friction on first and third soil layer

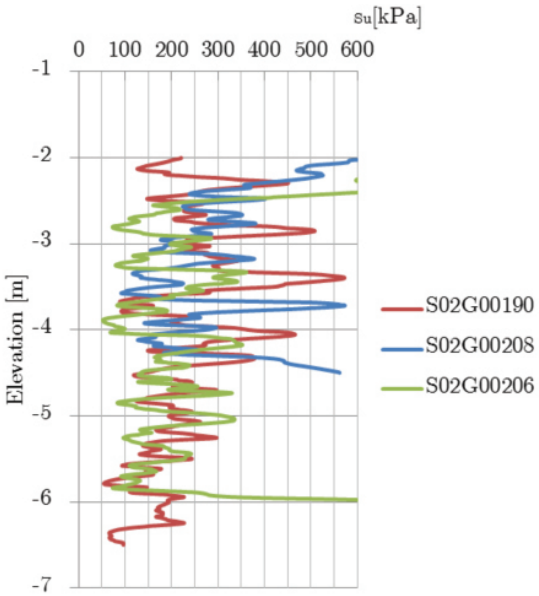

Figure 4.10: Plotted results for undrained shear strength on the second layer layer

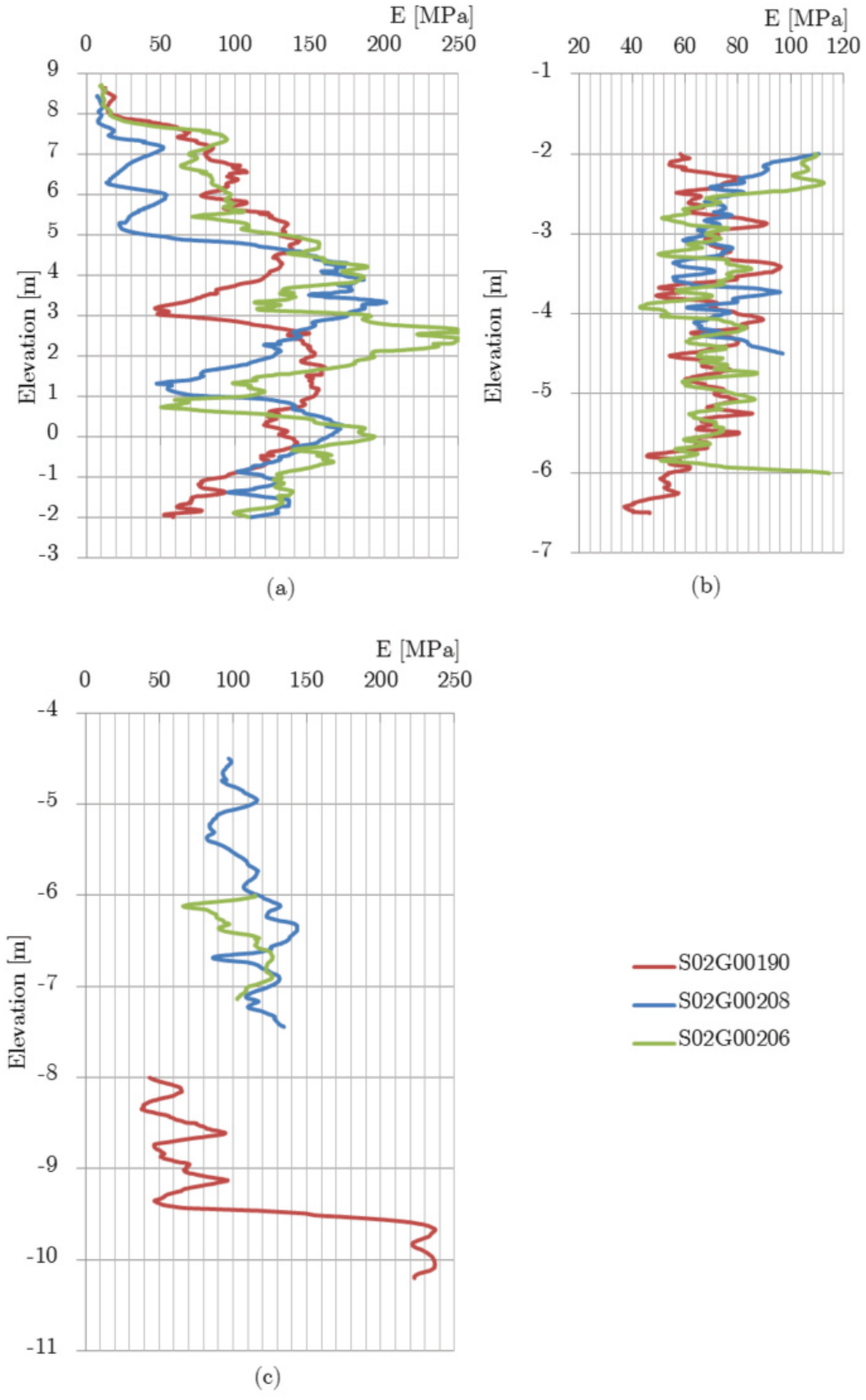

Figure 4.11: Plotted results for the elastic modulus on all soil layers

- Layer dimensions
- Shear strength parameters ϕ' and s_u
- Elastic modulus (E)
- Poisson ratio (ν)

As for layer definition, Figure 4.12 illustrates the soil model dimensions as well as the parameters that define mechanically each layer. The soil is modeled as having three layers with first being related to the dike's material. Both the first and third layers are characterized as having their shear strength defined purely by an angle of friction while the second layer is described as behaving like an undrained type of soil and therefore having it's shear strength characterized by just the undrained shear strength. In terms of elevation, the three CPTs executed do not start at same height, so the surface quota was defined as the average of all CPTs head elevation with a value of 8.7 m. The second layer is 4 meter thick and it starts at around -2 m height. The last layer starts at -6 meters and the longest CPT ends at about -10 m not having information after this depth.

In the interest of choosing soil parameters it was taken a moderately conservative posture, meaning that since CPT is our only test and all parameters are based on correlations, it is prudent to take into account the variability of the results and proceed to a safe choice of the mechanical parameters. Table 4.3 shows the chosen values for all the mechanical parameters. These values were chosen based on the plots presented in the previous section. It should be noted that each person may have a different view over parameter choice depending on the experience, geotechnical application and available data.

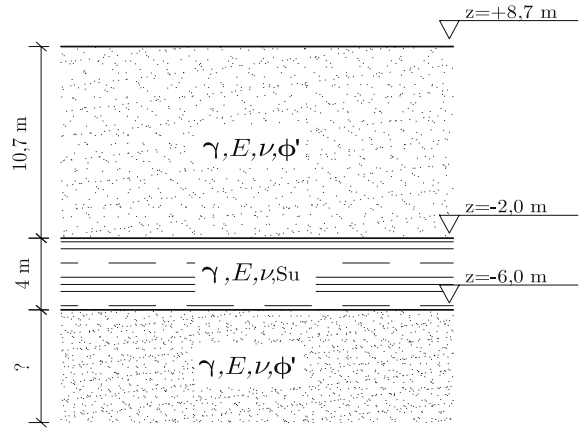

Figure 4.12: Mechanical diagram of the soil medium

Table 4.3: Estimated soil parameters

Layer	$\phi'[^\circ]$	$s_u\ [kPa]$	$\gamma_t\ [kN/m^3]$	$E\ [MPa]$	ν
1	39	-	20	90	0,35
2	-	200	18	65	0,4
3	33	-	19	100	0,35

Regarding Poisson's ratio, since no other information was available, values suggested by bibliography were adopted, more precisely values proposed by (Bowles, 1998). Here the author suggests a value range of 0.3 to 0.4 for sands and for undrained type of soils from 0.3(silty soils) to 0.5(saturated clay soils). Since no information was given, it was chosen the average value as being the representative for each layer.

4.3 Foundation Preliminary Design

As mentioned before, the foundation being analyzed is a foundation composed by a group of piles. Piles are structural members that are used to transmit surface loads to lower levels in the soil mass. This transfer may be mainly vertical distribution of the load along the pile shaft by means of friction (floating pile) or direct load application to the pile tip (end-bearing pile). Nonetheless, all piles support loads as a combination of shaft resistance and tip resistance. The quality of a deep foundation depends on the construction technique, equipment among other factors. Such parameters are not easy to quantify or take into account in normal design procedures. For this reason the Canadian Geotechnical Society refers that it is desirable to design deep foundations on a loading test basis of actual foundation units, also, monitor construction to ensure that design requirements are fulfilled. However, it is easily understandable that most projects may not have this kind of resources available.

In this section a preliminary design of a piled group foundation is made using well-known analytical solutions derived from plasticity theory and using Eurocode 7 in order to meet safety requirements.

4.3.1 Adopted foundation Loads

Loadings on the wind turbine were computed in chapter 3. Since wind is a dynamic action, response is time varying and therefore loads differ in time. When designing a foundation a design load must be assigned to the model. In this case the choice was to select the highest loads exhibited over the simulation time. As mentioned in section 3.4.2, the plots

for the shear force in y_t direction and the consequent bending moment , M_x, exhibit a transient behavior due to start up effects and therefore these values cannot be considered for the calculation of maximum loads. Table 4.4 gives the maximum absolute values of the simulations made in section 3.4.

Table 4.4: Maximum acting loads on wind turbine foundation

V_x $[kN]$	N $[kN]$	M_y $[kNm]$	M_z $[kNm]$
1173	6975	104700	5230

The cap is considered to be 2 m thick which is a common value seen in bibliography and it allows considering the pile cap as a rigid body. For this reason and the fact that the foundation is symmetric, when the cap is loaded vertically or horizontally it can be assumed that the force is distributed equally on all piles. Wind loading can act in every direction, thus the foundation must be able to handle the maximum load in every direction. This means that despite having the loads in all three directions, it is possible to treat this problem as 2D considering the maximum occurred load during analysis as the relevant one. In this case, shear force in x direction and bending moment acting along y axis are the higher loads and will be considered for this approach. Figure 4.13 illustrates the two dimension model considered for the calculation of the forces acting on all piles. Here, F_a and F_b are be assumed as the total reaction on each side of the pile cap. Each reaction can be written as the summation of the applied vertical forces(W_{cap} and N) and the additional vertical force(F_M) caused by the rotation of the cap:

$$F = F_G + F_M \tag{4.10}$$

with,

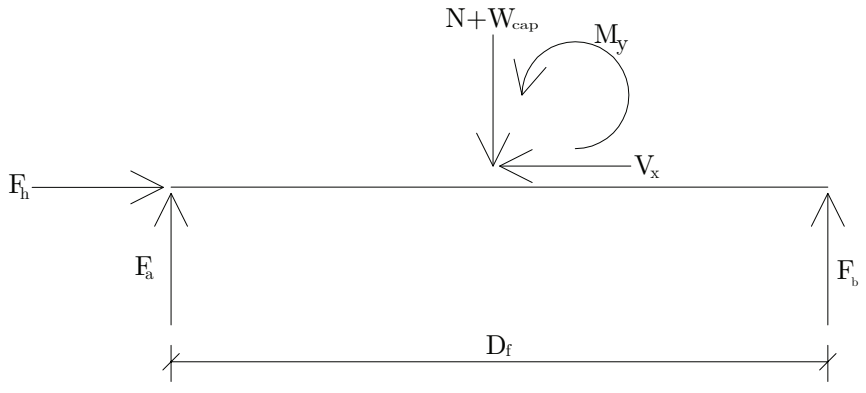

Figure 4.13: Two-dimensional force diagram of the foundation

$$F_G = \frac{N + W_{cap}}{2} \tag{4.11}$$

and,

$$F_M = \frac{M_y}{D_f} \tag{4.12}$$

As already mentioned, the rotation on the cap due to the applied bending moment will cause piles to suffer additional vertical loading. This occurs unevenly on piles because the ones located further away from the rotation axis suffer higher vertical solicitation than the ones closer. Given this, it is necessary to distribute this vertical force on all piles. Two situations may have to be analyzed in order to identify the worst case for vertical pile loading. An example of a foundation with 8 piles is given in Figure 4.14. The case at the left(a) has its rotation axis situated above two piles leaving three piles to bear the caused load due to the rotation. Also, pile A has the greatest arm in both cases so it is possible to suffer the highest solicitation. As for the figure on the right(b), the rotation axis is not situated above any piles which leads to a situation where there are more piles resisting the bending moment but two of them are close to the axis which may cause the distribution of loads to be considerably higher to the other two piles located further away. In order to determine the maximum additional vertical load due to the bending moment acting on a pile, the following force equilibrium can be made:

$$\begin{aligned} R \times F_M = \sum_{j=1}^{\frac{n_p}{2}} \left(R \times \sin\left(\theta_j\right) \times F_j\right) = R \times \sum_{j=1}^{\frac{n_p}{2}} \left(\sin\left(\theta_j\right) \times \sin\left(\theta_j\right) \times F_{M;max}\right) = \\ = R \times \sum_{j=1}^{\frac{n_p}{2}} \left(\sin^2\left(\theta_j\right) \times F_{M;max}\right) \end{aligned} \tag{4.13}$$

with,
n_p - number of piles
θ_j - angle between a pile and the foundation center
F_j - additional vertical force on pile j
$F_{M;max}$ - additional maximum vertical force on the most loaded pile
R - foundation radius

Finally Equation 4.14 gives the maximum additional loading on a single pile due to the rotation of the cap by re-arranging Expression 4.13:

$$F_{M:max} = \frac{F_M}{\sum_{j=1}^{\frac{n_p}{2}} \left(\sin^2 \theta_j\right)} \tag{4.14}$$

As said before, all piles bear the same vertical force caused by the cap's weight(W_{cap}) and the normal force transmitted from the turbine(N). Therefore, the total vertical load on a single pile can be written as:

$$F_{vp} = \frac{N + W_{cap}}{n_p} \pm F_{M;max} \tag{4.15}$$

Given the small value of the horizontal forces, the lateral effects are neglected in this preliminary pile design. Regard that, many design practices first design the pile system for vertical loads and only after verify the lateral action. This is because usually the effects caused by vertical loading are the conditional design situations when it comes to security verifications. Nevertheless, in common design practice this ought to be verified using approaches such as p-y curves or the Broms method (Bowles, 1998).

4.3.2 Pile capacity for axial loading

The ultimate axial bearing capacity of a pile subjected to compression can be given by the sum of two terms, tip resistance(R_b) and skin friction resistance(R_s). For traction piles there is no tip resistance, and therefore, the equation only has the R_s term .

Tip resistance is written as:

$$R_b = A_b \left(c' N_c + \sigma'_0 N_q\right) \tag{4.16}$$

where, A_b $[m^2]$ is the tip area of the pile, c $[kPa]$ the soil cohesion, σ'_0 $[kPa]$ the soil vertical tension at the pile tip, N_c are N_q the bearing capacity factors. Many authors mention that the capacity factor for sands (N_q) is very sensible to the geometric configuration of rupture surface and the contribution from the soil above the pile tip. For the present thesis it was chosen to calculate capacity factor using Sokolovski (1960) approach:

$$N_q = \frac{1 + \sin\left(\phi'\right)}{1 - \sin\left(\phi'\right)} e^{\pi \tan(\phi')} \tag{4.17}$$

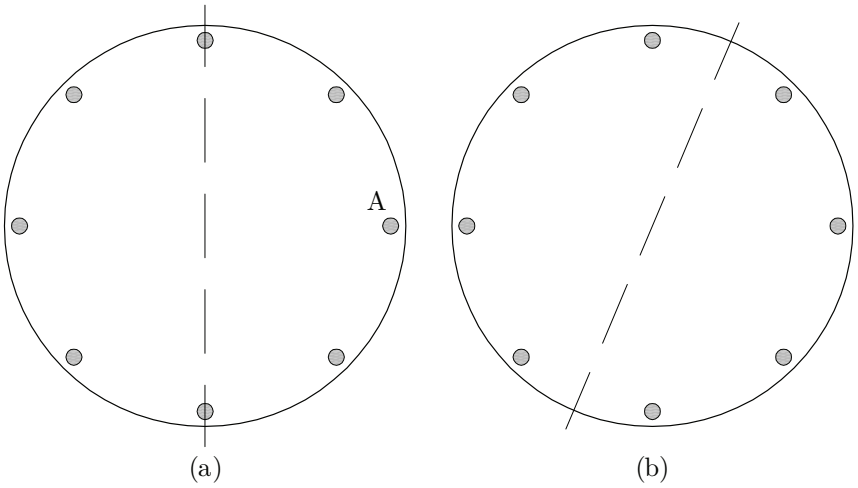

Figure 4.14: Two possible scenarios for vertical loading due to cap rotation

Regarding the factor N_c, the divergence between authors is smaller, being usual to consider $N_c = 9$ (Santos, 2008).

The second term of the total bearing capacity, given by Expression 4.18, has a higher degree of uncertainty because some parameters are strongly influenced by the construction process. Given this, it is necessary to select the type of piles, which for the present thesis these are assumed to be driven. This kind of piles penetrate the soil causing significant displacements and therefore densifying the soil around the piles. This leads to greater friction between the soil and the concrete when compared with other pile solutions such as bored piles.

$$R_s = A_s \left(\alpha c' + K \tan(\delta) \sigma'_v \right) \tag{4.18}$$

with,
A_s - shaft area of the pile $[m^2]$
α - dimensionless adhesion coefficient
K - coefficient of lateral pressure
δ - angle of friction between materials (soil-structure) $[^\circ]$
σ'_v - mean vertical effective stress along the pile shaft $[kPa]$

Lateral pressure coefficient determination depends on the pile construction method, i.e, it depends on the displaced soil volume. API[1] and DNV/Risø[2] recommend using K=1 for closed end piles. Concerning the soil-structure angle of friction it is a parameter of difficult

[1] American Petroleum Institute
[2] Det Norske Veritas and RisøNational Laboratory

evaluation, so the common criterion in engineering practice of considering $\delta = \frac{2}{3}\phi'$ is used.

The factor α can be calculated using the proposed equations by API:

$$\alpha = \begin{cases} 0.5\psi^{-0.5} & \text{if } \psi \leq 1 \\ 0.5\psi^{-0.25} & \text{if } \psi > 1 \end{cases} \tag{4.19}$$

where,

$$\psi = \frac{c'}{\sigma'_v} \tag{4.20}$$

Note that when more than one soil layer is present (which is the case), R_s must be calculated by summing the contribution from each layer.

In order to meet Eurocode 7 safety requirements, it is verified if after applying safety coefficients to the actions, materials and resistance, the calculated ultimate bearing capacity is greater than the applied loads. All these calculations are in a Mathcad sheet presented in appendix C.

4.3.3 Final foundation model

Designing a foundation is an iterative process. The designer evaluates several solutions until one meets all functional, economical and security requirements. Table 4.5 aggregates the parameters of the foundation that meet the intended requirements for the present work. It is a piled foundation with a cap of 2 m thickness(t_c) and a 20 m diameter(D_f). It has 24 piles each one with a 0.8 m diameter(D_p) and a length(l_p) of 21 meters. In terms of pile resistance, each pile has a shaft friction resistance(R_s) of 3938 kN and a tip resistance(R_b) of 3708 kN.

Table 4.5: Considered foundation parameters

Cap		Piles		
t_c $[m]$	D_f $[m]$	n_p	D_p $[m]$	l_p $[m]$
2	20	24	0.8	21

When having a pile group with many piles, caution may be taken not to have very small spacings. If pile spacing is not enough, soil stresses produced on either side are expected to overlap and soil may fail or the settlements be excessive. (Bowles, 1998) specifies that

optimum spacing seems to be on the order of 2.5 to $3.5D_p$ to vertical loads. As it will be dealt later on this thesis, the spacing between adjacent piles is $2.611m$ and therefore inside the given interval. Also, the Canadian geotechnical society refers that driven piles in cohesionless soils develop larger individual capacities when installed as a group since both lateral earth pressure and sand density increase. Therefore, it is conservative to use the sum of the individual pile capacities as an estimate of the pile group capacity. Given this facts it is reasonable(and on the safety side) to assume that the pre-designed pile group efficiency equals to one.

4.4 Conclusions

In this chapter the geotechnical and foundation models were defined. Data from three CPT tests was provided which with the proper treatment and correlations a soil model was created. The medium it is considered have three layers with the first being characterized as cohesionless and ending at -2 m elevation with a thickness of 10.7 meters. The following layer is 4 m thick with a undrained like behavior, while third layer has it's shear strength again characterized by just the angle of friction.

After assembling the soil model, a foundation pre-design was calculated taking into account Eurocode 7. The calculation model was assumed to be two-dimensional with the necessary precautions. In the end it was justified that the total piled foundation bearing capacity can be assumed as being the sum each pile contribution.

Having the wind loads caused by wind computed in Chapter 3 and the geotechnical model created in this one, we are now in conditions to analyze pile-soil-pile interaction in the following chapter.

Chapter 5

Pile-Soil-Pile Interaction

5.1 Introduction

After defining all problem variables in chapters 3 and 4 it is now time to proceed to the dynamic analysis of pile-soil-pile interaction. The problem studied is the stiffness of a group of floating cylindrical piles subjected to a harmonic excitation at the top. The materials are modeled as a linear material of young modulus E, Poisson ratio ν with each pile being a solid cylinder of length l_p and diameter D_p. A common model used for dynamic soil-structure engineering problems is to consider the structure connected to a series of springs and dashpots reproducing the system dynamic stiffness.

In this chapter stiffness and damping coefficients are computed using two distinct methods. First, the generalized pile-soil-pile solution which is a frequency-domain approach to the problem. Second, a numerical time-domain approach to the problem is made using the commercial finite element software PLAXIS 3D. The analyzed frequencies are in the range of the ones calculated in Chapter 3. Also, to study the applicability of the finite element solution to this frequency dependent behavior, verification calculations were made for higher frequencies and afterwards compared with the rigorous solution of Kaynia & Kausel (1982).

5.2 Generalized Pile-Soil-Pile Theory

As mentioned in Chapter 2 pile-soil-pile interaction focuses on the problematic of a piled foundation subjected to a dynamic load. The response may considerably change by slightly switching the frequency of excitation. Properly describing the solution and its variables

is then important to properly compute the dynamic stiffness of the foundation.

A simple analytical solution was proposed by Dobry and Gazetas (1988) where it is possible to compute the dynamic stiffness of a rigidly-caped pile group. The model assumes that cylindrical waves emanate simultaneously from all points along the pile axis length and propagate radially outward. Also it's considered by the model the soil as homogeneous, vertical piles, regular spacing of identical piles and that the dynamic stiffness of the single pile is known. Generalized pile-soil-pile theory is based on Dobry and Gazetas (1988) simple solution.

The position of the piles is defined in Cartesian coordinates x_j and y_j with j being the sequential pile number. If we consider n_p as the total number of piles, $j = 1 : n_p$. In the present thesis, this theory is only applied to a circular foundation with one row of piles along it's perimeter. Therefore, x_j and y_j can be written as:

$$x_j = R\cos\left(2\pi\frac{j-1}{n_p}\right) \tag{5.1}$$

$$y_j = R\sin\left(2\pi\frac{j-1}{n_p}\right) \tag{5.2}$$

with,
R - radius of the circular row of piles $[m]$
n_p - number of piles
j - pile number

Matrix Δ_{ij} gives the distance between piles i and j:

$$\Delta_{ij} = \sqrt{(x_j - x_i)^2 + (y_j - y_i)^2} \tag{5.3}$$

Dobry and Gazetas (1988) analyze the dynamic interaction between piles by proposing a dynamic interaction factor which is function of frequency. Later Hölscher (2014a) describes this as a matrix defined by:

$$A_{ij} = \begin{cases} \sqrt{\frac{r_0}{\Delta_{ij}}}\exp\left(-\beta\omega\frac{\Delta_{ij}}{c_s}\right)\exp\left(-i\omega\frac{\Delta_{ij}}{c_s}\right) & \text{if } i \neq j \\ 1 & \text{if } i = j \end{cases} \tag{5.4}$$

where,
A_{ij} - interaction matrix between piles i and j
r_0 - radius of the piles $[m]$
β - damping ratio of the soil
c_s - shear wave speed in the soil $[m/s]$

A_{ij} can also be seen as:

$$A_{ij} = \frac{Displacement\ on\ pile\ i\ due\ to\ a\ load\ applied\ on\ pile\ j}{Displacement\ on\ pile\ j\ when\ subjected\ to\ its\ own\ load} \tag{5.5}$$

Defining matrix A_{ij} allows to describe the displacement of all piles when the displacement on one pile is known. In other words, the displacement on pile i can be given by multiplying A_{ij} with the displacement on pile j. As known, displacements and forces are related by means of the stiffness. Equation (5.6) allows to describe the displacement on pile i when a force is applied on pile j.

$$w_i = A_{ij}\frac{F_j}{\mathscr{K}_d} \tag{5.6}$$

with,
F_j - force on pile j [N]
$\mathscr{K}_d$ - dynamic stiffness of a single pile [N/m]

Assuming that matrix A_{ij} is not singular, this relation can be written as seen in Expression 5.7. This equation makes it possible to know and describe all the forces or displacements on a pile group.

$$F_j = \mathscr{K}_d A_{ij}^{-1} w_i \tag{5.7}$$

Finally, the dynamic complex stiffness is frequency dependent and its generalized expression can be written in the following way:

$$\mathscr{K}_d = K_d(\omega) + i\omega C_d(\omega) \tag{5.8}$$

An important point worth mentioning about the stiffness of the single pile is that this

should be the stiffness of the single pile at the frequency of interest. However, the dynamic stiffness of a single pile does not present significant variations for relatively low frequencies having the same value as the static stiffness. For this reason and in order to save time in calculations, it is considered to be good enough the usage of the static stiffness as the single pile stiffness value. The calculation of the dynamic stiffness of a single pile applies to all the motions studied in this thesis and these are defined just as seen in Equation 5.8. As seen, this equation returns a complex number. However, it is possible to present its results using the stiffness and damping coefficients. The real part is the stiffness coefficient while the damping coefficient can be written as the imaginary part divided by the angular frequency being analyzed. Note that this applies to all dynamic stiffness written in the same way as in Equation 5.8.

5.2.1 Vertical Stiffness

For vertical loads, the total applied force on the foundation can be written as the summation of the forces on all the piles(F_{vert}). As for the displacement (w_{vert}), these are all considered to have the same displacement due to the rigid cap:

$$F_{vert} = \sum_{j=1}^{n_p} F_j \tag{5.9}$$

Applying Equation (5.7) to piled foundation we get:

$$F_{vert} = \mathscr{K}_v \left(\sum_{j=1}^{n_p} A_{ij}^{-1} e_i \right) w_{vert} \tag{5.10}$$

with e_i being a vector with n_p elements equal to 1. Knowing that the force dividing by the displacement gives the stiffness and that the summation can be replaced by the vector ${}^t e_j$ the group vertical stiffness is:

$$K_{vg} = \mathscr{K}_v \left({}^t e_j A_{v_{ij}}^{-1} e_i \right) \tag{5.11}$$

where,
${}^t e_j$ - Transposed matrix of e_i

5.2.2 Horizontal Stiffness

For horizontal loading, the pile-soil-pile interaction depends not only on the spacing between piles, but also on the angle θ between the line of the two piles and the direction of the horizontal applied force. Depending on this angle, the waves that emanate from piles can be pure shear waves if $\theta = 90°$ or compression waves if $\theta = 0°$.

If we consider the force pointing in y-axis direction (due to foundation symmetry for x-axis direction, the same logic applies) θ can be defined as:

$$\theta_{ij} = \begin{cases} \arcsin\left(\dfrac{\Delta y_{ij}}{\Delta_{ij}}\right) & \text{if } i \neq j \\ 1 & \text{if } i = j \end{cases} \tag{5.12}$$

(Dobry and Gazetas, 1988) present the horizontal dynamic interaction factor as:

$$\alpha_h(\theta) = \alpha_h\left(0°\right)\cos^2\left(\theta\right) + \alpha_h\left(90°\right)\sin^2\left(\theta\right) \tag{5.13}$$

where, $\alpha_h\left(90°\right)$ is the same as the vertical interaction factor and $\alpha_h\left(0°\right)$ the horizontal interaction factor. This expression can be easily written using interaction matrices using another notation. Hölscher (2014a) writes this expression as:

$$A_{h,ij} = A_{p,ij}\cos^2\left(\theta_{ij}\right) + A_{s,ij}\sin^2\left(\theta_{ij}\right) \tag{5.14}$$

with,
$A_{p,ij}$ - compression interaction matrix (see Equation 5.15)
$A_{s,ij}$ - shear or vertical interaction matrix already shown in Equation 5.4

$$A_{h_{ij}} = \begin{cases} \sqrt{\dfrac{r_0}{\Delta_{ij}}}\exp\left(-\beta\omega\dfrac{\Delta_{ij}}{c_{LA}}\right)\exp\left(-i\omega\dfrac{\Delta_{ij}}{c_{LA}}\right) & \text{if } i \neq j \\ 1 & \text{if } i = j \end{cases} \tag{5.15}$$

According to Dobry and Gazetas (1988), a pile making 90° is affected essentially only by S-waves which emanate from the active pile and which have a phase velocity c_s. However, a pile with $\theta = 0°$ is affected by compression-extension waves propagated with an apparent phase velocity which is approximate equal to the Lysmer's analog velocity (see

Expression 5.16).

$$c_{LA} = 3.4\frac{c_s}{\pi(1-\nu)} \tag{5.16}$$

Just like in the vertical case, the group stiffness can be calculated as summation of all individual piles stiffness($\mathscr{K}_h$) and their interaction effects on adjacent piles. Eq (5.17) shows the horizontal group stiffness.

$$K_{hg} = \mathscr{K}_h \left({}^t e_j A_{h_{ij}}^{-1} e_i \right) \tag{5.17}$$

5.2.3 Rocking Stiffness

In this section is assumed that the foundation rotates along one axis. Once again, since the foundation is symmetric we may assume the rocking stiffness being the same in every direction. Let us assume that the foundation is loaded by a rocking moment around the x-axis. Since the cap it is assumed as being infinitely stiff, the force and the rotation of each pile can be easily calculated if we know the moment and the rotation on the pile cap:

$$M = \sum_{j=1}^{n_p} y_j F_j \tag{5.18}$$

$$w_i = y_j \phi \tag{5.19}$$

with,
M - Bending moment on the cap $[Nm]$
ϕ - Rotation of the cap $[rad]$

Combining Equations 5.18 and 5.19 with the same logic seen in Equation 5.10 we get the bending stiffness of the foundation:

$$K_{\theta g} = \mathscr{K}_v \left(\sum_{j=1}^{n_p} y_j A_{ij}^{-1} y_j \right) \phi \tag{5.20}$$

It is assumed in rocking stiffness that no interaction takes place due to the rotational

deformation of each pile. According to Dobry and Gazetas (1988), such deformation (under zero lateral head displacement) is felt only a few diameters down from the pile head, and produces a rapidly decaying stress field around the pile. Hence the neighboring piles fall outside each others zone of influence. Although the simple method considers both axial and bending deformation of a pile due to its own load, the generalized pile-soil-pile theory only accounts for the axial deformation and interaction because the effects of bending deformation assume neglectable values when compared to the axial ones.

5.2.4 Analytical results

Dynamic stiffness for a foundation composed by a group of piles and a rigid cap was computed and it will be presented in this section. As already mentioned, dynamic stiffness is a complex number with a similar expression as the one seen in Equation 5.8. Likewise, the stiffness and damping coefficients are calculated in the same way as presented for the single pile. As calculated in appendix A and referred in section 3.3.1, NREL 5-MW Baseline wind turbine has a natural frequency of 0.302 Hz and its main response reaches values close to 1 Hz and bellow. It is important then, to effectuate a dynamic stiffness analysis to frequencies close to the natural and working frequencies. For this work, it was considered enough to analyze from a static state(0 Hz) to 1.2 Hz in 0.3 Hz intervals, i.e., 0, 0.3,... 1.2 Hz.

The effects on pile spacing are usually of great importance both for static and dynamic type of analysis. For static models, the decrease in pile spacing can mean a increase of foundation displacements thus a decreasing in group stiffness. As referred by Dobry and Gazetas (1988) and Hölscher (2014a), dynamic stiffness is dependent on frequency and thus the wavelength. A change in pile spacing alters clearly this interaction between the piles and the wavelength of the action propagating through the soil. This means that depending on the frequency, the increase on pile spacing may lead to a increase or decrease on the foundation stiffness depending if piles vibrate in counter-phase or in-phase respectively. For this reason it is important to analyze the effects on pile spacing. To perform this investigation first the dynamic stiffness of a foundation with few piles is investigated and gradually the number of piles is increased. Table 5.1 exhibits the number of piles on each foundation and the corresponding dimensionless spacing which is often used in literature.

Table 5.1: Different pile configurations analyzed

n_p	4	8	16	24
s/d	17,7	9,6	4,9	3,3

Note that generalized pile-soil-pile theory assumes that the pile penetrates a homogeneous

soil. As seen in the previous chapter, the foundation crosses three different soil layers. At first sight, this may constitute a problem of application. However, the stresses in fixed head piles tend to decay over depth. Kaynia and Kausel (1991) showed that the behavior of piles is influenced by near surface soil properties, specially for low frequencies. Since the first layer has considerable thickness, it is assumed that most of the phenomena takes place on the dike's material.

The Mathcad sheet for the calculation of a foundation with 24 piles($s/d = 3.3$) at $1.2Hz$ frequency is exhibited in appendix D.

Figure 5.1 shows the plotted results of the stiffness and damping coefficients for a vertically loaded foundation. At first sight the stiffness increases with decreasing pile spacing and increasing number of piles. Also, a more or less constant trend with very small variations for the frequencies studied. This may be different from the expected peaks and valleys seen in Figure 2.4 but a proper explanation can be given. For very low frequencies like the ones studied in this thesis, the wavelengths are much greater than the pile spacings. This causes the soil mass between piles to vibrate in phase with the piles and therefore the system responds as block since no effect of the wavelength is yet felt. This explanation also applies for the trend difference between greater and smaller spacings between piles. For the smaller spacings ($s/d = 4.9$ and 3.3) the wavelengths are much greater than the spacing and therefore the foundation still responds as a isolated block. With increasing spacing some effects of the wave length are starting to be seen(even if the variation may be neglectable for practical applications) with stiffness increasing which indicates the beginning of an out of phase behavior.

This trend is the same for the horizontal dynamic stiffness seen in Figure 5.2. Again the stiffness increases with decreasing pile spacing and the plots show even shorter variation

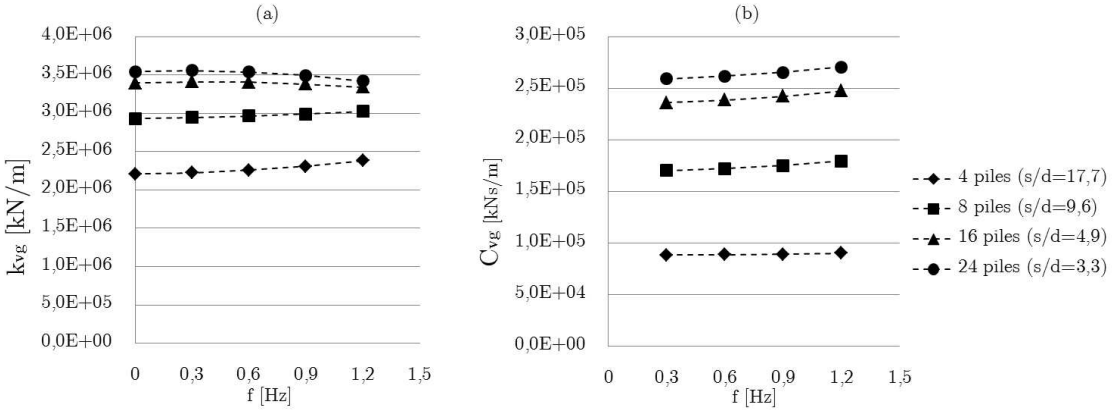

Figure 5.1: Results for vertical group stiffness(a) and damping(b) coefficients

with along the frequency range.

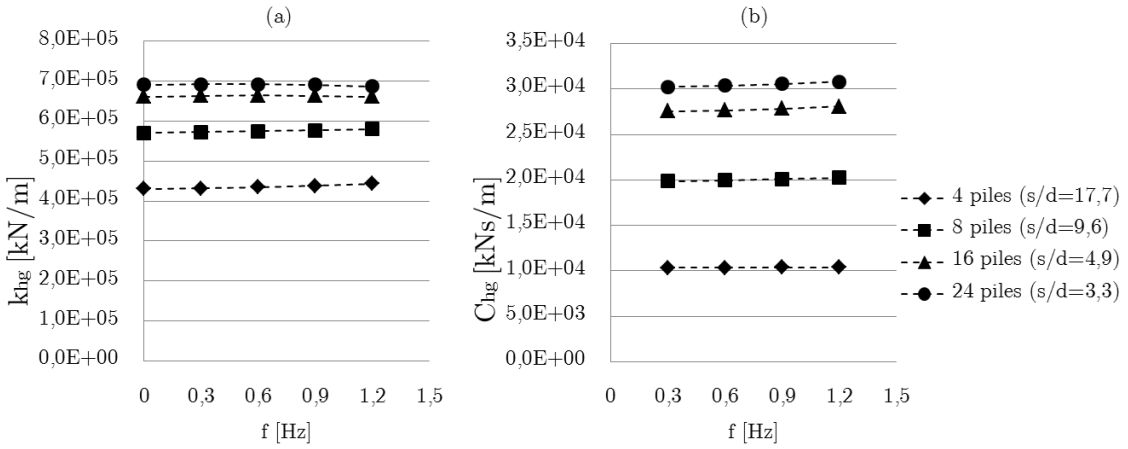

Figure 5.2: Results for horizontal group stiffness(a) and damping(b) coefficients

Finally plots for rocking dynamic stiffness are present in Figure 5.3. Here the stiffness coefficient invariably decreases over the analyzed frequencies. The calculated values for the damping coefficient shows rather strange values. For all spacings a negative damping coefficient is returned by the method. Physically this means that instead of a amplitude decrease due to material resistance we would have energy generation. This phenomenon is hardly understandable in real world which leads to the assumption that for low frequencies the damped behavior is not yet fully established. With increasing frequency within the considered values, the damping coefficient rapidly increases which leads to believing that quickly a undoubted dynamic behavior will be established and thus the damping coefficient will assume real physical meaning.

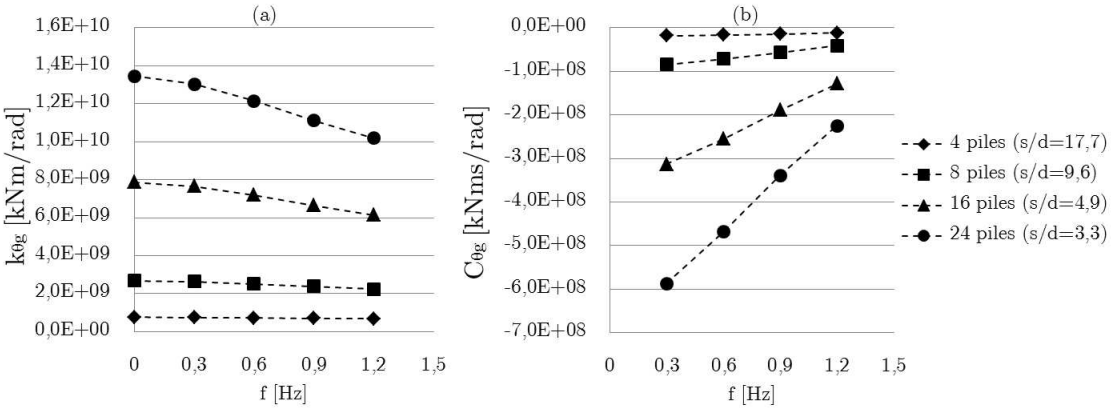

Figure 5.3: Results for rocking group stiffness(a) and damping(b) coefficients

5.3 3D Numerical Solution

For three-dimensional numerical modeling the software PLAXIS 3D is used. This is a commercial finite element tool developed by PLAXIS bv for the analysis of geotechnical problems. For the assessment of dynamic behavior, PLAXIS's add-on dynamics is used. All simulations were made using PLAXIS 3D 2013 version.

5.3.1 Numerical aspects in PLAXIS

In this section a brief description of PLAXIS 3D will be made. The goal is to describe briefly how the software works and what are the relevant parameters to take into consideration towards having a good model of the geotechnical problem in question.

The equation used in PLAXIS to describe the time-dependent movement of a volume is the generalized equation of motion:

$$\boldsymbol{F} = \boldsymbol{K}\boldsymbol{u} + \boldsymbol{C}\dot{\boldsymbol{u}} + \boldsymbol{M}\ddot{\boldsymbol{u}} \tag{5.21}$$

where, $\boldsymbol{K}$,$\boldsymbol{C}$ and $\boldsymbol{M}$ are the stiffness, damping and mass matrices respectively, $\boldsymbol{F}$ is the load vector and $\boldsymbol{u}$ the displacement vector. The dots above the **u** mean that these are time derivatives, with $\dot{\boldsymbol{u}}$ being the velocity and $\ddot{\boldsymbol{u}}$ the acceleration of the volume in question.

In many finite element formulations, $\boldsymbol{C}$ is often formulated as function of the mass and stiffness matrices which is the so called Rayleigh damping, where $\boldsymbol{C}$ is expressed as:

$$\boldsymbol{C} = \alpha_R \boldsymbol{M} + \beta_R \boldsymbol{K} \tag{5.22}$$

The parameters α_R and β_R are called the Rayleigh coefficients and each one determines the influence of the mass or stiffness in the damping of the system. The higher α_R is, the more the lower frequencies are damped while the higher β_R is, the more higher frequencies are damped (Brinkgreve et al., 2013). These parameters are automatically calculated by PLAXIS when given the damping ratio(ξ) which relates to these coefficients by the following expression:

$$\alpha_R + \beta_R \, \omega^2 = 2\omega\xi \tag{5.23}$$

PLAXIS calculates then coefficients α_R and β_R when given two different target frequencies

as seen in expressions 5.24 and 5.25.

$$\alpha_R = 2\omega_1\omega_2\frac{\omega_1\xi_2 - \omega_2\xi_1}{\omega_1^2 - \omega_2^2} \tag{5.24}$$

$$\beta_R = 2\frac{\omega_1\xi_1 - \omega_2\xi_2}{\omega_1^2 - \omega_2^2} \tag{5.25}$$

Time integration is also a important factor when dealing with numerical implementation of dynamics. PLAXIS uses the implicit time integration scheme of Nathan M. Newmark. Equations 5.26 and 5.27 express the displacement and velocity at the point of time $t + \Delta t$ and where Δt is the time step.

$$\boldsymbol{u}^{t+\Delta t} = \boldsymbol{u}^t + \dot{\boldsymbol{u}}^t\Delta t + \left(\left(\frac{1}{2} - \alpha\right)\ddot{\boldsymbol{u}}^t + \alpha\ddot{\boldsymbol{u}}^{t+\Delta t}\right)\Delta t^2 \tag{5.26}$$

$$\dot{\boldsymbol{u}}^{t+\Delta t} = \dot{\boldsymbol{u}}^t + \left((1-\beta)\,\ddot{\boldsymbol{u}}^t + \beta\ddot{\boldsymbol{u}}^{t+\Delta t}\right)\Delta t \tag{5.27}$$

where, α and β determine the accuracy of the numerical time integration. It is considered that the solution is unconditionally stable if these parameters satisfy the conditions set in 5.28. The used default values are 0.5 for β and 0.25 for α. Since the explanation of the time integration is not the main goal here, the work of Clough and Penzien (2003) can be consulted for further understanding and development of the method.

$$\beta \geq 0.5 \qquad \alpha \geq \frac{1}{4}\left(\frac{1}{2} + \beta\right)^2 \tag{5.28}$$

The time step(Δt) used for dynamic calculations is constant and it can be automatically determined by the software or specified by the user. If *Time step determination* is set to default, PLAXIS calculates the time step based on material, mesh and number of data points. Basically, the calculated time step is the one that ensures that a wave during a single step does not move a distance larger than the minimum dimension of an element (Brinkgreve et al., 2013). Nonetheless, there can be situations where there is the need to specify the time step. In this case the time step is defined as:

$$\Delta t = \frac{t_{total}}{m \times n} \tag{5.29}$$

with,
t_{total} - total calculation time(dynamic time) $[s]$
m - maximum number of steps
n - number of sub-steps

The *Max steps* parameter, m, is the number of calculation points which are saved for plotting in the output program. Increasing this parameter allows to have smother curves and animations but it will also increase the required storage memory. The sub steps are calculation steps but where data is not stored. The multiplication of this two parameters gives the total number of steps, which is important because the definition of a proper number of steps allows to properly describe the dynamic signal.

Another important aspect worth mentioning is the finite element mesh. Defining an adequate mesh is a matter of relevance. A sufficiently fine mesh must be defined in order to obtain accurate results, but at the same time, elements cannot be too small that increase the calculation times to unpractical durations. Naturally, and for the same reasons, the size of the model should be also carefully chosen, it is important not to create an oversized geometry because this means more elements in the system, but, the model should be big enough in order to avoid boundary interference. The size of the elements assume even more importance when dynamics are involved since the propagating waves should be properly described. As referred by Semblat and Brioist (2000) the size of the elements should lie between a tenth and a twentieth of the wavelength. The soil elements in PLAXIS 3D are 10-node tetrahedral elements(Figure 5.4) with three nodes per element which means that a second degree approximation of the displacement field is possible.

In PLAXIS, the average element size(l_e) is defined according to Equation 5.30, where the calculation of l_e is based on total size of the model and the relative element size factor(r_e) which varies from very fine($r_e = 0.5$) to very coarse($r_e = 2$). As default the relative element size is set to medium which corresponds to an r_e value of 1.

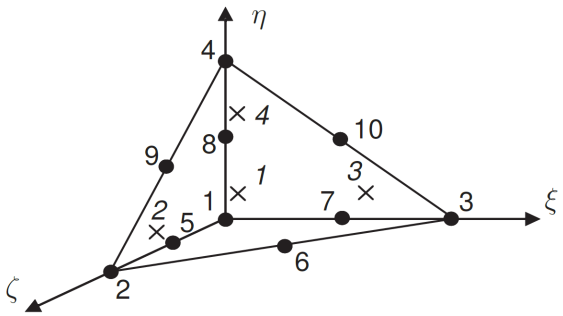

Figure 5.4: 10-node tetrahedral element used in PLAXIS 3D

$$l_e = \frac{r_e}{20} \times \sqrt{(x_{max} - x_{min})^2 + (y_{max} - y_{min})^2 + (z_{max} - z_{min})^2} \tag{5.30}$$

It is considered good practice to refine the finite element mesh in areas where large deformation gradients are expected. This allows on one side to have more accurate results and on the other to save calculation time since elements laying outside this areas do not need to have such dimensions. For this purpose PLAXIS 3D allows to refine geometrical entities through the *Fineness factor* parameter. By default this parameter assumes a value of 1 which means that no refinement was undertaken. On the other hand, values below unity will decrease the element size while using a value larger than 1 coarsens the mesh locally.

Defining proper model boundaries should also be a matter of attention. These should be located far enough from the area of interest in order to avoid interference and consequently inaccurate results. By default, PLAXIS applies to the boundaries of the geometrical model a set of general fixities. This means that the base if fully fixed($u_x = u_y = u_z = 0$), the ground surface can move freely and the vertical planes cannot move in their transversal direction. For example the vertical geometric boundary parallel to the yz plane is fixed in the x-direction($u_x = 0$ and $u_y = u_z = free$). When dealing with a dynamic problem, special care of the subject is needed. If no special measures are taken, the propagating waves reflect in the boundaries leading to artificial energy in the problem and distortion of results. PLAXIS deals with this problem by implementing viscous boundaries. These are dampers located at the boundaries that are used to ensure that an increase in stress on the boundary is observed without rebounding. Equations 5.31 and 5.32 represent the normal(σ_n) and shear(τ) stresses absorbed by a damper located at the boundary in x-direction.

$$\sigma_n = -C_1 \rho c_p \dot{u}_x \tag{5.31}$$

$$\tau = -C_2 \rho c_s \dot{u}_y \tag{5.32}$$

where, ρ is the density of the materials and c_p and c_s the pressure and shear wave velocities defined in expression 5.33. C_1 and C_2 are relaxation coefficients that were introduced in order ajust absorption if necessary. However, Brinkgreve et al. (2013) refer that further research is necessary to fully master the effects on this coefficients changes. Nevertheless, using $C_1 = 1$ and $C_2 = 1$ for practical calculations is considered to be sufficient.

$$c_p = \sqrt{\frac{E_{oed}}{\rho}} \qquad c_s = \sqrt{\frac{G}{\rho}} \tag{5.33}$$

with,
E_{oed} - oedometer modulus
G - shear modulus

In terms of loading, a dynamic impulse is specified multiplying the input value with a dynamic multiplier. An harmonic loading is defined in PLAXIS by the following equation:

$$F = \hat{M}\hat{F}\sin(\omega t + \phi_0) \tag{5.34}$$

with,
$\hat{M}$ - amplitude multiplier
$\hat{F}$ - input value of the load $[kN/m]$
ω - angular frequency $[rad]$
ϕ_0 - initial phase angle $[^\circ]$

5.3.2 PLAXIS model

5.3.2.1 Soil definition

One of PLAXIS important features is the wide range of soil models that this software offers in order to help to solve particular geotechnical problems. Since generalized pile-soil-pile theory assumes the soil as a linear elastic material it makes sense to use linear elasticity to model all soils in the finite element program. Using linear elasticity in this model seems to be a satisfactory approximation since strains in these dynamic calculations will assume very small values.

The soil stratigraphy is assumed to be the one defined in section 4.2.4. As for the soil, the needed parameters for input are shown in table 5.2 with their respective values. All other inputs are calculated from this basic inputs. Additionally Rayleigh damping parameters α and β are also defined in the parameters tabsheet. As mentioned in the previous section, these are automatically calculated by PLAXIS when damping ratio(ξ) and frequency are defined. For every calculated frequency it was considered $\xi = 5\%$.

Table 5.2: Adopted soil parameters in PLAXIS

Parameter	First layer	Second layer	Third layer
$\gamma\ [kN/m^3]$	20	18	19
$E\ [MPa]$	90	65	100
$c_p\ [m/s]$	266	276	288
$c_s\ [m/s]$	128	112	138
ν	0.35	0.40	0.35

5.3.2.2 Adopted geometry

The defined final model geometry is presented in Figure 5.5. The viscous boundaries are located at a distance of 2 pile lengths in x and y directions away from the foundation. The total thickness of the soil deposit is considered to be also 2 pile lengths which means a total deep of 42 m for both the single pile and pile group models, also, the model considers the bottom boundary as fully fixed. In the other two directions, the group of piles model is 104 m wide and the single pile 84 m. These dimensions are considered to be good enough because no boundary interference was evidenced in the obtained results.

5.3.2.3 Structural model

After defining soil model and geometry it is necessary to define the structural model in detail. The foundation cap is modeled as a plate element and for pile the *embedded pile* element was chosen. Plate elements are two dimensional structures composed of 6-node triangular elements with 6 degrees of freedom per node(3 translational and 3 rotational). These elements account for deflections due to shearing as well as bending. So in fact, these structural elements have no thickness but behave in such way. The PLAXIS embedded pile is considered as a beam which connects to the surrounding soil by means of special skin

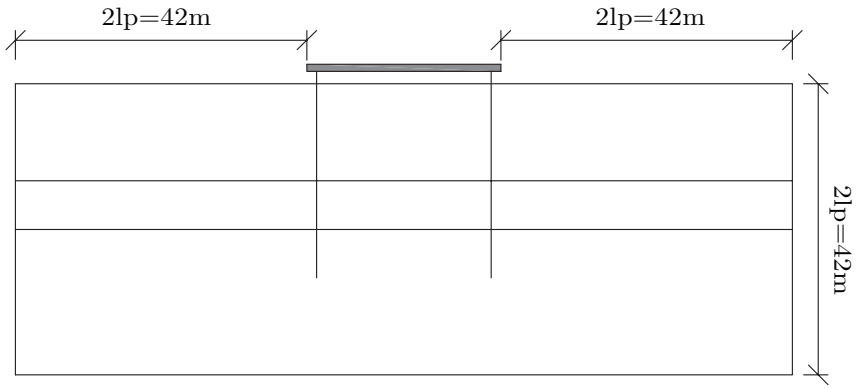

Figure 5.5: Adopted model dimensions in PLAXIS simulation

and foot interfaces. As illustrated in Figure 5.6, these interfaces are modeled as a series of springs located on each pile node and pile tip. K_s denotes the elastic shear stiffness while K_n and K_t are the normal elastic stiffness of the embedded interface elements.

Although volume is not considered, an elastic volume with equivalent diameter around the pile is assumed which makes the embedded pile behave like a volume pile. However, installation effects of the pile are not taken into account which may constitute a problem if these are important to the geotechnical problem. In comparison with volume elements both plate and embedded pile elements have their benefits. Since these are not made of volume elements the total number of elements in the mesh is lower, which allows to reduce calculation time. Also, these structural elements allow to directly evaluate the forces using PLAXIS 3D output processor. Table 5.3 shows the material parameters chosen for plate and embedded pile elements where d is plate thickness, T_{max} the skin resistance and F_{max} is foot resistance. The pile is set to be rigidly connected to the plate and in order to prevent the plate from interacting with the soil this is situated 1 centimeter above the soil surface, as depict in Figure 5.5.

Table 5.3: Adopted plate and embedded pile parameters

Parameter	Plate	Embedded pile
E_p $[GPa]$	30	30
γ $[kN/m^3]$	25	25
d $[m]$	2	-
ν $[m]$	0.15	-
$diameter$ $[m]$	-	0.8
T_{max} $[kN/m]$	-	187.5
F_{max} $[kN]$	-	3708

Forces are also defined in PLAXIS *Structures mode*. The loading is considered to be harmonic and described as seen in Equation 5.34. Here the amplitude multiplier($\hat{M}$) assumes 1 if the force is enabled and 0 if not. The initial phase angle(ϕ_0) is always set to zero and frequency is a variable input assuming the value of the frequency being analyzed at the time. Vertical and horizontal forces were chose to be applied as distributed loads which allows a smoother load distribution along the plate. As for the bending moment this cannot be directly applied in PLAXIS. This is achieved by applying two point loads with opposite direction at each plate edge and thus creating a rotation about the cap symmetry axis.

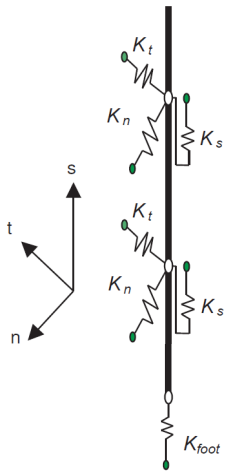

Figure 5.6: Embedded pile model, adapted from Brinkgreve et al. (2013)

5.3.2.4 Mesh

As mentioned in section 5.3.1, the finite element mesh is something that should be chosen with special care since choices clearly affect both accuracy of results and calculation time. First, the minimum element size must be defined, and at the region of analysis some refinement of the mesh is usually necessary. It was previously mentioned that the element size should be in the order of $\lambda/10 \leq l_e \leq \lambda/20$, but since the adopted elements by the software are quadratic, these allow for a better approximation and thus $l_e \approx \lambda/10$ was considered a good element size to properly describe the wave motion.

After defining the average element size, the area of interest was refined in order to get better results. For groups of piles with 4 and 8 piles a volume with $4D_p \times 4D_p \times 1.5l_p$ dimensions was created in order to later refine around the piles. For the other two groups, 16 and 24 piles, in order to facilitate the modeling it was chosen to refine the whole foundation creating a soil block with $22m \times 22m \times 1.5l_p$. Refinement can be made automatically by PLAXIS, or it can be done manually by changing the *Fineness factor* which will multiply by the average element size in order to coarsen or refine the mesh. In order to find out what the optimal element size around the pile should be, vertical static calculations were made decreasing the element size progressively. The optimal solution was defined as the one whose static results didn't differ more than 5% from the following results obtained with smaller elements. Table 5.4 shows the obtained displacements for each element size, and given these results, the chosen element size on the refined area was 2 m.

An example of the adopted mesh for the frequency of 1.2 Hz is given in Figure 5.7. Table 5.5 summarizes the adopted average element size, with the respective relative element size factor. Note that for the frequency of 0.3 Hz, l_e could not have a value close to $\lambda/10$

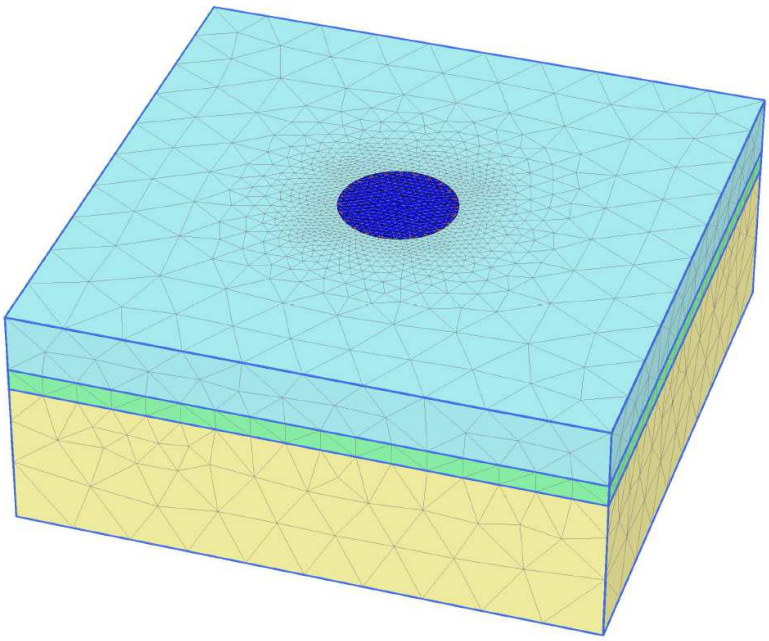

Figure 5.7: Adopted mesh for $f = 1.2\ Hz$

Table 5.4: Influence evaluation of the the element size around the piles

$l_e\ [m]$	r_e	$u_z\ [m]$	$\Delta\ [\%]$
2.5	0.523	$-5,95E^{-5}$	-
2.0	0.421	$-5,17E^{-5}$	13.1
1.5	0.316	$-5,21E^{-5}$	0.62

because otherwise the elements would be to big and the required refinement around the piles would not be possible since PLAXIS does not accept *Fineness factor* values smaller than 0.0625. For this reason, the average element size for 0.3 Hz is approximately $\lambda/15$.

Table 5.5: Adopted average element size

$f\ [Hz]$	$\lambda\ [m]$	r_e	$l_e\ [m]$
0	-	1	7,6
0,3	426,7	3,719	28,4
0,6	213,3	2,789	21,3
0,9	142,2	1,860	14,2
1,2	106,7	1,395	10,7

5.3.2.5 Staged construction

PLAXIS allows its calculations to be divided into several sequential calculation phases where each phase corresponds to a particular construction stage or loading case. Also, it

is on a *Stage construction* phase where specific calculation parameters are detailed. For the present study, three calculation phases where considered:

- Initial phase
- Building phase
- Loading phase

In the initial phase the initial stresses in the model's soil body are characterized. These initial stresses are influenced by the weight of the soil material and the history of its formation (Brinkgreve et al., 2013). This stress state is usually characterized by an initial vertical effective stress and its related with horizontal stresses by calculating the coefficient of lateral earth pressure K_0. The initial phase is automatically added by PLAXIS. Second it is defined the building phase. On this stage, the building is simulated by activating structural elements which in this case are the plate and all piles. Finally, the loading phase is where the load is activated and the dynamic action is defined. All displacements were set to zero before the loading phase.

When selecting a dynamic type of calculation, additional parameters have to be defined. First the viscous boundaries are activated in order to filter out reflecting waves. Then, dynamic time interval must be defined. This is the total time period considered in the dynamic phase, i.e, the duration of the dynamic action. For this parameter it was considered the amount of time that would take the response between two consecutive peaks to have less than 5% difference, so that the response can be considered as stationary. Given this, three periods were considered for 0.3, 0.6 and 0.9 Hz and 4 periods for $f = 1.2\ Hz$. Table 5.6 exhibits the total time for each calculated frequency.

Table 5.6: Dynamic time

$f\ [Hz]$	$t\ [s]$
0,3	10,0
0,6	5,00
0,9	3,33
1,2	3,33

If the user does not specify the time step, PLAXIS will automatically determine Δt. Here caution must be taken. Dynamic response stiffness and damping coefficients calculated from the model are phase dependent. For low frequencies, the phase angle is so small that a too large time step can induce unsatisfactory errors in the results. An example is given

in table 5.7. Here it is shown the possible error when calculating the damping coefficient with automatic time step and a chosen Δt of 0.005 seconds.

Table 5.7: Evaluation of the induced error by time step

$f\ [Hz]$	Automatic $\Delta t\ [s]$	$error\ [\%]$	$\Delta t\ [s]$	$error\ [\%]$
0,3	0.042	10,72	0.005	1,24
0,6	0.021	10,72	0.005	2,71
0,9	0.014	10,73	0.005	3,79
1,2	0.010	8,590	0.005	4,66

As seen, choosing automatic time step calculation will cause PLAXIS to attribute different time steps for each frequency. Also, the possible error fall in the unacceptable category. As for $\Delta t = 0.005\ s$ the maximum error was smaller than 5% ,this was considered an adequate value for all calculations.

5.3.2.6 Output model

The necessary output values from PLAXIS calculation are the time history of displacements. An example for a foundation with 24 piles vertically loaded at a frequency of 0.3 Hz can be seen in Figure 5.8.

Since the excitation is defined as harmonic, it may be assumed that the displacements caused by this force are harmonic as well, but with a phase difference(φ) between excitation and response. The basic equation is the same as Equation 5.21 but for a one degree-of-freedom system:

$$ku + c\dot{u} + m\ddot{u} = F \tag{5.35}$$

where,

$$F = \hat{F}\sin(\omega t) \tag{5.36}$$

$$u = \hat{u}\sin(\omega t - \varphi) \tag{5.37}$$

$$\dot{u} = \hat{u}\,\omega\cos(\omega t - \varphi) \tag{5.38}$$

$$\ddot{u} = -\hat{u}\,\omega^2\sin(\omega t - \varphi) \tag{5.39}$$

Here, m is the mass of the cap, $\hat{u}$ is the displacement amplitude of the foundation cap while k and c are the stiffness and damping coefficients respectively. As for $\hat{F}$, this is the

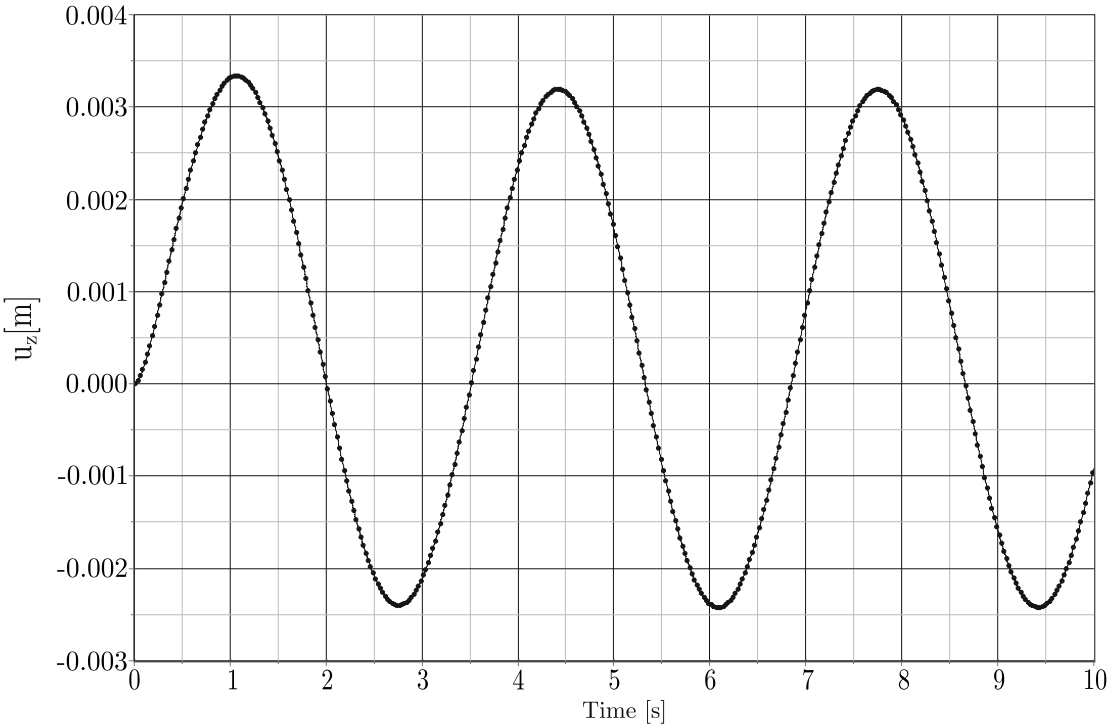

Figure 5.8: Cap displacement over time for a group of 24 piles loaded at a frequency of 0.3 Hz

force amplitude in vertical or horizontal direction depending on which type of motion is being analyzed. Combining Equation 5.35 with Equations 5.36, 5.37, 5.38 and 5.39 we get:

$$\hat{F}\sin(\omega t) = k\,\hat{u}\sin(\omega t - \varphi) + c\,\hat{u}\,\omega\cos(\omega t - \varphi) - m\,\hat{u}\,\omega^2\sin(\omega t - \varphi) \tag{5.40}$$

The values of $\hat{F}$ and ω are input parameters, $\hat{u}$ is read from the last peak displacement value and the phase difference is the horizontal distance between the displacement curve and excitation curve multiplied by the angular frequency (see Equation 5.41). For example, Figure 5.9 shows the normalized force and displacement curves where it can be seen the time lag(δt) between the peaks.

$$\varphi = \omega\,\delta t \tag{5.41}$$

Having determined $\hat{u}$ and φ it is possible to calculate the stiffness and damping coefficients at the specific moments $\omega t - \phi = \pi/2$ and $\omega t = \varphi$. The resulting equations are:

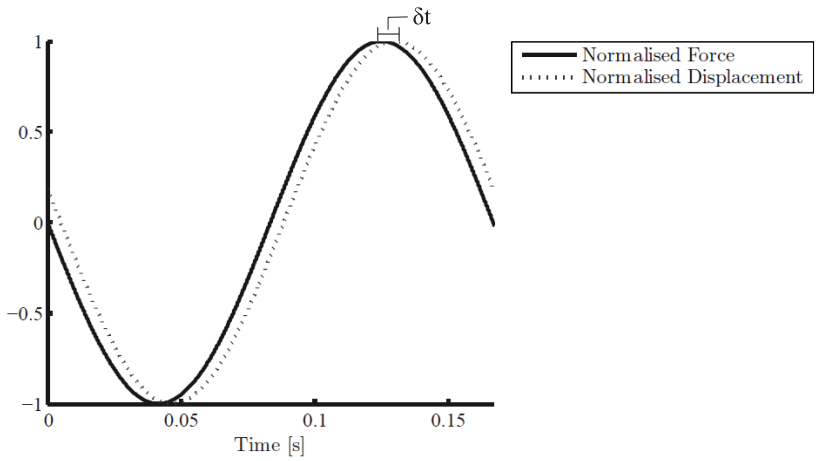

Figure 5.9: Normalized curves for force and displacement from where φ is read

$$k = \frac{\hat{F}}{\hat{u}} \cos(\varphi) + m\,\omega^2 \tag{5.42}$$

$$c = \frac{\hat{F}}{\hat{u}\,\omega} \sin(\varphi) \tag{5.43}$$

Likewise, the rocking stiffness is calculated by replacing $\hat{u}$ and $\hat{F}$ for the cap rotation($\hat{\theta}$) and bending moment($\hat{M}$) amplitude. The rotation of the cap is calculated as seen in Equation 5.44 where $\hat{u}_z$ is the maximum displacement amplitude at the tip of the foundation and R is the foundation radius.

$$\hat{\theta} = \arctan\left(\frac{\hat{u}_z}{R}\right) \tag{5.44}$$

5.4 Results and discussion

After presenting how the result treatment was held, it is time to exhibit the returned results by finite element calculation using PLAXIS 3D software. Figures 5.10, 5.11 and 5.12 show the plots for the stiffness and damping coefficients over the given frequencies.

As it can be seen, results for the finite element approach are not as smooth as the ones computed by the generalized pile-soil-pile theory. Plots 5.10-a and 5.12-a show overall the same tendency. Here most values of the static stiffness are higher than the dynamic stiffness with an increasing gap between static and dynamic behavior with increasing number of piles. As for the horizontal stiffness coefficient seen in Figure 5.11-a, the trend

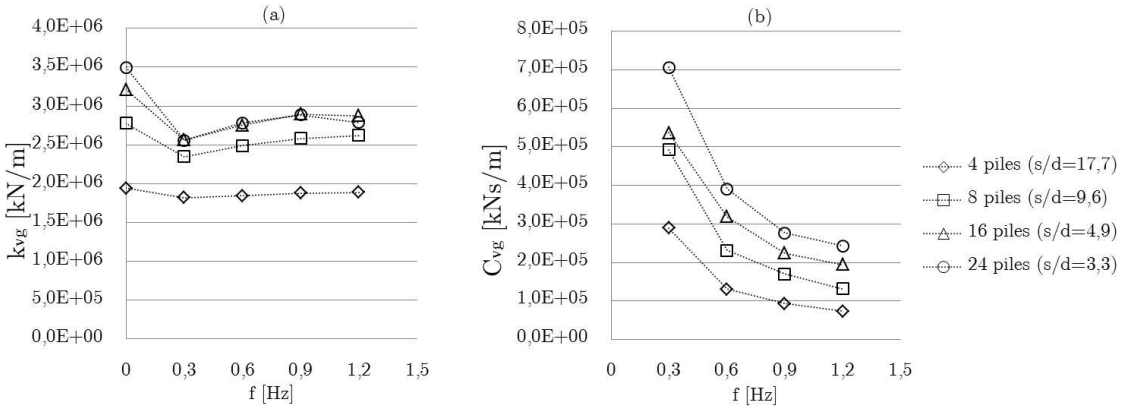

Figure 5.10: Vertical group stiffness(a) and damping(b) coefficients calculated using PLAXIS

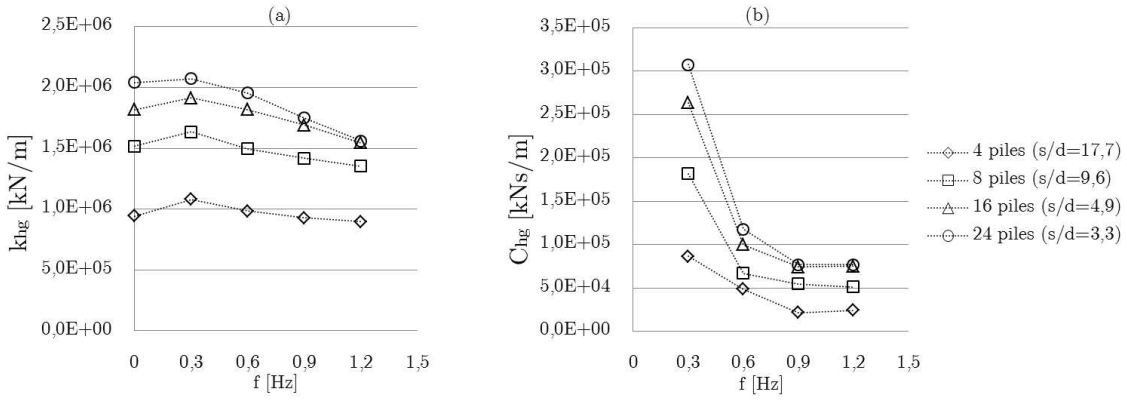

Figure 5.11: Horizontal group stiffness(a) and damping(b) coefficients calculated using PLAXIS

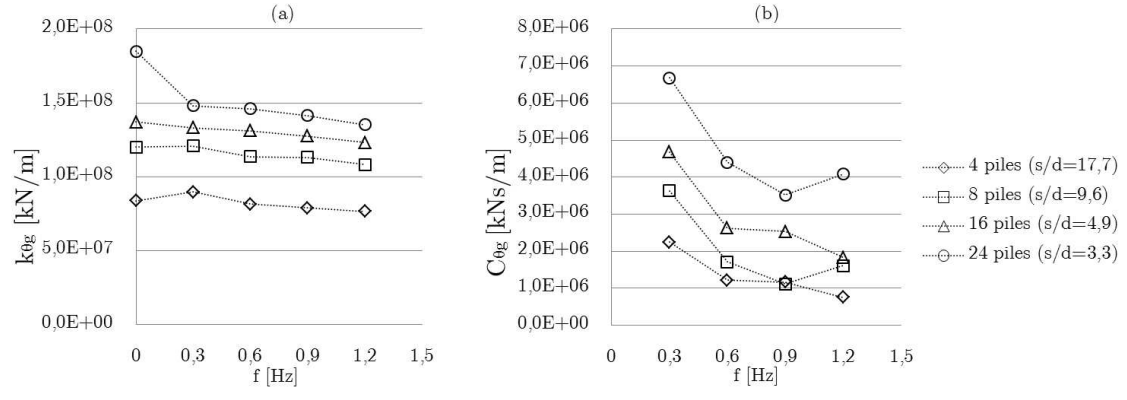

Figure 5.12: Rocking group stiffness(a) and damping(b) coefficients calculated using PLAXIS

is not the same as in Figures 5.10-a and 5.12-a but also a clear difference between static and dynamic analysis can be seen. In all plots, the damping coefficient exhibits the same shape where damping values start really high and quickly decrease showing relatively small amplitude variations afterward. When compared with results obtained in section 5.2.4 for the generalized pile-soil-pile theory, once again, the trends between the two approaches do not match. It should be taken into account that the generalized pile-soil-pile theory accounts only for one soil layer, while the model in PLAXIS takes all three layers in consideration. This may also play a role when evaluating the magnitude of results but in principle it should not have a considerable effect on results nor in the trends exhibited.

A common thing though, is that the values for the damping coefficient are lower than the stiffness by a factor of 10 to 10^2, which means that the damping coefficient does not play a significant role on the total dynamic stiffness of the group. Given this, and because in practice the dynamic stiffness of the group for the analyzed frequencies could be characterized by just the real part(i.e just by a stiffness coefficient) it may be assumed that the exhibited behavior is still more static alike than a clear dynamic state. Abstractly the "wavelength" of a static action can be seen as being infinite. For the frequencies studied in this thesis the wavelengths are rather high and in all cases these are bigger than the problem geometry for the FEM calculation. The damping plots in Figures 5.10-b, 5.11-b and 5.12-b may also be explained by this line of thought. The trend seems to be affected by the frequency which is a divisor when computing the coefficient. Then, with increasing frequency this trend ceases to be so pronounced appearing to converge to a stable solution. However, it should be mentioned that for the lowest frequencies the solution should converge to zero as seen in Equation 5.45. Also, the previous assumption may clarify the clear difference the static behavior and the first considered frequency. Dampers are velocity dependent, when the excitation exhibits high velocity, the damper's response is much stronger than when a slow moving action is applied, and this is may be exactly what happens for low frequency behaviors. If the dampers installed on the viscous boundaries do not work efficiently, the waves will reflect on the boundaries and the system will have higher energy than if these were working properly.

$$\lim_{\omega\to 0} c = \lim_{\omega\to 0} \frac{\hat{F}}{\hat{u}\,\omega}\sin(\varphi) = \lim_{\omega\to 0} \frac{\hat{F}}{\hat{u}\,\omega}\sin(\omega\delta t) = \frac{\hat{F}\delta t}{\hat{u}} \lim_{\omega\to 0} \frac{\sin(\omega\delta t)}{\omega\delta t} = \frac{\hat{F}\delta t}{\hat{u}} = 0 \quad (5.45)$$

Given this, it seemed prudent to ask if finite element calculations are able to capture and reproduce the effects of pile-soil-pile interaction. For this it was decided to calculate the vertical stiffness of a square foundation with 9 piles and compare it with the known rigorous solution of Kanya and Kausel (1982). All model considerations are the same as

mentioned in section 5.3.2 and the soil is described by Dobry and Gazetas (1988). It is a homogeneous halfspace with $E_p/E_p = 1000$ and $L/D_p = 15$. Other parameters were kept the same as in previous simulations. The results for the rigorous solution are plotted as function of the dimensionless frequency defined in Equation 2.2 and the dynamic stiffness coefficients are defined as the ratio between the group stiffness/damping coefficient and the sum of the static stiffness of the single piles. The dimensionless frequencies analyzed are presented in Table 5.8 as well as their corresponding linear frequencies.

Table 5.8: Analyzed dimensionless frequencies and corresponding liner frequency values

a_0	$f[Hz]$
0	0
0.025	0.367
0,05	0.734
0.075	1.101
0.1	1.468
0.2	2.937
0.3	4.405

Also, another fact must be taken into account. On the proposed solution by Kanya and Kausel (1982) the dynamic stiffness is given as $\mathscr{K}(\omega) = k(\omega) + ia_0C(\omega)$ and therefore special care must be taken when comparing the damping coefficient given from the finite element calculation with the one from the rigorous solution. This relation is given in Equation 5.46.

$$i\omega\, C_{PLAXIS} = i\, a_0 C_{rigorous} \Leftrightarrow C_{rigorous} = C_{PLAXIS}\frac{c_s}{D_p} \tag{5.46}$$

The results shown in Figure 5.13 sustain this line of thought. For the low frequencies the behavior is the same as seen in Figure 5.10 and with increasing frequency the results show that PLAXIS is capable of capturing the pile-soil-pile phenomenon by displaying more or less the same trend as the one followed by the rigorous solution. However, results for the stiffness coefficient(Figure 5.13-a) present better agreement in terms of magnitude than values for the damping coefficient seen in Figure 5.13-b. Nevertheless, finite element solution continues to have a drawback. With increasing frequency the element size decreases in order to be able to properly describe the waves. This fact will cause the number of elements to quickly increase and hence increasing the calculation time. For example, for the last calculated frequency of the example shown in Figure 5.13 which is the equivalent of 4.4 Hz with 109807 elements required it took about 79 minutes to calculate.

This is an aspect to take into account when evaluating dynamic problems using time domain solutions such as the finite element method. For high frequencies the computing

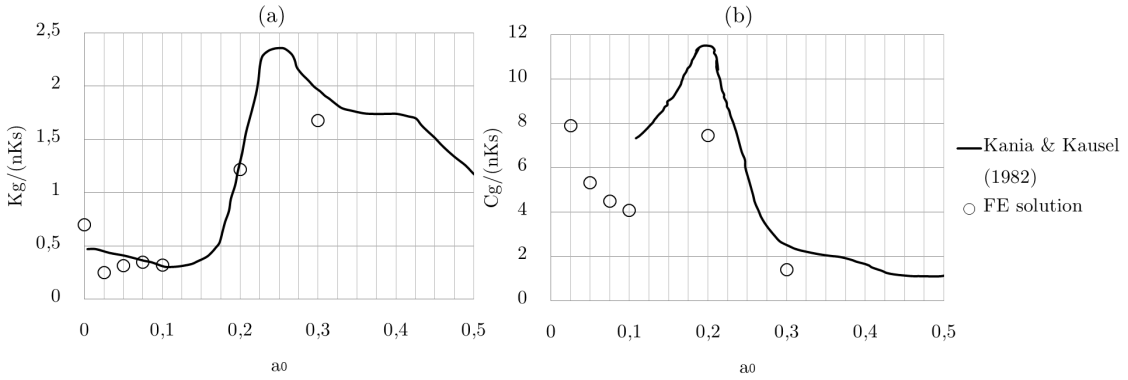

Figure 5.13: Comparison between PLAXIS results and rigorous solution from Kaynia & Kausel (1982)

effort needed and the calculation time may exceed by far the resources available in common engineering companies. Nevertheless, for low frequencies although the calculation time is still considerably higher than in static calculations it falls into the practical range of day by day engineering practice.

5.5 Conclusions

In this chapter two methods to calculate the dynamic stiffness of a piled foundation were addressed. Both consider the soil and structure as an elastic material and the foundation cap to be indefinitely stiff. The generalized pile-soil-pile theory approaches the problem in the frequency domain while a finite element analysis is a time domain method.

Overall, the generalized pile-soil-pile solution seems to behave better for the analyzed frequencies than the finite element approach. It is clear that the typical frequency dependent behavior on this kind of problem is not yet establish since the wave lengths are still too big to play a role in this soil-structure interaction problem. Results from both methods give low damping which indicates that the foundation response is yet governed mainly by the stiffness coefficient. Solutions returned by PLAXIS 3D do not present good results for the low frequencies which may be due to the low efficiency of the viscous boundaries when dealing with low frequencies.

At high frequencies, three dimensional finite element calculations seem to properly describe the interaction between the propagating waves on the soil and piles showing good agreement with the rigorous solution proposed by Kaynia & Kausel (1982). However, high frequency calculations using time domain approaches lead to big computing efforts increasing the total calculation time.

Chapter 6

Conclusions and Future Developments

6.1 Conclusions

This thesis addresses the soil-structure interaction of a foundation composed by a group of piles dynamically loaded by a wind turbine subjected to wind action. This interaction is often called as pile-soil-pile interaction. In order to perform this analysis, loads on the piles caused by the wind turbine were computed using the software package FAST. From this wind-turbine interaction study it was possible to conclude, as expected, that the main loads are registered on the primary wind flow direction and therefore, for the computation of forces and moments a two dimensional wind turbine model is adequate since the foundation has to resist the maximum registered loads in any direction.Also, the relevant frequencies were analyzed. Both natural and response frequencies are very similar and lay outside the 1P and 3P intervals.

As for the pile-soil-pile interaction study, numerical and analytical solutions were computed. At low frequencies such as the ones observed in this thesis, the piles and the soil between them still behave similarly to a shallow foundation which means that moves a block. This means that no pile-soil-pile interaction is yet establish due the fact that the wavelengths are still large in order to establish a frequency dependent behavior as shown by Kanya and Kausel (1982) and Dobry and Gazetas (1988). This type of behavior is confirmed by the analytical solution, were plots exhibit no peaks or valleys. However, for the last frequencies some effects are starting to be seen since the wavelengths get smaller.

The numerical solution computed with PLAXIS 3D showed different behavior when com-

pared with the generalized pile-soil-pile solution. Here the stiffness coefficient plots show a difference of behavior when transiting from the static to dynamic behavior and then having smaller variations in terms of magnitude as the frequency increases. Also, the damping coefficients do not present significant influence on the total result of the dynamic stiffness. This suggests that a fully dynamic behavior is not yet fully establish and also the viscous boundaries may not be effective for very low frequencies.

In order to investigate the capability of the numerical approach to reproduce the wave dependent behavior, an analysis on a foundation with 9 piles was performed and compared with the rigorous solution of Kanya and Kausel (1982). Results for the stiffness coefficient were closer to the rigorous solution than results for the damping component of the solution. Nevertheless, it was possible to conclude that PLAXIS 3D was able to reproduce the peaks and valleys which indicate a frequency dependent response. However, it is important to state that this result improvement with the increase of frequency comes at computational cost which may lead to unpractical calculation times.

6.2 Future Developments

Regarding further developments on the problematic of soil-structure interaction for a dynamically loaded foundation composed by a group of piles, further studies may be done. First the effects of cycling loading must be evaluated. Wind turbines are built to last many decades which means that cyclic loadings might lead to degrading conditions of the soil that may cause lower stiffness with time. If this long term effects are accountable, measures to ensure no significant loss of stiffness must be taken.

Many dynamic methods assume the soil an elastic material. This assumption is justified by the small strains that the soil is subjected to. However, introducing plasticity on the constitutive model of the soil may be interesting. First to fully understand the effects on plasticity on the pile-soil-pile interaction and also, how possible soil weakness due to long term effects may introduce strains that are already past by the plastic frontier.

On this thesis, the effects of the dike geometry were not evaluated. Since the foundations may have large dimensions, it is important to study if common dike design practices are adequate in order to avoid failure. The dynamic nature of working wind turbines, may introduce vibrations to the soil mass that were not considered in this study. Also, the effects of wave loading on the dike were not considered. It is important to study if this effects are relevant, the wave action may lead to different frequencies other than the ones studied on this work and it is additional loading on the foundation. In The Netherlands seismic risk is very low which leads this analysis to be very often neglected. Nevertheless,

if the there is high risk of seismicity, this analysis must be held, again, for the same reasons mentioned above.

Finally, the best way to study and fully understand this problematic is to collect data from full-scale field tests performed on dynamically loaded pile groups. This analysis would enable to compare and validate the used solutions, allowing to substantially reduce the uncertainty of the methods.

Bibliography

O.A Bauchau. Modeling rotorcraft dynamics with finite element multibody procedures. In *ASME 2009 International Design Engineering Technical Conferences and Computers and Information in Engineering Conference*, pages 31–40. American Society of Mechanical Engineers, 2009.

J.E. Bowles. *Foundation analysis and design.* McGraw-Hill, fifth edition, 1998.

R.B.J Brinkgreve, E. Engin, and W.M Swolfs. *Plaxis 3D 2013 Manual.* Delft, The Netherlands, 2013.

R. Castro. *Introduction to wind energy (In Portuguese).* IST, 4th edition, 2009.

R.W. Clough and J. Penzien. *Dynamics of Structures.* McGraw-Hill, Inc, 2nd edition, 2003. ISBN 0-07-113241-4.

DINOloket, Consulted on May 2014. URL `http://www.dinoloket.nl/`.

DNV/Risø. *Guidelines for Design of Wind Turbines.* Det Norske Veritas and Wind Energy Department, RisøNational laboratory, second edition edition, 2002.

R. Dobry and G. Gazetas. Simple method for dynamic stiffness and damping of floating pile groups. *Geotechnique*, 38(4):557–574, 1988.

European Standard. *EN 1997:Eurocode 7 Geotechnical design - Part 1: General rules.* Brussels, 1997.

H. Gerritsen. What happened in 1953? the big flood in the netherlands in retrospect. *Philosophical Transactions of the Royal Society A: Mathematical, Physical and Engineering Sciences*, 363(1831):1271–1291, 2005.

P. Guedes de Melo. Valores de parâmetros de cálculo para maciços terrosos. Geotechnical works lecture notes (in Portuguese), 2012.

P. Hölscher. Dynamics piled foundation - application to on-shore wind turbines. Technical report, Delft University of Technology, 2014a.

P. Hölscher. *Soil dynamics in urban areas*, 2014b. Soil dynamics lecture notes.

American Petroleum Institute. *Recommended Practice for Planning, Designing and Constructing Fixed Offshore Platforms: Working Stress Design.* American Petroleum Institute, twenty-first edition edition, 2005.

B.J. Jonkman and L. Kilcher. Turbsim users guide version 1.06.00 (draft version). Technical Report NREL/TP-xxx-xxxx, National Renewable Energy Laboratory, Golden, Colorado, 2012.

J.M. Jonkman. Dynamics modeling and loads analysis of an offshore floating wind turbine. Technical Report NREL/TP-500-41958, National Renewable Energy Laboratory, Golden, Colorado, November 2007.

J.M. Jonkman and M. L. Buhl Jr. Fast users guide. Technical report, National Renewable Energy Laboratory, Golden, Colorado, 2005.

J.M Jonkman, S. Butterfield, W. Musial, and G. Scott. Definition of a 5-mw reference wind turbine for offshore system development. Technical Report NREL/TP-500-38060, National Renewable Energy Laboratory, Golden, Colorado, February 2009.

A.M. Kanya and E. Kausel. Dynamic behavior of pile groups. In *2nd Inter. Conf. Numer. Meth. Offshore pilling*, 1982.

A.M Kaynia and E. Kausel. Dynamics of piles and pile groups in layered soil media. *Soil Dynamics and Earthquake Engineering*, 10(8):386–401, 1991.

W. Liu and M. Novak. Dynamic response of single piles embedded in transversely isotropic layered media. *Earthquake Engineering & Structural Dynamics*, 23(11):1239–1257, 1994.

Germanischer Lloyd. Fast and adams, June 2005.

P.J. Moriarty and A. C. Hansen. Aerodyn theory manual. Technical Report NREL/EL-500-36881, National Renewable Energy Laboratory, Golden, Colorado, 2005.

H.G. Poulos. Analysis of the settlement of pile groups. *Geotechnique*, 4(3), 1968.

H.G. Poulos. Behavior of laterally loaded piles ii. pile groups. *Journal of Soil Mechanics & Foundations Div*, 1971.

P.K. Robertson. The james k. mitchell lecture: Interpretation of in-situ tests–some insights. In *Proc. 4th Int. Conf. on Geotechnical and Geophysical Site Characterization–ISC'4*, pages 3–24, 2012.

P.K. Robertson and K.L. Cabal. *Guide to cone penetration testing for geotechnical engineering.* Gregg drilling,, 5th edition, 2012.

J.A. Santos. Dinâmica de fundações. Foundation dynamics lecture notes (in Portuguese), 2002.

J.A. Santos. Fundações por estacas - acções verticais. Geotechnical works lecture notes (in Portuguese), 2008.

B. Schoenmaker. Numerical approach to machine foundation. Master thesis, TU Delft, Delft University of Technology, February 2014.

O. Schwertassek, R.and Wallrapp and A. Shabana. Flexible multibody simulation and choice of shape functions. *Nonlinear Dynamics*, 20(4):361–380, 1999. ISSN 0924-090X. doi: 10.1023/A:1008314826838.

J.F. Semblat and J.J. Brioist. Efficiency of higher order finite elements for the analysis of seismic wave propagation. *Journal of Sound and Vibration*, 231(2):460467, March 2000.

Canadian Geotechnical Society. *Canadian Foundation Engineering Manual*. Canadian Geotechnical Society, fourth edition, 2006.

IEC technical committee 88: Wind Turbines. *IEC 61400-1. Wind Turbines - Part 1: Design Requirements*. Geneva, Switzerland, third edition, 2005.

J. van der Tempel and D. Molenaar. Wind turbine structural dynamics - a review of the principles for modern power generation, onshore and offshore. *Wind Engineering*, 26 (4):211–222, 2002.

Appendix A

Natural frequency calculation using Rayleigh-Ritz analysis

$M_{hub} := 56.780\ tonnes$ – Blade mass

$M_{blade} := 17.740\ \ tonnes$ – Hub mass

$M_{nacelle} := 240.000\ \ tonnes$ – Nacelle mass

$H_{hub} := 90\ \ m$

$E_{steel} := 210 \cdot 10^{6}\ \ kPa$

$M_{total} := 3 \cdot M_{blade} + M_{hub} + M_{nacelle} = 350$ tonnes

$\phi(x) := x^{3} - 3 \cdot 84 \cdot x^{2}$

$\phi'(x) := 3\ x^{2} - x \cdot 6 \cdot 84$

$\phi''(x) := 6\ x - 6 \cdot 84$

$\rho := 8.5\ \ \frac{tonnes}{m^{3}}$

Tower Base:

$Dext_b := 6\ \ m$

$t_b := 0.027\ \ m$

$Dint_b := Dext_b - 2 \cdot t_b = 5.946\ m$

Tower Top:

$Dext_t := 3.87\ \ m$

$t_t := 0.019\ \ m$

$Dint_t := Dext_t - 2 \cdot t_t = 3.832\ m$

$m_1 := 0.023667$

$m_2 := 0.0234889$

$$D_{ext}(x) := Dext_b - m_1 \cdot x$$

$$D_{int}(x) := Dint_b - m_2 \cdot x$$

$$I(x) := \frac{\pi \cdot \left(D_{ext}(x)^{4} - D_{int}(x)^{4}\right)}{64}$$

$$A(x) := \frac{\pi \cdot \left(D_{ext}(x)^{2} - D_{int}(x)^{2}\right)}{4}$$

Stiffness:

$$K := \int_{0}^{H_{hub}} I(x)\ E_{steel} \cdot \phi''(x)^{2}\ \mathrm{d}x = 2.486 \cdot 10^{15}\ \ \frac{kN}{m}$$

Mass:

$m(x) := A(x)\ \rho$

$$M := \int_{0}^{H_{hub}} m(x) \cdot \phi(x)^{2}\ \mathrm{d}x + M_{total} \cdot \phi\left(H_{hub}\right)^{2} = 6.895 \cdot 10^{14} tonnes$$

Frequency:

$$w_n := \sqrt{\frac{K}{M}} = 1.899\ \ \frac{rad}{s} \qquad f := \frac{w_n}{2 \cdot \pi} = 0.302\ \ Hz$$

Appendix B

FAST, TurbSim and AeroDyn input files

B.1 FAST input file

```
------------------------ FAST INPUT FILE -------------------------------
      NREL 5.0 MW Baseline Wind Turbine for Use in Offshore Analysis
  Properties from Dutch Offshore Wind Energy Converter (DOWEC) 6MW Pre-
         Design (10046_009.pdf) and REpower 5M 5MW (5m_uk.pdf)
                      Compatible with FAST v6.0.
---------------------- SIMULATION CONTROL ------------------------------
False       Echo        - Echo input data to "echo.out" (flag)
   1        ADAMSPrep   - ADAMS preprocessor mode {1: Run FAST, 2: use
                          FAST as a preprocessor to create an ADAMS model
                          3: do both} (switch)
   1        AnalMode    - Analysis mode {1: Run a time-marching
                          simulation
                          2: create a periodic linearized model} (switch)
   3        NumBl       - Number of blades (-)
630.0       TMax        - Total run time (s)
0.0125      DT          - Integration time step (s)
---------------------- TURBINE CONTROL ---------------------------------
   0        YCMode      - Yaw control mode {0: none, 1: user-defined from
                          routine UserYawCont
                          2: user-defined from Simulink} (switch)
9999.9      TYCOn       - Time to enable active yaw control (s
   1        PCMode      - Pitch control mode {0: none, 1: user-defined
                          from routine PitchCntrl, 2: user-defined from
                          Simulink} (switch)
   0.0      TPCOn       - Time to enable active pitch control (s
   1        VSContrl    - Variable-speed control mode {0: none,
                          1: simpleVS
                          2: user-defined from routine UserVSCont
                          3: user-defined from Simulink} (switch)
1173.7      VS_RtGnSp   - Rated generator speed for simple variable-speed
                          generator control (HSS side) (rpm)
43093.55    VS_RtTq     - Rated generator torque/constant generator
                          torque in Region 3 for simple variable-speed
                          generator control (HSS side) (N-m
0.0255764   VS_Rgn2K    - Generator torque constant in Region 2 for
                          simple variable-speed generator control (N-
                          m/rpm^2)
9999.9E-9   VS_SlPc     - Rated generator slip percentage in Region 2 1/2
                          for simple variable-speed generator control (%)
   1        GenModel    - Generator model {1: simple, 2: Thevenin,
                          3: user-defined from routine UserGen} (switch)
True        GenTiStr    - Method to start the generator {T: timed using
                          TimGenOn, F: generator speed using SpdGenOn}
True        GenTiStp    - Method to stop the generator {T: timed using
                          TimGenOf, F: when generator power = 0}
9999.9      SpdGenOn    - Generator speed to turn on the generator for a
                          startup (HSS speed) (rpm)
   0.0      TimGenOn    - Time to turn on the generator for a startup (s)
9999.9      TimGenOf    - Time to turn off the generator (s
   1        HSSBrMode   - HSS brake model {1: simple, 2: user-defined
from
                          routine UserHSSBr} (switch)
   0        THSSBrDp    - Time to initiate deployment of the HSS brake(s)
9999.9      TiDynBrk    - Time to initiate deployment of the dynamic
                          generator brake (s)
9999.9      TTpBrDp(1)  - Time to initiate deployment of tip brake 1 (s)
9999.9      TTpBrDp(2)  - Time to initiate deployment of tip brake 2 (s)
```

```
9999.9      TTpBrDp(3)  - Time to initiate deployment of tip brake 3 (s)
9999.9      TBDepISp(1) - Deployment-initiation speed for the tip brake
                          on blade 1 (rpm)
9999.9      TBDepISp(2) - Deployment-initiation speed for the tip brake
                          on blade 2 (rpm)
9999.9      TBDepISp(3) - Deployment-initiation speed for the tip brake
                          on blade 3 (rpm)
9999.9      TYawManS    - Time to start override yaw maneuver and end
                          standard yaw control (s)
9999.9      TYawManE    - Time at which override yaw maneuver reaches
                          final yaw angle (s)
   0.0      NacYawF     - Final yaw angle for yaw maneuvers (degrees)
9999.9      TPitManS(1) - Time to start override pitch maneuver for blade
                          1 and end standard pitch control (s)
9999.9      TPitManS(2) - Time to start override pitch maneuver for blade
                          2 and end standard pitch control (s)
9999.9      TPitManS(3) - Time to start override pitch maneuver for blade
                          3 and end standard pitch control (s)
9999.9      TPitManE(1) - Time at which override pitch maneuver for blade
                          1 reaches final pitch (s)
9999.9      TPitManE(2) - Time at which override pitch maneuver for blade
                          2 reaches final pitch (s)
9999.9      TPitManE(3) - Time at which override pitch maneuver for blade
                          3 reaches final pitch (s)
  90.0      BlPitch(1)  - Blade 1 initial pitch (degrees)
  90.0      BlPitch(2)  - Blade 2 initial pitch (degrees)
  90.0      BlPitch(3)  - Blade 3 initial pitch (degrees)
  90.0      B1PitchF(1) - Blade 1 final pitch for pitch maneuvers
                          (degrees)
  90.0      B1PitchF(2) - Blade 2 final pitch for pitch maneuvers
                          (degrees)
  90.0      B1PitchF(3) - Blade 3 final pitch for pitch maneuvers
                          (degrees)
---------------------- ENVIRONMENTAL CONDITIONS -------------------------
   9.80665      Gravity     - Gravitational acceleration (m/s^2)
---------------------- FEATURE FLAGS ------------------------------------
True        FlapDOF1    - First flapwise blade mode DOF (flag)
True        FlapDOF2    - Second flapwise blade mode DOF (flag)
True        EdgeDOF     - First edgewise blade mode DOF (flag)
False       TeetDOF     - Rotor-teeter DOF (flag)
True        DrTrDOF     - Drivetrain rotational-flexibility DOF (flag)
False       GenDOF      - Generator DOF (flag)
False       YawDOF      - Yaw DOF (flag)
True        TwFADOF1    - First fore-aft tower bending-mode DOF (flag)
True        TwFADOF2    - Second fore-aft tower bending-mode DOF (flag)
True        TwSSDOF1    - First side-to-side tower bending-mode DOF
True        TwSSDOF2    - Second side-to-side tower bending-mode DOF
True        CompAero    - Compute aerodynamic forces (flag)
False       CompNoise   - Compute aerodynamic noise (flag)
---------------------- INITIAL CONDITIONS -------------------------------
   0.0      OoPDefl     - Initial out-of-plane blade-tip displacement (m)
   0.0      IPDefl      - Initial in-plane blade-tip deflection (m)
   0.0      TeetDefl    - Initial or fixed teeter angle (degrees)
   0.0      Azimuth     - Initial azimuth angle for blade 1 (m)
   0.0      RotSpeed    - Initial or fixed rotor speed (rpm)
   0.0      NacYaw      - Initial or fixed nacelle-yaw angle (m)
   0.0      TTDspFA     - Initial fore-aft tower-top displacement (m)
```

```
   0.0      TTDspSS     - Initial side-to-side tower-top displacement (m)
---------------------- TURBINE CONFIGURATION --------------------------
  63.0      TipRad      - The distance from the rotor apex to the blade
                          tip (m)
   1.5      HubRad      - The distance from the rotor apex to the blade
                          root (m)
   1        PSpnElN     - Number of the innermost blade element which is
                          still part of the pitchable portion of the
                          blade for partial-span pitch control [1 to
                          BldNodes]
   0.0      UndSling    - Undersling length [distance from teeter pin to
                          the rotor apex] (m)
   0.0      HubCM       - Distance from rotor apex to hub mass [positive
                          downwind] (m)
  -5.01910  OverHang    - Distance from yaw axis to rotor apex [3 blades]
                          or teeter pin [2 blades] (m)
   1.9      NacCMxn     - Downwind distance from the tower-top to the
                          nacelle CM (m)
   0.0      NacCMyn     - Lateral  distance from the tower-top to the
                          nacelle CM (m)
   1.75     NacCMzn     - Vertical distance from the tower-top to the
                          nacelle CM (m)
   87.6     TowerHt     - Height of tower above ground level [onshore] or
                          MSL [offshore] (m)
   1.96256  Twr2Shft    - Vertical distance from the tower-top to the
                          rotor shaft (m)
   0.0      TwrRBHt     - Tower rigid base height (m)
  -5.0      ShftTilt    - Rotor shaft tilt angle (degrees)
   0.0      Delta3      - Delta-3 angle for teetering rotors (degrees)
  -2.5      PreCone(1)  - Blade 1 cone angle (degrees)
  -2.5      PreCone(2)  - Blade 2 cone angle (degrees)
  -2.5      PreCone(3)  - Blade 3 cone angle (degrees)
   0.0      AzimB1Up    - Azimuth value to use for I/O when blade 1
                          points up (degrees)
---------------------- MASS AND INERTIA -------------------------------
   0.0      YawBrMass   - Yaw bearing mass (kg)
 240.00E3   NacMass     - Nacelle mass (kg)
  56.78E3   HubMass     - Hub mass (kg)
   0.0      TipMass(1)  - Tip-brake mass, blade 1 (kg)
   0.0      TipMass(2)  - Tip-brake mass, blade 2 (kg)
   0.0      TipMass(3)  - Tip-brake mass, blade 3 (kg)
2607.89E3   NacYIner    - Nacelle inertia about yaw axis (kg m^2)
 534.116    GenIner     - Generator inertia about HSS (kg m^2)
 115.926E3  HubIner     - Hub inertia about rotor axis [3 blades] or
                          teeter axis [2 blades] (kg m^2)
---------------------- DRIVETRAIN -------------------------------------
 100.0      GBoxEff     - Gearbox efficiency (%)
  94.4      GenEff      - Generator efficiency [ignored by the Thevenin
                          and user-defined generator models] (%)
  97.0      GBRatio     - Gearbox ratio (-)
False       GBRevers    - Gearbox reversal {T: if rotor and generator
                          rotate in opposite directions} (flag)
  28.1162E3 HSSBrTqF    - Fully deployed HSS-brake torque (N-m)
   0.6      HSSBrDT     - Time for HSS-brake to reach full deployment
                          once initiated (sec)
            DynBrkFi    - File containing a mech-gen-torque vs HSS-speed
                          curve for a dynamic brake [CURRENTLY IGNORED]
```

```
 867.637E6  DTTorSpr    - Drivetrain torsional spring (N-m/rad)
   6.215E6  DTTorDmp    - Drivetrain torsional damper (N-m/(rad/s))
---------------------- SIMPLE INDUCTION GENERATOR ----------------------
9999.9      SIG_SlPc    - Rated generator slip percentage (%)
9999.9      SIG_SySp    - Synchronous (zero-torque) generator speed (rpm)
9999.9      SIG_RtTq    - Rated torque (N-m)
9999.9      SIG_PORt    - Pull-out ratio (Tpullout/Trated) (-)
---------------------- THEVENIN-EQUIVALENT INDUCTION GENERATOR ----------
9999.9      TEC_Freq    - Line frequency [50 or 60] (Hz)
9998        TEC_NPol    - Number of poles [even integer > 0] (-)
9999.9      TEC_SRes    - Stator resistance (ohms)
9999.9      TEC_RRes    - Rotor resistance (ohms)
9999.9      TEC_VLL     - Line-to-line RMS voltage (volts)
9999.9      TEC_SLR     - Stator leakage reactance (ohms)
9999.9      TEC_RLR     - Rotor leakage reactance (ohms)
9999.9      TEC_MR      - Magnetizing reactance (ohms)
---------------------- PLATFORM -----------------------------------------
   0        PtfmModel   - Platform model {0: none, 1: onshore,
                          2: fixed bottom offshore
                          3: floating offshore} (switch)
"Platform.dat" PtfmFile - Name of file containing platform properties
---------------------- TOWER --------------------------------------------
  20        TwrNodes    - Number of tower nodes used for analysis (-)
"NRELOffshrBsline5MW_Tower_Onshore.dat"  TwrFile     - Name of file
                          containing tower properties
---------------------- NACELLE-YAW --------------------------------------
9028.32E6   YawSpr      - Nacelle-yaw spring constant (N-m/rad)
  19.16E6   YawDamp     - Nacelle-yaw damping constant (N-m/(rad/s))
                             0.0      YawNeut     - Neutral yaw position-
                          -yaw spring force is zero at this yaw (degrees)
---------------------- FURLING ------------------------------------------
False       Furling     - Read in additional model properties for furling
                          turbine (flag)
            FurlFile    - Name of file containing furling properties
---------------------- ROTOR-TEETER -------------------------------------
   0        TeetMod     - Rotor-teeter spring/damper model {0: none,
                          1: standard,
                          2: user-defined from routine UserTeet}
   0.0      TeetDmpP    - Rotor-teeter damper position (degrees)
   0.0      TeetDmp     - Rotor-teeter damping constant (N-m/(rad/s))
   0.0      TeetCDmp    - Rotor-teeter rate-independent Coulomb-damping
                          moment (N-m)
   0.0      TeetSStP    - Rotor-teeter soft-stop position (degrees)
   0.0      TeetHStP    - Rotor-teeter hard-stop position (degrees)
   0.0      TeetSSSp    - Rotor-teeter soft-stop linear-spring constant
                          (N-m/rad)
   0.0      TeetHSSp    - Rotor-teeter hard-stop linear-spring constant
                          (N-m/rad)
---------------------- TIP-BRAKE ----------------------------------------
   0.0      TBDrConN    - Tip-brake drag constant during normal
                          operation, Cd*Area (m^2)
   0.0      TBDrConD    - Tip-brake drag constant during fully-deployed
                          operation, Cd*Area (m^2)
   0.0      TpBrDT      - Time for tip-brake to reach full deployment
                          once released (sec)
---------------------- BLADE --------------------------------------------
"NRELOffshrBsline5MW_Blade.dat"    BldFile(1)  - Name of file containing
```

```
                                                    properties for blade 1
"NRELOffshrBsline5MW_Blade.dat"    BldFile(2)   - Name of file containing
                                                    properties for blade 2
"NRELOffshrBsline5MW_Blade.dat"    BldFile(3)   - Name of file containing
                                                    properties for blade 3
---------------------- AERODYN -------------------------------------------
"NRELOffshrBsline5MW_AeroDyn.ipt"  ADFile       - Name of file containing
                                                    AeroDyn input parameters
---------------------- NOISE ---------------------------------------------
                                   NoiseFile    - Name of file containing
                                       aerodynamic noise input parameters
---------------------- ADAMS ---------------------------------------------
"NRELOffshrBsline5MW_ADAMSSpecific.dat" ADAMSFile - Name of file
                              containing ADAMS-specific input parameters
---------------------- LINEARIZATION CONTROL -----------------------------
"NRELOffshrBsline5MW_Linear.dat"   LinFile      - Name of file containing
                                                 FAST linearization parameters
---------------------- OUTPUT --------------------------------------------
True        SumPrint    - Print summary data to "<RootName>.fsm" (flag)
1           OutFileFmt  - Format for tabular (time-marching) output
                          file(s)(1: text file [<RootName>.out],
                          2: binary file [<RootName>.outb], 3: both)
True        TabDelim    - Generate a tab-delimited tabular output file
"ES10.3E2"  OutFmt      - Format used for tabular output except time.
   30.0      TStart     - Time to begin tabular output (s)
   4        DecFact     - Decimation factor for tabular output {1: output
                          every time step} (-)
   1.0      SttsTime    - Amount of time between screen status messages
                          (s)
  -3.09528  NcIMUxn     - Downwind distance from the tower-top to the
                          nacelle IMU (m)
   0.0      NcIMUyn     - Lateral  distance from the tower-top to the
                          nacelle IMU (m)
   2.23336  NcIMUzn     - Vertical distance from the tower-top to the
                          nacelle IMU (m)
   1.912    ShftGagL    - Distance from rotor apex [3 blades] or
                          teeter pin [2 blades] to shaft strain gages (m)
   0        NTwGages    - Number of tower nodes that have strain gages
                          for output [0 to 9] (-)
            TwrGagNd    - List of tower nodes that have strain gages
                          [1 to TwrNodes] (-)
   0        NBlGages    - Number of blade nodes that have strain gages
                          for output [0 to 9] (-)
 5,9,13     BldGagNd    - List of blade nodes that have strain gages
                          [1 to BldNodes] (-)
            OutList     - The next line(s) contains a list of output
parameters.  See OutList.txt for a listing of available output channels:

"TwrBsFxt,TwrBsFyt,TwrBsFzt,TwrBsMxt,TwrBsMyt,TwrBsMzt"  - Tower Base
Loads
"PtfmFxt,PtfmFyt,PtfmFzt,PtfmMxt,PtfmMyt,PtfmMzt"  - Support platform
Loads
"LSSTipVxa"                                        - Rotor speed
END of FAST input file (the word "END" must appear in the first 3 columns
of this last line).
---------------------------------------------------------------------------
```

B.2 TurbSim input file

```
            TurbSim Input File. Valid for TurbSim v1.06.00
---------Runtime Options-----------------------------------------------
2318682    RandSeed1    - First random seed  (-2147483648 to 2147483647)
RANLUX     RandSeed2    - Second random seed (-2147483648 to 2147483647)
                          for intrinsic pRNG, or an alternative pRNG:
                          "RanLux" or "RNSNLW"
False      WrBHHTP      - Output hub-height turbulence parameters in
                          binary form?  (Generates RootName.bin)
False      WrFHHTP      - Output hub-height turbulence parameters in
                          formatted form?  (Generates RootName.dat)
False      WrADHH       - Output hub-height time-series data in AeroDyn
                          form?  (Generates RootName.hh)
False      WrADFF       - Output full-field time-series data in
                          TurbSim/AeroDyn form? (Generates Rootname.bts)
True       WrBLFF       - Output full-field time-series data in
                          BLADED/AeroDyn form?  (Generates RootName.wnd)
False      WrADTWR      - Output tower time-series data?
                          (Generates RootName.twr)
False      WrFMTFF      - Output full-field time-series data in formatted
                          (readable) form? (Generates RootName.u,
                          RootName.v, RootName.w)
False      WrACT        - Output coherent turbulence time steps in
                          AeroDyn form? (Generates RootName.cts)
True       Clockwise    - Clockwise rotation looking downwind?
 0         ScaleIEC     - Scale IEC turbulence models to exact target
                          standard deviation? [0=no additional scaling;
                          1=use hub scale uniformly;
                          2=use individual scales]
--------Turbine/Model Specifications----------------------------------
13         NumGrid_Z    - Vertical grid-point matrix dimension
13         NumGrid_Y    - Horizontal grid-point matrix dimension
0.0125     TimeStep     - Time step [seconds]
660        AnalysisTime - Length of analysis time series [seconds]
                          (program will add time if necessary:
                          AnalysisTime= MAX(AnalysisTime,
                          UsableTime+GridWidth/MeanHHWS))
630        UsableTime   - Usable length of output time series [seconds]
                          (program will add GridWidth/MeanHHWS seconds)
90         HubHt        - Hub height [m] (should be > 0.5*GridHeight)
150.00     GridHeight   - Grid height [m]
150.00     GridWidth    - Grid width [m] (should be >= 2*(RotorRadius+
                          ShaftLength))
0          VFlowAng     - Vertical mean flow (uptilt) angle [degrees]
0          HFlowAng     - Horizontal mean flow (skew) angle [degrees]
--------Meteorological Boundary Conditions-------------------------------
--
"IECKAI"   TurbModel    - Turbulence model ("IECKAI"=Kaimal,
                          "IECVKM"=von Karman, "GP_LLJ", "NWTCUP",
                          "SMOOTH", "WF_UPW", "WF_07D", "WF_14D",
                          "TIDAL", or "NONE")
"1-ED3"    IECstandard  - Number of IEC 61400-x standard (x=1,2, or 3
                          with optional 61400-1 edition number (i.e. "1-
                          Ed2"))
"A"        IECturbc     - IEC turbulence characteristic ("A", "B", "C" or
                          the turbulence intensity in percent) ("KHTEST"
                     option with NWTCUP model, not used for other models)
```

```
"NTM"      IEC_WindType - IEC turbulence type ("NTM"=normal,
                          "xETM"=extreme turbulence, "xEWM1"=extreme 1-
                          year wind,"xEWM50"=extreme 50-year wind, where
                          x=wind turbine class 1, 2, or 3)
default    ETMc         - IEC Extreme Turbulence Model "c" parameter[m/s]
default    WindProfileType - Wind profile type ("JET";"LOG"=logarithmic;
                          "PL"=power law;"H2L"=Log law for TIDAL spectral
                          model;"IEC"=PL on rotor disk, LOG elsewhere;
                          or "default")
90         RefHt        - Height of the reference wind speed [m]
33.4       URef         - Mean (total) wind speed at the reference height
                          [m/s] (or "default" for JET wind profile)
default    ZJetMax      - Jet height [m] (used only for JET wind profile,
                          valid 70-490 m)
default    PLExp        - Power law exponent [-] (or "default")
default    Z0           - Surface roughness length [m] (or "default")
--------Non-IEC Meteorological Boundary Conditions------------------------
default    Latitude     - Site latitude [degrees] (or "default")
0.05       RICH_NO      - Gradient Richardson number
default    UStar        - Friction or shear velocity [m/s] (or "default")
default    ZI           - Mixing layer depth [m] (or "default")
default    PC_UW        - Hub mean u'w' Reynolds stress (or "default")
default    PC_UV        - Hub mean u'v' Reynolds stress (or "default")
default    PC_VW        - Hub mean v'w' Reynolds stress (or "default")
default    IncDec1      - u-component coherence parameters (e.g. "10.0
                          0.3e-3" in quotes) (or "default")
default    IncDec2      - v-component coherence parameters (e.g. "10.0
                          0.3e-3" in quotes) (or "default")
default    IncDec3      - w-component coherence parameters (e.g. "10.0
                          0.3e-3" in quotes) (or "default")
default    CohExp       - Coherence exponent (or "default")
--------Coherent Turbulence Scaling Parameters---------------------------
"M:\coh_events\eventdata"  CTEventPath     - Name of the path where event
                                             data files are located
"Random"   CTEventFile  - Type of event files ("LES", "DNS", or "RANDOM")
true       Randomize    - Randomize the disturbance scale and locations?
                          (true/false)
 1.0       DistScl      - Disturbance scale (ratio of wave height to
                          rotor disk). (Ignored when Randomize = true.)
 0.5       CTLy         - Fractional location of tower centerline from
                    right (looking downwind) to left side of the dataset.
 0.5       CTLz         - Fractional location of hub height from the
                          bottom of the dataset. (Ignored when Randomize
                          = true.)
30.0       CTStartTime  - Minimum start time for coherent structures in
                          RootName.cts [seconds]
================================================================================
             NOTE: Do not add or remove any lines in this file!
================================================================================
```

B.3 AeroDyn input file

```
       NREL 5.0 MW offshore baseline aerodynamic input properties;
                    Compatible with AeroDyn v12.58.
SI          SysUnits    - System of units for used for input and output
                          [must be SI for FAST] (unquoted string)
BEDDOES     StallMod    - Dynamic stall included [BEDDOES or STEADY]
NO_CM       UseCm       - Use aerodynamic pitching moment model?
                          [USE_CM or NO_CM] (unquoted string)
EQUIL       InfModel    - Inflow model [DYNIN or EQUIL] (unquoted string)
SWIRL       IndModel    - Induction-factor model [NONE or WAKE or SWIRL]
                           0.005      AToler      - Induction-factor
                          tolerance (convergence criteria)
PRANDtl     TLModel     - Tip-loss model (EQUIL only) [PRANDtl, GTECH, or
                          NONE] (unquoted string)
PRANDtl     HLModel     - Hub-loss model (EQUIL only) [PRANdtl or NONE]
"33.4ms.wnd" WindFile    - Name of file containing wind data
  90.0      HH          - Wind reference (hub) height
                          [TowerHt+Twr2Shft+OverHang*SIN(ShftTilt)] (m)
   0.0      TwrShad     - Tower-shadow velocity deficit (-)
9999.9      ShadHWid    - Tower-shadow half width (m)
9999.9      T_Shad_Refpt- Tower-shadow reference point (m)
   1.225    AirDens     - Air density (kg/m^3)
   1.464E-5 KinVisc     - Kinematic air viscosity [CURRENTLY IGNORED]
                          (m^2/sec)
   0.0125   DTAero      - Time interval for aerodynamic calculations
(sec)
   8        NumFoil     - Number of airfoil files (-)
"Cylinder1.dat"  FoilNm - Names of the airfoil files [NumFoil lines]
"Cylinder2.dat"
"DU40_A17.dat"
"DU35_A17.dat"
"DU30_A17.dat"
"DU25_A17.dat"
"DU21_A17.dat"
"NACA64_A17.dat"
  62        BldNodes    - Number of blade nodes used for analysis (-)
RNodes   AeroTwst  DRNodes  Chord    NFoil  PrnElm
2.000000 13.308000 1.000000 3.542000 1 NOPRINT
3.000000 13.308000 1.000000 3.557216 1 NOPRINT
4.000000 13.308000 1.000000 3.671364 1 NOPRINT
5.000000 13.308000 1.000000 3.785511 1 NOPRINT
6.000000 13.308000 1.000000 3.899805 1 NOPRINT
7.000000 13.308000 1.000000 4.014319 1 NOPRINT
8.000000 13.308000 1.000000 4.128833 1 NOPRINT
9.000000 13.308000 1.000000 4.243101 2 NOPRINT
10.000000 13.308000 1.000000 4.357246 2 NOPRINT
11.000000 13.308000 1.000000 4.471391 2 NOPRINT
12.000000 13.196537 1.000000 4.562793 3 NOPRINT
13.000000 12.750683 1.000000 4.585963 3 NOPRINT
14.000000 12.304829 1.000000 4.609134 3 NOPRINT
15.000000 11.858976 1.000000 4.632305 3 NOPRINT
16.000000 11.431780 1.000000 4.644902 4 NOPRINT
17.000000 11.110317 1.000000 4.597585 4 NOPRINT
18.000000 10.788854 1.000000 4.550268 4 NOPRINT
19.000000 10.467390 1.000000 4.502951 4 NOPRINT
20.000000 10.147963 1.000000 4.455451 4 NOPRINT
21.000000 9.867232 1.000000 4.404476 4 NOPRINT
22.000000 9.586500 1.000000 4.353500 4 NOPRINT
```

```
23.000000 9.305768 1.000000 4.302524 4 NOPRINT
24.000000 9.025037 1.000000 4.251549 4 NOPRINT
25.000000 8.729244 1.000000 4.192927 5 NOPRINT
26.000000 8.432659 1.000000 4.133902 5 NOPRINT
27.000000 8.136073 1.000000 4.074878 5 NOPRINT
28.000000 7.839488 1.000000 4.015854 5 NOPRINT
29.000000 7.535646 1.000000 3.953305 6 NOPRINT
30.000000 7.230524 1.000000 3.890134 6 NOPRINT
31.000000 6.925402 1.000000 3.826963 6 NOPRINT
32.000000 6.620280 1.000000 3.763793 6 NOPRINT
33.000000 6.327598 1.000000 3.703000 6 NOPRINT
34.000000 6.039061 1.000000 3.643000 6 NOPRINT
35.000000 5.750524 1.000000 3.583000 6 NOPRINT
36.000000 5.461988 1.000000 3.523000 6 NOPRINT
37.000000 5.175037 1.000000 3.463000 7 NOPRINT
38.000000 4.888939 1.000000 3.403000 7 NOPRINT
39.000000 4.602841 1.000000 3.343000 7 NOPRINT
40.000000 4.316744 1.000000 3.283000 7 NOPRINT
41.000000 4.045402 1.000000 3.223000 7 NOPRINT
42.000000 3.786134 1.000000 3.163000 7 NOPRINT
43.000000 3.526866 1.000000 3.103000 7 NOPRINT
44.000000 3.267598 1.000000 3.043000 7 NOPRINT
45.000000 3.036537 1.000000 2.983000 8 NOPRINT
46.000000 2.839951 1.000000 2.923000 8 NOPRINT
47.000000 2.643366 1.000000 2.863000 8 NOPRINT
48.000000 2.446780 1.000000 2.803000 8 NOPRINT
49.000000 2.251305 1.000000 2.743000 8 NOPRINT
50.000000 2.057890 1.000000 2.683000 8 NOPRINT
51.000000 1.864476 1.000000 2.623000 8 NOPRINT
52.000000 1.671061 1.000000 2.563000 8 NOPRINT
53.000000 1.477488 1.000000 2.503000 8 NOPRINT
54.000000 1.283441 1.000000 2.443001 8 NOPRINT
55.000000 1.089395 1.000000 2.383001 8 NOPRINT
56.000000 0.895348 1.000000 2.323002 8 NOPRINT
57.000000 0.712699 1.000000 2.243795 8 NOPRINT
58.000000 0.532331 1.000000 2.160745 8 NOPRINT
59.000000 0.360341 1.000000 2.061597 8 NOPRINT
60.000000 0.263755 1.000000 1.817570 8 NOPRINT
61.000000 0.167168 1.000000 1.573543 8 NOPRINT
62.000000 0.077559 1.000000 1.038267 8 NOPRINT
62.750000 0.019390 0.500000 0.259567 8 NOPRINT
```

Appendix C

Pile pre-design

Foundation Design

- Soil parameters:

$$\phi' := \begin{bmatrix} 39 \\ 0 \\ 33 \end{bmatrix} ^\circ \qquad c' := \begin{bmatrix} 0.001 \\ 200 \\ 0.001 \end{bmatrix} kPa \qquad \gamma_{soil} := \begin{bmatrix} 20 \\ 18 \\ 19 \end{bmatrix} \frac{kN}{m^3} \qquad \gamma_w := 10 \frac{kN}{m^3}$$

$$h_{layer} := \begin{bmatrix} 10.7 \\ 4 \end{bmatrix} m \qquad h_w := 8.7\ m$$

- Foundation parameters:

$$D_p := 0.8\ m \qquad l_p := 21\ m \qquad D_f := 20\ m \qquad n_p := 24$$

$$A_b := \pi \cdot \left(\frac{D_p}{2} \right)^2$$

$$A_s := \begin{bmatrix} \text{if } l_p < h_{layer_1} \\ \quad \pi \cdot D_p \cdot l_p \\ \text{else} \\ \quad \pi \cdot D_p \cdot h_{layer_1} \end{bmatrix} \quad \begin{bmatrix} \text{if } l_p \le h_{layer_1} \\ \quad 0 \\ \text{else if } h_{layer_1} < l_p < h_{layer_1} + h_{layer_2} \\ \quad \pi \cdot D_p \cdot \left(l_p - h_{layer_1} \right) \\ \text{else} \\ \quad \pi \cdot D_p \cdot h_{layer_2} \end{bmatrix} \quad \begin{bmatrix} \text{if } l_p < h_{layer_1} + h_{layer_2} \\ \quad 0 \\ \text{else} \\ \quad \pi \cdot D_p \cdot \left(l_p - h_{layer_1} - h_{layer_2} \right) \end{bmatrix}$$

- Initial design:

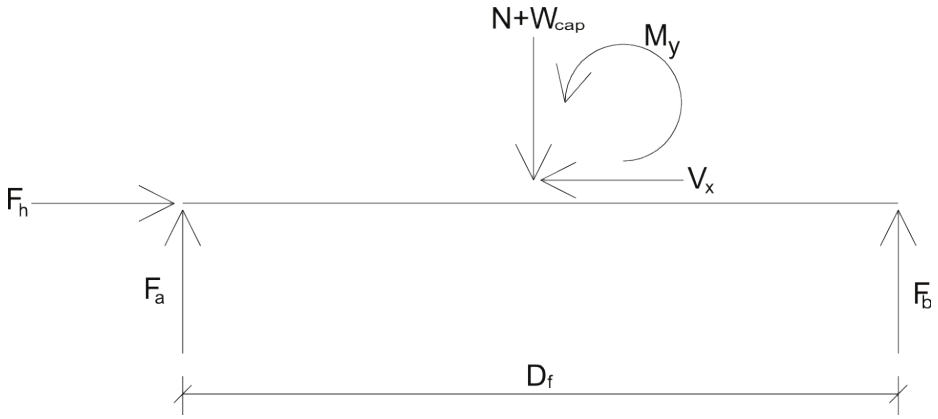

Forces on the cap:

$N := 6975\ kN$ $M_y := 104700\ kN \cdot m$ $V_x := 1173\ kN$

$\gamma_c := 25\ \frac{kN}{m^3}$ $t_c := 2\ m$ $V_{cap} := \pi \cdot \left(\frac{D_f}{2}\right)^2 \cdot t_c = 628.319\ m^3$

$W_{cap} := \gamma_c \cdot V_{cap} = \left(1.571 \cdot 10^4\right)\ kN$

The force on a pile can be written as the sum of normal and weight forces(Fj;G) and the aditional vertical force caused by the bending moment(Fj;M), for example, Fa can be written as:

Fa=Fa;G+Fa,M

Where,

$F_{a;G} := \frac{N + W_{cap}}{2}$

Aditional vertical force due to bending moment Fa;M:

$F_{a;M} := \frac{M_y}{D_f} = \left(5.235 \cdot 10^3\right)\ kN$

Forces on a single pile head:

All piles are assumed carry the same vertical force due to weight and normal force:

$F_G := \frac{N + W_{cap}}{n_p} = 945.123\ kN$

Force distribution due to the bending moment:

$j := 1, 2 .. \frac{n_p}{2}$

$y_{1,j} := \frac{D_f}{2} \cdot \sin\left(\pi \cdot \frac{j-1}{0.5 \cdot n_p}\right)$ $y_{2_{1,j}} := \frac{D_f}{2} \cdot \sin\left(\pi \cdot \frac{j}{0.5 \cdot n_p + 1}\right)$

$\theta_{1,j} := \operatorname{asin}\left(\operatorname{abs}\left(\frac{y_{1,j}}{\frac{D_f}{2}}\right)\right)$ $\theta_{2_{1,j}} := \operatorname{asin}\left(\operatorname{abs}\left(\frac{y_{2_{1,j}}}{\frac{D_f}{2}}\right)\right)$

The maximum force that a pile is subjected to due to the bending moment:

$$F_{M;max} := \frac{F_{a;M}}{min\left(\left(\sum_{j=1}^{\frac{n_p}{2}} \left(\sin\left(\theta_{1,j}\right)\right)^2, \sum_{j=1}^{\frac{n_p}{2}} \left(\sin\left(\theta 2_{1,j}\right)\right)^2\right)\right)} = 872.5\ kN$$

$$F_{vp;max} := F_G + F_{M;max} = \left(1.818 \cdot 10^3\right)\ kN$$

$$F_{vp;min} := F_G - F_{M;max} = 72.623\ kN$$

It can be concluded that all piles are always under compression.

Single pile axial resistance:

Tip resistance:

$$u := \begin{cases} 0 & \text{if } l_p < h_w \\ \gamma_w \cdot \langle l_p - h_w \rangle & \text{otherwise} \end{cases}$$

$$\sigma'_0 := \begin{cases} \gamma_{soil_1} \cdot l_p - u & \text{if } l_p \le h_{layer_1} \\ \gamma_{soil_1} \cdot h_{layer_1} + \gamma_{soil_2} \cdot \left(l_p - h_{layer_1}\right) - u & \text{if } h_{layer_1} < l_p < h_{layer_1} + h_{layer_2} \\ \gamma_{soil_1} \cdot h_{layer_1} + \gamma_{soil_2} \cdot h_{layer_2} + \gamma_{soil_3} \cdot \left(l_p - h_{layer_1} - h_{layer_2}\right) - u & \text{otherwise} \end{cases}$$

$$N_q := \begin{cases} \left(\frac{1+\sin\left(\phi'_1\right)}{1-\sin\left(\phi'_1\right)}\right) \cdot e^{\pi \cdot \tan\left(\phi'_1\right)} & \text{if } l_p \le h_{layer_1} \\ \left(\frac{1+\sin\left(\phi'_2\right)}{1-\sin\left(\phi'_2\right)}\right) \cdot e^{\pi \cdot \tan\left(\phi'_2\right)} & \text{else if } h_{layer_1} < l_p < h_{layer_1} + h_{layer_2} \\ \left(\frac{1+\sin\left(\phi'_3\right)}{1-\sin\left(\phi'_3\right)}\right) \cdot e^{\pi \cdot \tan\left(\phi'_3\right)} & \text{else} \end{cases}$$

– Sokolovski (1960)

$N_c := 9$ – Value sugested by several authors

$$R_b := \begin{cases} A_b \cdot \left(c'_1 \cdot N_c + \sigma'_0 \cdot N_q\right) & \text{if } l_p \le h_{layer_1} \\ A_b \cdot \left(c'_2 \cdot N_c + \sigma'_0 \cdot N_q\right) & \text{else if } h_{layer_1} < l_p < h_{layer_1} + h_{layer_2} \\ A_b \cdot \left(c'_3 \cdot N_c + \sigma'_0 \cdot N_q\right) & \text{else} \end{cases} = \left(3.708 \cdot 10^3\right)\ kN$$

Shaft resistance:

$$\delta := \phi' \cdot \frac{2}{3} = \begin{bmatrix} 26 \\ 0 \\ 22 \end{bmatrix} \circ$$

$K := 1$ – Coefficient of lateral earth pressure. It varies from 0.8 to 1 accoring to API (2000) 0.8 if the pile is open–ended and 1 if closed–ended.

$$\sigma'_{vmed} := \text{if } l_p \le h_{layer_1}$$

$$\begin{bmatrix} \dfrac{\gamma_{soil_1} \cdot l_p - u}{2} \\ 0 \\ 0 \end{bmatrix}$$

$$\text{else if } h_{layer_1} < l_p < h_{layer_1} + h_{layer_2}$$

$$\begin{bmatrix} \dfrac{\gamma_{soil_1} \cdot h_{layer_1} - \gamma_w \cdot \left(h_{layer_1} - h_w\right)}{2} \\ \dfrac{\left(\gamma_{soil_1} \cdot h_{layer_1} - \gamma_w \cdot \left(h_{layer_1} - h_w\right)\right) + \left(\gamma_{soil_1} \cdot h_{layer_1} + \gamma_{soil_2} \cdot \left(l_p - h_{layer_1}\right) - u\right)}{2} \\ 0 \end{bmatrix}$$

$$\text{else}$$

$$\begin{bmatrix} \dfrac{\gamma_{soil_1} \cdot h_{layer_1} - \gamma_w \cdot \left(h_{layer_1} - h_w\right)}{2} \\ \dfrac{2 \cdot \gamma_{soil_1} \cdot h_{layer_1} - \gamma_w \cdot \left(h_{layer_1} - h_w\right) + \gamma_{soil_2} \cdot h_{layer_2} - \gamma_w \cdot \left(h_{layer_1} + h_{layer_2} - h_w\right)}{2} \\ \dfrac{2 \cdot \gamma_{soil_1} \cdot h_{layer_1} + 2 \cdot \gamma_{soil_2} \cdot h_{layer_2} - \gamma_w \cdot \left(h_{layer_1} + h_{layer_2} - h_w\right) + \gamma_{soil_3} \cdot \left(l_p - h_{layer_1} - h_{layer_2}\right) - u}{2} \end{bmatrix}$$

$\psi := \text{if } l_p \le h_{layer_1}$ — API (2000)

$$\begin{bmatrix} \dfrac{c'_1}{\sigma'_{vmed_1}} & 0.1 & 0.1 \end{bmatrix}$$

$$\text{else if } h_{layer_1} < l_p < h_{layer_1} + h_{layer_2}$$

$$\begin{bmatrix} \dfrac{c'_1}{\sigma'_{vmed_1}} & \dfrac{c'_2}{\sigma'_{vmed_2}} & 0.1 \end{bmatrix}$$

$$\text{else}$$

$$\begin{bmatrix} \dfrac{c'_1}{\sigma'_{vmed_1}} & \dfrac{c'_2}{\sigma'_{vmed_2}} & \dfrac{c'_3}{\sigma'_{vmed_3}} \end{bmatrix}$$

$$\alpha_1 := \text{if } \psi_{1,1} \le 1 \quad \| \text{return } 0.5 \cdot \psi_{1,1}^{-0.5} \quad \text{else if } \psi_{1,1} > 1 \quad \| \text{return } 0.5 \cdot \psi_{1,1}^{-0.25}$$

$$\alpha_2 := \text{if } \psi_{1,2} \le 1 \quad \| \text{return } 0.5 \cdot \psi_{1,2}^{-0.5} \quad \text{else if } \psi_{1,2} > 1 \quad \| \text{return } 0.5 \cdot \psi_{1,2}^{-0.25}$$

$$\alpha_3 := \text{if } \psi_{1,3} \le 1 \quad \| \text{return } 0.5 \cdot \psi_{1,3}^{-0.5} \quad \text{else if } \psi_{1,3} > 1 \quad \| \text{return } 0.5 \cdot \psi_{1,3}^{-0.25}$$

$$\alpha := \begin{bmatrix} \alpha_1 \\ \alpha_2 \\ \alpha_3 \end{bmatrix}$$

$$R_{s;1} := A_{s_{1,1}} \cdot \left(\alpha_1 \cdot c'_1 + K \cdot \sigma'_{vmed_1} \cdot \tan\left(\delta_1\right) \right)$$

$$R_{s;2} := A_{s_{1,2}} \cdot \left(\alpha_2 \cdot c'_2 + K \cdot \sigma'_{vmed_2} \cdot \tan\left(\delta_2\right) \right)$$

$$R_{s;3} := A_{s_{1,3}} \cdot \left(\alpha_3 \cdot c'_3 + K \cdot \sigma'_{vmed_3} \cdot \tan\left(\delta_3\right) \right)$$

$$R_s := R_{s;1} + R_{s;2} + R_{s;3} = \left(3.938 \cdot 10^3\right)\ kN$$

$$R_t := R_b + R_s = \left(7.645 \cdot 10^3\right)\ kN$$

$$S := \text{if } F_{vp;max} < R_t \quad \| \text{return “Security verified”} \quad \text{else} \quad \| \text{“Security not verified”} \quad = \text{“Security verified”}$$

Partial security factors:

Actions:

$\gamma_{G;unf} := [1.35 \;\; 1.0]$ $\gamma_{G;fav} := [1.0 \;\; 1.0]$

$\gamma_{Q;unf} := [1.5 \;\; 1.3]$ $\gamma_{Q;fav} := [0 \;\; 0]$

Soil:

$\gamma_{\phi'} := [1.0 \;\; 1.25]$ $\gamma_{c'} := [1.0 \;\; 1.25]$ $\gamma_{cu} := [1.0 \;\; 1.4]$

Resistance: Note: This values apply to driven piles

$\gamma_b := [1.0 \;\; 1.1 \;\; 1.0 \;\; 1.3]$ $\gamma_{s;c} := [1.0 \;\; 1.1 \;\; 1.0 \;\; 1.3]$

$\gamma_t := [1.0 \;\; 1.1 \;\; 1.0 \;\; 1.3]$ $\gamma_{s;t} := [1.25 \;\; 1.15 \;\; 1.1 \;\; 1.6]$

Design Approaches:

Design Approach 1:

Combination 1: A1+M1+R1

Combination 2: A2+(M1 or M2)+R4 – M1 is for vertical loading
M2 is for lateral loading or negative friction

Design Approach 2:

A1+M1+R2

Design Approach 3:

(A1 or A2)+M2+R3

A1 is for structural actions
A2 is for geotechnical actions

Applying security coefficients:

- Design approach 1 – Combination 1:

$$F_{vd;1.1} := F_G \cdot \gamma_{G;unf_{1,1}} + F_{vp;max} \cdot \gamma_{Q;unf_{1,1}} = \left\langle 4.002 \cdot 10^3 \right\rangle \ kN$$

$$\phi'_d := \operatorname{atan}\left(\frac{\tan(\phi')}{\gamma_{\phi'_{1,1}}}\right) = \begin{bmatrix} 39 \\ 0 \\ 33 \end{bmatrix} ^\circ \qquad c'_d := \frac{c'}{\gamma_{c'_{1,1}}} = \begin{bmatrix} 0.001 \\ 200 \\ 0.001 \end{bmatrix} kPa$$

$$\delta_d := \operatorname{atan}\left(\frac{\tan(\delta)}{\gamma_{\phi'_{1,1}}}\right) = \begin{bmatrix} 26 \\ 0 \\ 22 \end{bmatrix} ^\circ$$

$$N_{qd} := \begin{cases} \left(\frac{1+\sin\left(\phi'_{d_1}\right)}{1-\sin\left(\phi'_{d_1}\right)}\right) \cdot e^{\pi \cdot \tan\left(\phi'_{d_1}\right)} & \text{if } l_p \le h_{layer_1} \\ \left(\frac{1+\sin\left(\phi'_{d_2}\right)}{1-\sin\left(\phi'_{2}\right)}\right) \cdot e^{\pi \cdot \tan\left(\phi'_{d_2}\right)} & \text{else if } h_{layer_1} < l_p < h_{layer_1} + h_{layer_2} \\ \left(\frac{1+\sin\left(\phi'_{d_3}\right)}{1-\sin\left(\phi'_{d_3}\right)}\right) \cdot e^{\pi \cdot \tan\left(\phi'_{d_3}\right)} & \text{else} \end{cases} = 26.092$$

$$R_{bd;1.1} := \text{if } l_p \le h_{layer_1} \quad = \left(3.708 \cdot 10^3\right)\ kN$$

$$\left\| \frac{A_b \cdot \left(c'_{d_1} \cdot N_c + \sigma'_0 \cdot N_{qd}\right)}{\gamma_{b_{1,1}}} \right.$$

$$\text{else if } h_{layer_1} < l_p < h_{layer_1} + h_{layer_2}$$

$$\left\| \frac{A_b \cdot \left(c'_{d_2} \cdot N_c + \sigma'_0 \cdot N_{qd}\right)}{\gamma_{b_{1,1}}} \right.$$

$$\text{else}$$

$$\left\| \frac{A_b \cdot \left(c'_{d_3} \cdot N_c + \sigma'_0 \cdot N_{qd}\right)}{\gamma_{b_{1,1}}} \right.$$

$$\psi_d := \text{if } l_p \le h_{layer_1}$$

$$\left\| \begin{bmatrix} \frac{c'_{d_1}}{\sigma'_{vmed_1}} & 0.1 & 0.1 \end{bmatrix} \right.$$

$$\text{else if } h_{layer_1} < l_p < h_{layer_1} + h_{layer_2}$$

$$\left\| \begin{bmatrix} \frac{c'_{d_1}}{\sigma'_{vmed_1}} & \frac{c'_{d_2}}{\sigma'_{vmed_2}} & 0.1 \end{bmatrix} \right.$$

$$\text{else}$$

$$\left\| \begin{bmatrix} \frac{c'_{d_1}}{\sigma'_{vmed_1}} & \frac{c'_{d_2}}{\sigma'_{vmed_2}} & \frac{c'_{d_3}}{\sigma'_{vmed_3}} \end{bmatrix} \right.$$

$$\alpha_{d_1} := \text{if } \psi_{d_{1,1}} \le 1$$

$$\left\| \text{return } 0.5 \cdot \psi_{d_{1,1}}^{-0.5} \right.$$

$$\text{else if } \psi_{d_{1,1}} > 1$$

$$\left\| \text{return } 0.5 \cdot \psi_{d_{1,1}}^{-0.25} \right.$$

$$\alpha_{d_2} := \text{if } \psi_{d_{1,2}} \le 1$$

$$\left\| \text{return } 0.5 \cdot \psi_{d_{1,2}}^{-0.5} \right.$$

$$\text{else if } \psi_{d_{1,2}} > 1$$

$$\left\| \text{return } 0.5 \cdot \psi_{d_{1,2}}^{-0.25} \right.$$

$$\alpha_{d_3} := \text{if } \psi_{d_{1,3}} \le 1$$

$$\left\| \text{return } 0.5 \cdot \psi_{d_{1,3}}^{-0.5} \right.$$

$$\text{else if } \psi_{d_{1,3}} > 1$$

$$\left\| \text{return } 0.5 \cdot \psi_{d_{1,3}}^{-0.25} \right.$$

$$\alpha_d := \begin{bmatrix} \alpha_{d_1} \\ \alpha_{d_2} \\ \alpha_{d_3} \end{bmatrix} = \begin{bmatrix} 155.724 \\ 0.512 \\ 252.166 \end{bmatrix}$$

$$R_{s;1} := A_{s_{1,1}} \cdot \left(\alpha_{d_1} \cdot c'_{d_1} + K \cdot \sigma'_{vmed_1} \cdot \tan\left(\delta_{d_1}\right) \right)$$

$$R_{s;2} := A_{s_{1,2}} \cdot \left(\alpha_{d_2} \cdot c'_{d_2} + K \cdot \sigma'_{vmed_2} \cdot \tan\left(\delta_{d_2}\right) \right)$$

$$R_{s;3} := A_{s_{1,3}} \cdot \left(\alpha_{d_3} \cdot c'_{d_3} + K \cdot \sigma'_{vmed_3} \cdot \tan\left(\delta_{d_3}\right) \right)$$

$$R_{sd;1.1} := \frac{R_{s;1} + R_{s;2} + R_{s;3}}{\gamma_{s;c_{1,1}}} = \left\langle 3.938 \cdot 10^3 \right\rangle \ kN$$

$$R_{td;1.1} := R_{bd;1.1} + R_{sd;1.1} = \left\langle 7.645 \cdot 10^3 \right\rangle \ kN$$

$$S := \begin{array}{l} \text{if } F_{vd;1.1} < R_{td;1.1} \\ \quad \text{return “Security verified”} \\ \text{else} \\ \quad \text{“Security not verified”} \end{array} \quad \Big| = \text{“Security verified”}$$

- <u>Design approach 1 – Combination 2:</u>

$$F_{vd;1.2} := F_G \cdot \gamma_{G;unf_{1,2}} + F_{vp;max} \cdot \gamma_{Q;unf_{1,2}} = \left\langle 3.308 \cdot 10^3 \right\rangle \ kN$$

$$\phi'_d := \operatorname{atan}\left(\frac{\tan(\phi')}{\gamma_{\phi'_{1,1}}} \right) = \begin{bmatrix} 39 \\ 0 \\ 33 \end{bmatrix} ^\circ \qquad c'_d := \frac{c'}{\gamma_{c'_{1,1}}} = \begin{bmatrix} 0.001 \\ 200 \\ 0.001 \end{bmatrix} \ kPa$$

$$\delta_d := \operatorname{atan}\left(\frac{\tan(\delta)}{\gamma_{\phi'_{1,1}}} \right) = \begin{bmatrix} 26 \\ 0 \\ 22 \end{bmatrix} ^\circ$$

$$N_{qd} := \begin{cases} \left(\frac{1+\sin\left(\phi'_{d_1}\right)}{1-\sin\left(\phi'_{d_1}\right)}\right) \cdot e^{\pi \cdot \tan\left(\phi'_{d_1}\right)} & \text{if } l_p \le h_{layer_1} \\ \left(\frac{1+\sin\left(\phi'_{d_2}\right)}{1-\sin\left(\phi'_{2}\right)}\right) \cdot e^{\pi \cdot \tan\left(\phi'_{d_2}\right)} & \text{else if } h_{layer_1} < l_p < h_{layer_1} + h_{layer_2} \\ \left(\frac{1+\sin\left(\phi'_{d_3}\right)}{1-\sin\left(\phi'_{d_3}\right)}\right) \cdot e^{\pi \cdot \tan\left(\phi'_{d_3}\right)} & \text{else} \end{cases} = 26.092$$

$$R_{bd;1.2} := \begin{cases} \frac{A_b \cdot \left(c'_{d_1} \cdot N_c + \sigma'_0 \cdot N_{qd}\right)}{\gamma_{b_{1,4}}} & \text{if } l_p \le h_{layer_1} \\ \frac{A_b \cdot \left(c'_{d_2} \cdot N_c + \sigma'_0 \cdot N_{qd}\right)}{\gamma_{b_{1,4}}} & \text{else if } h_{layer_1} < l_p < h_{layer_1} + h_{layer_2} \\ \frac{A_b \cdot \left(c'_{d_3} \cdot N_c + \sigma'_0 \cdot N_{qd}\right)}{\gamma_{b_{1,4}}} & \text{else} \end{cases} = \left(2.852 \cdot 10^3\right)\ kN$$

$$\psi_d := \begin{cases} \begin{bmatrix} \frac{c'_{d_1}}{\sigma'_{vmed_1}} & 0.1 & 0.1 \end{bmatrix} & \text{if } l_p \le h_{layer_1} \\ \begin{bmatrix} \frac{c'_{d_1}}{\sigma'_{vmed_1}} & \frac{c'_{d_2}}{\sigma'_{vmed_2}} & 0.1 \end{bmatrix} & \text{else if } h_{layer_1} < l_p < h_{layer_1} + h_{layer_2} \\ \begin{bmatrix} \frac{c'_{d_1}}{\sigma'_{vmed_1}} & \frac{c'_{d_2}}{\sigma'_{vmed_2}} & \frac{c'_{d_3}}{\sigma'_{vmed_3}} \end{bmatrix} & \text{else} \end{cases}$$

$$\alpha_{d_1} := \begin{cases} \text{return } 0.5 \cdot \psi_{d_{1,1}}^{-0.5} & \text{if } \psi_{d_{1,1}} \le 1 \\ \text{return } 0.5 \cdot \psi_{d_{1,1}}^{-0.25} & \text{else if } \psi_{d_{1,1}} > 1 \end{cases}$$

$$\alpha_{d_2} := \begin{cases} \text{return } 0.5 \cdot \psi_{d_{1,2}}^{-0.5} & \text{if } \psi_{d_{1,2}} \le 1 \\ \text{return } 0.5 \cdot \psi_{d_{1,2}}^{-0.25} & \text{else if } \psi_{d_{1,2}} > 1 \end{cases}$$

$$\alpha_{d_3} := \begin{cases} \text{return } 0.5 \cdot \psi_{d_{1,3}}^{-0.5} & \text{if } \psi_{d_{1,3}} \le 1 \\ \text{return } 0.5 \cdot \psi_{d_{1,3}}^{-0.25} & \text{else if } \psi_{d_{1,3}} > 1 \end{cases}$$

$$\alpha_d := \begin{bmatrix} \alpha_{d_1} \\ \alpha_{d_2} \\ \alpha_{d_3} \end{bmatrix} = \begin{bmatrix} 155.724 \\ 0.512 \\ 252.166 \end{bmatrix}$$

$$R_{s;1} := A_{s_{1,1}} \cdot \left(\alpha_{d_1} \cdot c'_{d_1} + K \cdot \sigma'_{vmed_1} \cdot \tan\left(\delta_{d_1}\right) \right)$$

$$R_{s;2} := A_{s_{1,2}} \cdot \left(\alpha_{d_2} \cdot c'_{d_2} + K \cdot \sigma'_{vmed_2} \cdot \tan\left(\delta_{d_2}\right) \right)$$

$$R_{s;3} := A_{s_{1,3}} \cdot \left(\alpha_{d_3} \cdot c'_{d_3} + K \cdot \sigma'_{vmed_3} \cdot \tan\left(\delta_{d_3}\right) \right)$$

$$R_{sd;1.2} := \frac{R_{s;1} + R_{s;2} + R_{s;3}}{\gamma_{s;c_{1,4}}} = \left\langle 3.029 \cdot 10^3 \right\rangle \ kN$$

$$R_{td;1.2} := R_{bd;1.2} + R_{sd;1.2} = \left(5.881 \cdot 10^{3}\right)\ kN$$

$$S := \begin{array}{l} \text{if } F_{vd;1.2} < R_{td;1.2} \\ \quad \text{return “Security verified”} \\ \text{else} \\ \quad \text{“Security not verified”} \end{array} \quad = \text{“Security verified”}$$

- Design approach 2:

$$F_{vd;2} := F_G \cdot \gamma_{G;unf_{1,1}} + F_{vp;max} \cdot \gamma_{Q;unf_{1,1}} = \left(4.002 \cdot 10^{3}\right)\ kN$$

$$\phi'_d := \operatorname{atan}\left(\frac{\tan(\phi')}{\gamma_{\phi'_{1,1}}}\right) = \begin{bmatrix} 39 \\ 0 \\ 33 \end{bmatrix} \cdot ^\circ \qquad c'_d := \frac{c'}{\gamma_{c'_{1,1}}} = \begin{bmatrix} 0.001 \\ 200 \\ 0.001 \end{bmatrix}\ kPa$$

$$\delta_d := \operatorname{atan}\left(\frac{\tan(\delta)}{\gamma_{\phi'_{1,1}}}\right) = \begin{bmatrix} 26 \\ 0 \\ 22 \end{bmatrix} \cdot ^\circ$$

$$N_{qd} := \begin{array}{l} \text{if } l_p \le h_{layer_1} \\ \quad \left(\frac{1+\sin\left(\phi'_{d_1}\right)}{1-\sin\left(\phi'_{d_1}\right)}\right) \cdot e^{\pi \cdot \tan\left(\phi'_{d_1}\right)} \\ \text{else if } h_{layer_1} < l_p < h_{layer_1} + h_{layer_2} \\ \quad \left(\frac{1+\sin\left(\phi'_{d_2}\right)}{1-\sin\left(\phi'_{2}\right)}\right) \cdot e^{\pi \cdot \tan\left(\phi'_{d_2}\right)} \\ \text{else} \\ \quad \left(\frac{1+\sin\left(\phi'_{d_3}\right)}{1-\sin\left(\phi'_{d_3}\right)}\right) \cdot e^{\pi \cdot \tan\left(\phi'_{d_3}\right)} \end{array} \quad = 26.092$$

$$R_{bd;2} := \text{if } l_p \le h_{layer_1} \quad = \left(3.371 \cdot 10^{3}\right)\ kN$$

$$\left\| \frac{A_b \cdot \left(c'_{d_1} \cdot N_c + \sigma'_0 \cdot N_{qd}\right)}{\gamma_{b_{1,2}}} \right.$$

$$\text{else if } h_{layer_1} < l_p < h_{layer_1} + h_{layer_2}$$

$$\left\| \frac{A_b \cdot \left(c'_{d_2} \cdot N_c + \sigma'_0 \cdot N_{qd}\right)}{\gamma_{b_{1,2}}} \right.$$

$$\text{else}$$

$$\left\| \frac{A_b \cdot \left(c'_{d_3} \cdot N_c + \sigma'_0 \cdot N_{qd}\right)}{\gamma_{b_{1,2}}} \right.$$

$$\psi_d := \text{if } l_p \le h_{layer_1}$$

$$\left\| \begin{bmatrix} \frac{c'_{d_1}}{\sigma'_{vmed_1}} & 0.1 & 0.1 \end{bmatrix} \right.$$

$$\text{else if } h_{layer_1} < l_p < h_{layer_1} + h_{layer_2}$$

$$\left\| \begin{bmatrix} \frac{c'_{d_1}}{\sigma'_{vmed_1}} & \frac{c'_{d_2}}{\sigma'_{vmed_2}} & 0.1 \end{bmatrix} \right.$$

$$\text{else}$$

$$\left\| \begin{bmatrix} \frac{c'_{d_1}}{\sigma'_{vmed_1}} & \frac{c'_{d_2}}{\sigma'_{vmed_2}} & \frac{c'_{d_3}}{\sigma'_{vmed_3}} \end{bmatrix} \right.$$

$$\alpha_{d_1} := \text{if } \psi_{d_{1,1}} \le 1$$

$$\left\| \text{return } 0.5 \cdot \psi_{d_{1,1}}^{-0.5} \right.$$

$$\text{else if } \psi_{d_{1,1}} > 1$$

$$\left\| \text{return } 0.5 \cdot \psi_{d_{1,1}}^{-0.25} \right.$$

$$\alpha_{d_2} := \text{if } \psi_{d_{1,2}} \le 1$$

$$\left\| \text{return } 0.5 \cdot \psi_{d_{1,2}}^{-0.5} \right.$$

$$\text{else if } \psi_{d_{1,2}} > 1$$

$$\left\| \text{return } 0.5 \cdot \psi_{d_{1,2}}^{-0.25} \right.$$

$$\alpha_{d_3} := \text{if } \psi_{d_{1,3}} \le 1$$

$$\left\| \text{return } 0.5 \cdot \psi_{d_{1,3}}^{-0.5} \right.$$

$$\text{else if } \psi_{d_{1,3}} > 1$$

$$\left\| \text{return } 0.5 \cdot \psi_{d_{1,3}}^{-0.25} \right.$$

$$\alpha_d := \begin{bmatrix} \alpha_{d_1} \\ \alpha_{d_2} \\ \alpha_{d_3} \end{bmatrix} = \begin{bmatrix} 155.724 \\ 0.512 \\ 252.166 \end{bmatrix}$$

$$R_{s;1} := A_{s_{1,1}} \cdot \left(\alpha_{d_1} \cdot c'_{d_1} + K \cdot \sigma'_{vmed_1} \cdot \tan\left(\delta_{d_1}\right) \right)$$

$$R_{s;2} := A_{s_{1,2}} \cdot \left(\alpha_{d_2} \cdot c'_{d_2} + K \cdot \sigma'_{vmed_2} \cdot \tan\left(\delta_{d_2}\right) \right)$$

$$R_{s;3} := A_{s_{1,3}} \cdot \left(\alpha_{d_3} \cdot c'_{d_3} + K \cdot \sigma'_{vmed_3} \cdot \tan\left(\delta_{d_3}\right) \right)$$

$$R_{sd;2} := \frac{R_{s;1} + R_{s;2} + R_{s;3}}{\gamma_{s;c_{1,2}}} = \left(3.58 \cdot 10^3\right)\ kN$$

$$R_{td;2} := R_{bd;2} + R_{sd;2} = \left(6.95 \cdot 10^3\right)\ kN$$

$$S := \text{if } F_{vd;2} < R_{td;2} \ \| \ \text{return “Security verified”} \ \text{else} \ \| \ \text{“Security not verified”} = \text{“Security verified”}$$

- <u>Design approach 3:</u>

$$F_{vd;3} := F_G \cdot \gamma_{G;unf_{1,1}} + F_{vp;max} \cdot \gamma_{Q;unf_{1,1}} = \left(4.002 \cdot 10^3\right)\ kN$$

$$\phi'_d := \operatorname{atan}\left(\frac{\tan(\phi')}{\gamma_{\phi'_{1,2}}} \right) = \begin{bmatrix} 32.936 \\ 0 \\ 27.453 \end{bmatrix} ^\circ \qquad c'_d := \frac{c'}{\gamma_{c'_{1,2}}} = \begin{bmatrix} 8 \cdot 10^{-4} \\ 160 \\ 8 \cdot 10^{-4} \end{bmatrix} kPa$$

$$\delta_d := \operatorname{atan}\left(\frac{\tan(\delta)}{\gamma_{\phi'_{1,2}}} \right) = \begin{bmatrix} 21.315 \\ 0 \\ 17.912 \end{bmatrix} ^\circ$$

$$N_{qd} := \begin{cases} \left(\frac{1+\sin\left(\phi'_{d_1}\right)}{1-\sin\left(\phi'_{d_1}\right)}\right) \cdot e^{\pi \cdot \tan\left(\phi'_{d_1}\right)} & \text{if } l_p \le h_{layer_1} \\ \left(\frac{1+\sin\left(\phi'_{d_2}\right)}{1-\sin\left(\phi'_{2}\right)}\right) \cdot e^{\pi \cdot \tan\left(\phi'_{d_2}\right)} & \text{else if } h_{layer_1} < l_p < h_{layer_1} + h_{layer_2} \\ \left(\frac{1+\sin\left(\phi'_{d_3}\right)}{1-\sin\left(\phi'_{d_3}\right)}\right) \cdot e^{\pi \cdot \tan\left(\phi'_{d_3}\right)} & \text{else} \end{cases} = 13.865$$

$$R_{bd;3} := \begin{cases} \frac{A_b \cdot \left(c'_{d_1} \cdot N_c + \sigma'_0 \cdot N_{qd}\right)}{\gamma_{b_{1,3}}} & \text{if } l_p \le h_{layer_1} \\ \frac{A_b \cdot \left(c'_{d_2} \cdot N_c + \sigma'_0 \cdot N_{qd}\right)}{\gamma_{b_{1,3}}} & \text{else if } h_{layer_1} < l_p < h_{layer_1} + h_{layer_2} \\ \frac{A_b \cdot \left(c'_{d_3} \cdot N_c + \sigma'_0 \cdot N_{qd}\right)}{\gamma_{b_{1,3}}} & \text{else} \end{cases} = \left\langle 1.97 \cdot 10^3 \right\rangle \ kN$$

$$\psi_d := \text{if } l_p \le h_{layer_1}$$
$$\quad \begin{bmatrix} \frac{c'_{d_1}}{\sigma'_{vmed_1}} & 0.1 & 0.1 \end{bmatrix}$$
$$\text{else if } h_{layer_1} < l_p < h_{layer_1} + h_{layer_2}$$
$$\quad \begin{bmatrix} \frac{c'_{d_1}}{\sigma'_{vmed_1}} & \frac{c'_{d_2}}{\sigma'_{vmed_2}} & 0.1 \end{bmatrix}$$
$$\text{else}$$
$$\quad \begin{bmatrix} \frac{c'_{d_1}}{\sigma'_{vmed_1}} & \frac{c'_{d_2}}{\sigma'_{vmed_2}} & \frac{c'_{d_3}}{\sigma'_{vmed_3}} \end{bmatrix}$$

$$\alpha_{d_1} := \text{if } \psi_{d_{1,1}} \le 1$$
$$\quad \text{return } 0.5 \cdot \psi_{d_{1,1}}^{-0.5}$$
$$\text{else if } \psi_{d_{1,1}} > 1$$
$$\quad \text{return } 0.5 \cdot \psi_{d_{1,1}}^{-0.25}$$

$$\alpha_{d_2} := \text{if } \psi_{d_{1,2}} \le 1$$
$$\quad \text{return } 0.5 \cdot \psi_{d_{1,2}}^{-0.5}$$
$$\text{else if } \psi_{d_{1,2}} > 1$$
$$\quad \text{return } 0.5 \cdot \psi_{d_{1,2}}^{-0.25}$$

$$\alpha_{d_3} := \text{if } \psi_{d_{1,3}} \le 1$$
$$\quad \text{return } 0.5 \cdot \psi_{d_{1,3}}^{-0.5}$$
$$\text{else if } \psi_{d_{1,3}} > 1$$
$$\quad \text{return } 0.5 \cdot \psi_{d_{1,3}}^{-0.25}$$

$$\alpha_d := \begin{bmatrix} \alpha_{d_1} \\ \alpha_{d_2} \\ \alpha_{d_3} \end{bmatrix} = \begin{bmatrix} 174.105 \\ 0.573 \\ 281.93 \end{bmatrix}$$

$$R_{s;1} := A_{s_{1,1}} \cdot \left(\alpha_{d_1} \cdot c'_{d_1} + K \cdot \sigma'_{vmed_1} \cdot \tan\left(\delta_{d_1}\right) \right)$$

$$R_{s;2} := A_{s_{1,2}} \cdot \left(\alpha_{d_2} \cdot c'_{d_2} + K \cdot \sigma'_{vmed_2} \cdot \tan\left(\delta_{d_2}\right) \right)$$

$$R_{s;3} := A_{s_{1,3}} \cdot \left(\alpha_{d_3} \cdot c'_{d_3} + K \cdot \sigma'_{vmed_3} \cdot \tan\left(\delta_{d_3}\right) \right)$$

$$R_{sd;3} := \frac{R_{s;1} + R_{s;2} + R_{s;3}}{\gamma_{s;c_{1,3}}} = \left\langle 3.248 \cdot 10^3 \right\rangle \ kN$$

$$R_{td;3} := R_{bd;3} + R_{sd;3} = \left\langle 5.218 \cdot 10^{3} \right\rangle \ kN$$

$$S := \text{if } F_{vd;3} < R_{td;3} \ \Big\| \text{return “Security verified”} \ \text{else} \ \Big\| \text{“Security not verified”} \quad \Big| = \text{“Security verified”}$$

$$F_d := \begin{bmatrix} F_{vd;1.1} \\ F_{vd;1.2} \\ F_{vd;2} \\ F_{vd;3} \end{bmatrix} = \begin{bmatrix} 4.002 \cdot 10^{3} \\ 3.308 \cdot 10^{3} \\ 4.002 \cdot 10^{3} \\ 4.002 \cdot 10^{3} \end{bmatrix} kN \qquad R_d := \begin{bmatrix} R_{td;1.1} \\ R_{td;1.2} \\ R_{td;2} \\ R_{td;3} \end{bmatrix} = \begin{bmatrix} 7.645 \cdot 10^{3} \\ 5.881 \cdot 10^{3} \\ 6.95 \cdot 10^{3} \\ 5.218 \cdot 10^{3} \end{bmatrix} kN$$

$$\frac{R_d}{F_d} = \begin{bmatrix} 1.91 \\ 1.778 \\ 1.737 \\ 1.304 \end{bmatrix}$$

Appendix D

Generalized pile-soil-pile theory Mathcad sheet

Circular pile group

Input parameters

Foundation:

$n_p := 24$ $R := 10\ m$ $r_0 := 0.4\ m$

Soil:

$E := 90\ MPa$ $\nu := 0.35$ $G := \frac{E}{2 \cdot (1+\nu)} = 33.333\ MPa$

$\gamma := 20\ \frac{kN}{m^3}$ $c_s := \sqrt{\frac{G \cdot g}{\gamma}} = 127.845\ \frac{m}{s}$ $\beta := 0.05$

Frequency:

$f := 1.2\ Hz$ $\omega := 2 \cdot \pi \cdot f = 7.54\ \frac{rad}{s}$

Sitffness of a single pile:

Vertical stiffness

$k_v := 8.16 \cdot 10^5\ \frac{kN}{m}$

Horizontal stiffness

$k_h := 1.59 \cdot 10^5\ \frac{kN}{m}$

Rocking stiffness

$k_\theta := 1.78 \cdot 10^5\ kN \cdot m$

Coordinates and spacing

$i := 1,2..n_p$ $j := 1,2..n_p$

$x_{1,j} := R \cdot \cos\left(2\ \pi \cdot \frac{j-1}{n_p}\right)$ $y_{1,j} := R \cdot \sin\left(2\ \pi \cdot \frac{j-1}{n_p}\right)$

$\Delta_{i,j} := \sqrt{\left(x_{1,j} - x_{1,i}\right)^2 + \left(y_{1,j} - y_{1,i}\right)^2}$

$$\Delta = \begin{bmatrix} 0 & 2.611 & 5.176 & 7.654 & 10 & 12.175 & 14.142 & \\ 2.611 & 0 & 2.611 & 5.176 & 7.654 & 10 & 12.175 & \\ 5.176 & 2.611 & 0 & 2.611 & 5.176 & 7.654 & 10 & \\ 7.654 & 5.176 & 2.611 & 0 & 2.611 & 5.176 & 7.654 & \\ 10 & 7.654 & 5.176 & 2.611 & 0 & 2.611 & 5.176 & \\ 12.175 & 10 & 7.654 & 5.176 & 2.611 & 0 & 2.611 & \\ 14.142 & 12.175 & 10 & 7.654 & 5.176 & 2.611 & 0 & \\ 15.867 & 14.142 & 12.175 & 10 & 7.654 & 5.176 & 2.611 & \\ & & & & & & & \ddots \end{bmatrix} m$$

Vertical impedance

$$p := \sqrt{-1}$$

$$A_{v_{i,j}} := \left\| \begin{array}{l} \text{if } i = j \\ \quad \text{return } 1 \\ \text{else} \\ \quad \text{return } \sqrt{\frac{r_0}{\Delta_{i,j}}} \cdot e^{\left(-\beta \cdot \omega \cdot \frac{\Delta_{i,j}}{c_s}\right)} \cdot e^{\left(-p \cdot \omega \cdot \frac{\Delta_{i,j}}{c_s}\right)} \end{array} \right.$$

$$A_v = \begin{bmatrix} 1 & 0.384 - 0.06i & 0.261 - 0.082i & 0.201 - 0.097i & \\ 0.384 - 0.06i & 1 & 0.384 - 0.06i & 0.261 - 0.082i & \\ 0.261 - 0.082i & 0.384 - 0.06i & 1 & 0.384 - 0.06i & \\ 0.201 - 0.097i & 0.261 - 0.082i & 0.384 - 0.06i & 1 & \\ 0.161 - 0.108i & 0.201 - 0.097i & 0.261 - 0.082i & 0.384 - 0.06i & \\ & & & & \ddots \end{bmatrix}$$

$$e_i := 1 \qquad e = \begin{bmatrix} 1 \\ 1 \\ 1 \\ \vdots \end{bmatrix}$$

$$K_{vg} := k_v \cdot e^{\mathrm{T}} \cdot A_v^{-1} \cdot e = \left(3.421 \cdot 10^6 + 2.039i \cdot 10^6\right) \frac{kN}{m}$$ – Group vertical dynamic stiffness

Group vertical stiffness coefficient

$$k_{vg} := \mathrm{Re}\left(K_{vg}\right) = \left(3.421 \cdot 10^6\right) \frac{kN}{m}$$

Group vertical damping coefficient

$$C_{vg} := \frac{\mathrm{Im}\left(K_{vg}\right)}{\omega} = \left(2.705 \cdot 10^5\right) \frac{kN \cdot s}{m}$$

Horizontal impedance

$$\theta_{i,j} := \begin{cases} \text{if } i = j \\ \quad \text{return } 0 \\ \text{else} \\ \quad \text{return } \operatorname{asin}\left(\dfrac{\operatorname{abs}\left(y_{1,j} - y_{1,i}\right)}{\Delta_{i,j}}\right) \end{cases}$$

– Angle between piles

$$\theta = \begin{bmatrix} 0 & 1.44 & 1.309 & 1.178 & 1.047 & 0.916 & 0.785 & 0.654 & \\ 1.44 & 0 & 1.178 & 1.047 & 0.916 & 0.785 & 0.654 & 0.524 & \\ 1.309 & 1.178 & 0 & 0.916 & 0.785 & 0.654 & 0.524 & 0.393 & \\ 1.178 & 1.047 & 0.916 & 0 & 0.654 & 0.524 & 0.393 & 0.262 & \\ 1.047 & 0.916 & 0.785 & 0.654 & 0 & 0.393 & 0.262 & 0.131 & \\ & & & & & & & & \ddots \end{bmatrix}$$

$$c_{LA} := 3.4 \cdot \frac{c_s}{\pi \cdot (1 - \nu)} = 212.863 \ \frac{m}{s}$$

$$A_{h_{i,j}} := \begin{cases} \text{if } i = j \\ \quad \text{return } 1 \\ \text{else} \\ \quad \text{return } \sqrt{\dfrac{r_0}{\Delta_{i,j}}} \cdot e^{\left(-\beta \cdot \omega \cdot \frac{\Delta_{i,j}}{c_{LA}}\right)} \cdot e^{\left(-p \cdot \omega \cdot \frac{\Delta_{i,j}}{c_{LA}}\right)} \end{cases}$$

$$A_h = \begin{bmatrix} 1 & 0.388 - 0.036\text{i} & 0.271 - 0.05\text{i} & 0.217 - 0.06\text{i} & \\ 0.388 - 0.036\text{i} & 1 & 0.388 - 0.036\text{i} & 0.271 - 0.05\text{i} & \\ 0.271 - 0.05\text{i} & 0.388 - 0.036\text{i} & 1 & 0.388 - 0.036\text{i} & \\ 0.217 - 0.06\text{i} & 0.271 - 0.05\text{i} & 0.388 - 0.036\text{i} & 1 & \\ & & & & \ddots \end{bmatrix}$$

$$A_{i,j} := A_{v_{i,j}} \cdot \left(\sin\left(\theta_{i,j}\right)\right)^2 + A_{h_{i,j}} \cdot \left(\cos\left(\theta_{i,j}\right)\right)^2$$

$$K_{hg} := k_h \cdot e^{\mathrm{T}} \cdot A_h^{-1} \cdot e = \left(6.868 \cdot 10^5 + 2.32\mathrm{i} \cdot 10^5\right) \frac{kN}{m}$$ – Group horizontal stiffness

Group horizontal stiffness coefficient

$$k_{hg} := \mathrm{Re}\left(K_{hg}\right) = \left(6.868 \cdot 10^5\right) \frac{kN}{m}$$

Group horizontal damping coefficient

$$C_{hg} := \frac{\mathrm{Im}\left(K_{hg}\right)}{\omega} = \left(3.077 \cdot 10^4\right) s \cdot \frac{kN}{m}$$

Rocking impedance

Dynamic bending stiffness of the group

$$K_{\theta g} := k_v \cdot \sum_{j=1}^{n_p} y \cdot A_v^{-1} \cdot y^{\mathrm{T}} = \left(1.019 \cdot 10^{10} - 1.695\mathrm{i} \cdot 10^9\right) kN \cdot m$$

Group bending stiffness coefficient

$$k_{\theta g} := \mathrm{Re}\left(K_{\theta g}\right) = \left(1.019 \cdot 10^{10}\right) \frac{kN \cdot m}{rad}$$

Group bending damping coefficient

$$C_{\theta g} := \frac{\mathrm{Im}\left(K_{\theta g}\right)}{\omega} = -2.248 \cdot 10^8 \frac{kN \cdot m \cdot s}{rad}$$